APPLIED PHYSICS REVIEWS

Vertically aligned carbon nanofibers and related structures: Controlled synthesis and directed assembly

A. V. Melechko
Molecular-Scale Engineering and Nanoscale Technologies Research Group, Oak Ridge National Laboratory, P.O. Box 2008, MS 6006, Oak Ridge, Tennessee 37831-6006 and Materials Science and Engineering Department, University of Tennessee, Knoxville, Tennessee 37996-2200

V. I. Merkulov and T. E. McKnight
Molecular-Scale Engineering and Nanoscale Technologies Research Group, Oak Ridge National Laboratory, P.O. Box 2008, MS 6006, Oak Ridge, Tennessee 37831-6006

M. A. Guillorn
Cornell Nanoscale Science and Technology Facility, Cornell University, Ithaca, New York 14853-2000

K. L. Klein
Molecular-Scale Engineering and Nanoscale Technologies Research Group, Oak Ridge National Laboratory, P.O. Box 2008, MS 6006, Oak Ridge, Tennessee 37831-6006 and Materials Science and Engineering Department, University of Tennessee, Knoxville, Tennessee 37996-2200

D. H. Lowndes
Thin Film and Nanostructured Materials Physics Group, Oak Ridge National Laboratory, Oak Ridge, Tennessee 37831-6056 and Center for Nanophase Materials Science, Oak Ridge National Laboratory, Oak Ridge, Tennessee 37831-6056

M. L. Simpson[a)]
Molecular-Scale Engineering and Nanoscale Technologies Research Group, Oak Ridge National Laboratory, P.O. Box 2008, MS 6006, Oak Ridge, Tennessee 37831-6006, Materials Science and Engineering Department, University of Tennessee, Knoxville, Tennessee 37996-2200, and Center for Nanophase Materials Science, Oak Ridge National Laboratory, Oak Ridge, Tennessee 37831-6056

(Received 10 September 2004; accepted 17 December 2004; published online 3 February 2005)

The controlled synthesis of materials by methods that permit their assembly into functional nanoscale structures lies at the crux of the emerging field of nanotechnology. Although only one of several materials families is of interest, carbon-based nanostructured materials continue to attract a disproportionate share of research effort, in part because of their wide-ranging properties. Additionally, developments of the past decade in the controlled synthesis of carbon nanotubes and nanofibers have opened additional possibilities for their use as functional elements in numerous applications. Vertically aligned carbon nanofibers (VACNFs) are a subclass of carbon nanostructured materials that can be produced with a high degree of control using catalytic plasma-enhanced chemical-vapor deposition (C-PECVD). Using C-PECVD the location, diameter, length, shape, chemical composition, and orientation can be controlled during VACNF synthesis. Here we review the CVD and PECVD systems, growth control mechanisms, catalyst preparation, resultant carbon nanostructures, and VACNF properties. This is followed by a review of many of the application areas for carbon nanotubes and nanofibers including electron field-emission sources, electrochemical probes, functionalized sensor elements, scanning probe microscopy tips, nanoelectromechanical systems (NEMS), hydrogen and charge storage, and catalyst support. We end by noting gaps in the understanding of VACNF growth mechanisms and the challenges remaining in the development of methods for an even more comprehensive control of the carbon nanofiber synthesis process. © *2005 American Institute of Physics*. [DOI: 10.1063/1.1857591]

TABLE OF CONTENTS

I. INTRODUCTION. 2
A. Historical background. 2
B. Definitions. 2
C. Overview of applications of vertically aligned carbon nanofibers. 4
II. SYNTHESIS. 5
A. Methods of synthesis of carbon materials. . . . 5
B. Catalytic thermal chemical-vapor deposition. 5
1. Thermal CVD and catalytic thermal CVD. 5
2. C-TCVD growth mechanisms. 5

C. Catalytic plasma-enhanced chemical-vapor deposition. 7
1. Introduction to PECVD. 7
2. C-PECVD experimental systems and results. 8
3. C-PECVD specific aspects of carbon nanostructure growth control. 12
D. Substrates and catalysts. 17
1. Substrates. 17
2. Catalysts. 18
3. Methods of catalyst preparation. 18
4. Catalyst particle evolution. 21
III. PROPERTIES. 22
A. Structure. 22
B. Electrical properties. 24
C. Electron field emission. 24
D. Mechanical properties. 26
E. Chemical properties. 27
F. Electrochemical properties. 28
G. Postsynthesis processing. 29
IV. APPLICATIONS. 31
A. Microfabricated field-emission electron sources. 31
B. Microfabricated x-ray sources. 32
C. Electrochemical probes. 32
D. Intracellular gene delivery devices. 33
E. Scanning probe microscopy tips. 33
F. Nanoelectromechanical devices (NEMS). . . . 34
G. Nanoporous membranes. 34
H. Other applications. 34
V. FUTURE DEVELOPMENTS AND CONCLUSIONS. 35

I. INTRODUCTION

A. Historical background

It has been known for over a century that filamentous carbon can be formed by the catalytic decomposition of carbon-containing gas on a hot metal surface. In a U.S. Patent published in 1889,[1] it is reported that carbon filaments are grown from carbon-containing gases using an iron crucible. It is probable that this early material consisted of nanofibers arranged in larger filaments; however, the actual observation of discrete nanofibers had to await the development of high-resolution electron microscopy. Radushkevich and Lukyanovich obtained transmission electron micrographs of nanofibers, or "soot particles," in 1952.[2] Works in the 1950s established that carbon filaments could be produced by the interaction of a wide range of hydrocarbons and other gases with metals, the most effective of which were iron, cobalt, and nickel. Early detailed studies (1950s through 1970s) of carbon nanofiber growth were prompted by undesirable formation of carbon deposits in industrial steam cracker tubes used to produce a variety of olefins,[3] and in the nuclear industry in which use of gases containing hydrocarbons or CO for cooling and heat transfer created carbon deposits on fuel cladding.[4] It should be noted that in the current literature, the term "nanofiber" is preferentially used, featuring distinction in size scale, while in the past simply "filamentous carbon," "carbon filaments," and "carbon whiskers" were applied.[4] In 1985 a form of carbon, buckminsterfullerene C_{60}, was observed by a team headed by Kroto *et al.*,[5] which led to the Nobel Prize in chemistry in 1997. This discovery was followed by IIijima's demonstration in 1991 that carbon nanotubes are formed during arc-discharge synthesis of C_{60} (Ref. 6) and other fullerenes, triggering a deluge of interest in carbon nanofibers and nanotubes. In the 1990s the introduction of catalytic plasma-enhanced chemical-vapor deposition (C-PECVD) provided additional control mechanisms over the growth of carbon nanostructures. In 1997 Chen *et al.* used PECVD for nanofiber synthesis.[7] Their work was followed by the better known work of Ren *et al.*[8] The use of C-PECVD ultimately has allowed for the highly deterministic synthesis of carbon nanostructures,[9,10] where by deterministic synthesis we mean control over position, alignment, diameter, length, chemical composition, or other characteristics of individual nanostructures.

There are many excellent reviews devoted to various aspects of synthesis and properties and applications of carbon nanofibers and carbon nanotubes.[11–18] Here we focus on the interplay between controlled synthesis and the resultant applications of vertically aligned carbon nanofibers. That is, we show that the control of nanofiber properties during the synthesis process provides the means for accomplishing bottom-up assembly of microscale (or larger) structures, devices, or systems with functional nanoscale elements. Other classes of filamentous carbon-based nanomaterials will be reviewed as well since most of the fundamental aspects of their synthesis and resulting properties, apart from a few distinctive characteristics, are the same or similar to those of nanofibers.

B. Definitions

Carbon nanofibers (CNFs) are cylindrical or conical structures that have diameters varying from a few to hundreds of nanometers and lengths ranging from less than a micron to millimeters. The internal structure of carbon nanofibers varies and is comprised of different arrangements of modified graphene sheets. A graphene layer can be defined as a hexagonal network of covalently bonded carbon atoms or a single two-dimensional (2D) layer of a three-dimensional (3D) graphite [Fig. 1(a)]. In general, a nanofiber consists of stacked curved graphite layers that form cones [Fig. 1(b)] or "cups."[19,20] The stacked cone structure is often referred to as herringbone (or fishbone) as their cross-sectional transmission electron micrographs (TEM) resemble a fish skeleton, while the stacked cups structure is most often referred to as a bamboo type, resembling the compartmentalized structure of a bamboo stem. Currently there is no strict classification of nanofiber structures. The main distinguishing characteristic of nanofibers from nanotubes is the stacking of graphene sheets of varying shapes.

We can define α as an angle between the fiber axis and the graphene sheet near the sidewall surface [Fig. 1(b)]. The nanofiber with $\alpha=0$ is a special case in which one or more

[a]Electronic mail: simpsonml1@ornl.gov

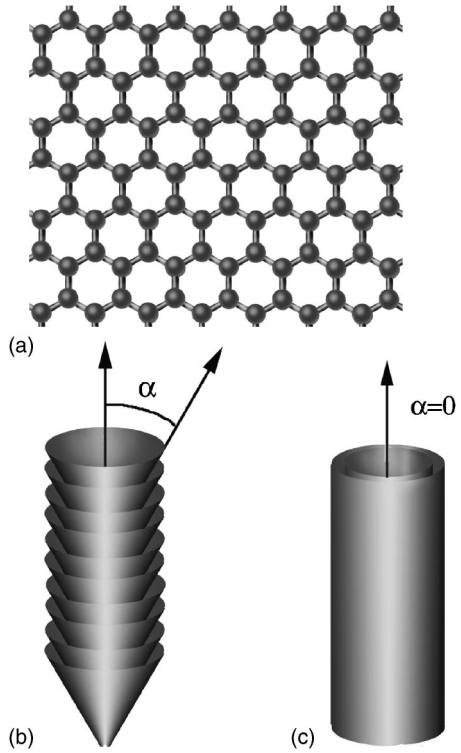

FIG. 1. Schematic structure of carbon nanofibers and nanotubes. (a) Graphene layer, (b) stacked cone (herringbone) nanofiber, and (c) nanotube.

graphene layers form cylinders that run the full length of the nanostructure [Fig. 1(c)]. This arrangement, with its closed and semi-infinite surface,[6] results in extraordinary properties that made this type of a nanofiber known to the world as a carbon nanotube (CNT). However, one cannot expect the same mechanical, electrical, and chemical properties for nanofibers with a nonzero α. In this case the nanostructure is assembled from graphene layers that are relatively short and poorly connected, spanning only a part of the nanofiber. For example, similar to graphite, charge transport along the nanofiber with $\alpha > 0$ is determined by both "in-plane" and "interplane" components that are quite different. The same is true for mechanical properties since the van der Waals bonding between the graphene planes differs drastically from the in-plane covalent bonding of true nanotubes. Similarly, the chemical properties of nanofibers and nanotubes are quite different since defect-free nanotube walls do not contain the exposed edges and unsaturated bonds of graphene planes, and as a result nanotubes are far less reactive than nanofibers. TEM images displaying nanofibers with various structures are shown in Fig. 2. TEM images of nanotubes are presented in Fig. 3. The clearly visible fringes correspond to graphene layers and run parallel to the axis of nanotubes throughout their entire length.

Although perhaps not completely warranted by utility, both the scientific community and the popular press have focused more on the special case of the CNT structure than the more general case that includes nanofibers. The reason for the attention given to nanotubes is clear: the beauty and perfection of their mathematical description and the resulting extraordinary mechanical and (ballistic) electron-transport properties. However, the distinctive properties of nanotubes

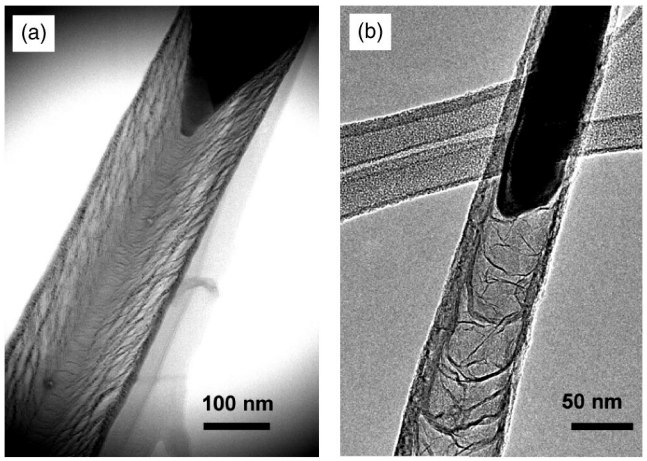

FIG. 2. (a) STEM image of a herringbone carbon nanofiber produced by dc C-PECVD with Ni catalyst; (b) TEM image of a bamboo-type carbon nanofiber grown at the same conditions with Fe catalyst.

call for a distinction in terminology that is not always made in literature. Instead, there is a tendency to call all these materials nanotubes, perhaps due to greater name recognition. For consistency and accuracy in this review, we refer to structures as nanotubes only if the graphene layers form cylinders that extend throughout the length of the material. If instead the graphene sheets form cones, cups, etc., we refer to them as nanofibers, even if that differs from the term used in a particular referenced work (if sufficient data are provided). Some authors, in order to distinguish this type of carbon nanostructure, refer to them as graphitic nanofibers[21] (GNF) or multiwalled carbon nanofibers (MWNFs).[22] The term nanostructure will be used in cases when some particular aspect is common to both nanotubes and other types of nanofibers.

Structures that are oriented perpendicular to the substrate on which they are grown are commonly called vertically aligned. In the case of a nanofiber or nanotube this means that the structure is straight and its axis is normal to the substrate (Fig. 4). In contrast, synthesis methods such as arc discharge, laser ablation, and certain types of chemical-vapor

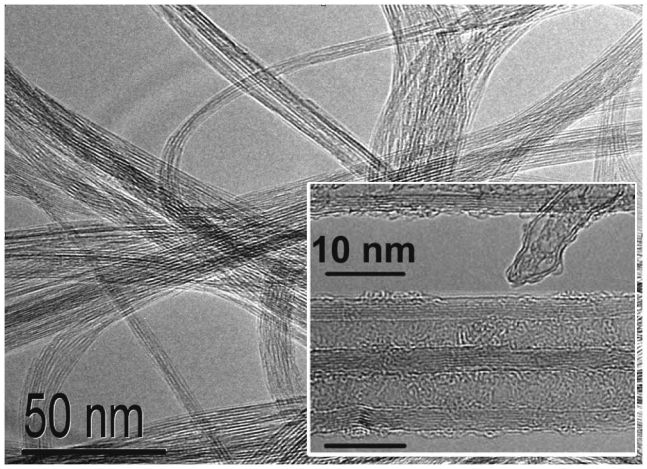

FIG. 3. TEM image of bundles of single-walled carbon nanotubes. Inset: TEM image of multiwalled carbon nanotubes (courtesy of D. B. Geohegan and H. Cui).

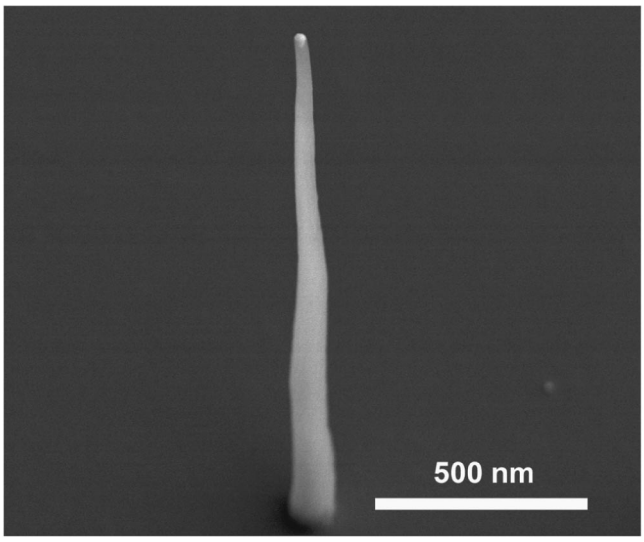

FIG. 4. SEM image of a VACNF produced by dc-PECVD in ammonia/acetylene plasma at 700 °C. The image is aquired at a 30° tilt angle, so that the apparent height is two times smaller than the actual height of the nanofiber.

deposition with floating catalyst produce nonaligned, entangled ropes of nanotubes. The CNT material produced this way can be used for a variety of applications such as reinforcement of composite materials, hydrogen storage, catalyst support, etc. However, for many applications that utilize nanofibers as individual elements, nanoelectronics, for example,[23] tedious manipulations on a microscale are often required if such entangled material is to be used. Accordingly, synthesis of aligned structures at defined positions on a substrate is preferred. Vertically aligned carbon nanofibers and carbon nanotubes can be prepared as a dense mat ("forest") or as individual freestanding structures (often arranged into a regular array), as can be seen in Fig. 5. Vertical alignment in very dense forests is provided by van der Waals interaction between nanotubes or nanofibers that keeps them aligned, while isolated elements may be aligned by interaction of the growing nanofiber with an electric field.[24]

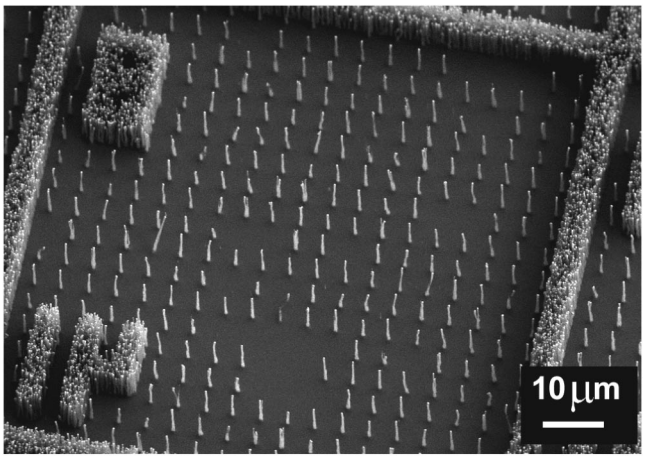

FIG. 5. SEM image of regular arrays of freestanding VACNFs and forests of VACNFs. Catalyst definition was produced by photolithography. VACNFs were grown by dc C-PECVD.

Throughout this article we will refer to deterministic synthesis as a method of growing individual nanostructures with precisely defined characteristics, such as size, location, chemical composition, internal structure, etc. Recently, it has been demonstrated that carbon nanofibers can be synthesized deterministically by PECVD.[9,10] In this synthesis process, the location of the VACNF is defined by patterning the catalyst material using photo- or electron-beam lithography with the size of the catalyst nanoparticle controlling the resultant nanofiber diameter, the nanofiber length is controlled by the growth rate and duration of the growth process, the alignment is controlled by the electric field present in the plasma sheath, and the sidewall chemical composition is defined by the selection of gas composition, substrate materials, and plasma power used during synthesis. In spite of this high degree of control, command over other VACNF attributes, such as specific internal crystalline structure, remains elusive. In particular, the ability to grow either individual freestanding vertically aligned nanofibers or single vertically aligned nanotubes by selecting appropriate growth conditions would represent a major advance in this field. While some fundamental questions remain unanswered, the technology of VACNF synthesis has matured to the point that it can be used as a standard processing step in complex device fabrication.[25–35]

C. Overview of applications of vertically aligned carbon nanofibers

There are many potential applications of carbon nanostructures which can be subdivided into two categories. The first category includes "bulk material" applications, in which carbon nanostructures are utilized as filler in composite materials, as catalyst support, for hydrogen storage, as electrodes for fuel cells, as supercapacitors, or for ultrafiltration membranes.[36] For these applications the properties of individual nanostructures are controlled to produce a functional ensemble. The second category includes applications in which each nanotube or nanofiber is used as an individual functional element of a device. For these applications it is highly important that the nanostructure is a high aspect ratio, mechanically and chemically robust conductor of electrons that can be deterministically produced on any substrate. The use of large-scale growth reactors created the opportunity to synthesize high-quality VACNFs in precisely defined locations on substrates compatible with microelectronic device manufacturing equipment (e.g., 100-mm-diameter Si and quartz wafers). These applications include field-emission devices such as field-emission displays and perhaps nanoscale electron sources for electron microscopy and electron-beam lithography, scanning probe tips and functionalized scanning probes, electrochemical probes, gene delivery arrays, membranes for microfluidic devices, and nanoelectronic devices. Some of these applications are discussed in Sec. IV in greater detail.

II. SYNTHESIS

A. Methods of synthesis of carbon materials

The methods for synthesizing carbon nanostructures include laser vaporization,[5] arc discharge,[6,37] catalytic chemical-vapor deposition (C-CVD), and catalytic plasma-enhanced chemical-vapor deposition (C-PECVD). While arc discharge and laser ablation are very efficient methods for producing high-quality nanotube material in large quantities, they do not offer control over the spatial arrangement of the produced nanostructures. Complex purification procedures are also required to remove amorphous carbon particles and entangled catalyst in order to obtain a useful material. At this time, only C-CVD allows controlled synthesis of carbon nanotubes and nanofibers and only C-PECVD allows deterministic synthesis in which the location, alignment, size, shape, and structure of each individual nanofiber are controlled during synthesis. The material obtained by this method can be considered phase pure, that is, no purification process is necessary. Furthermore, the defined and accessible position of the catalyst particle, especially at the tip, makes its optional extraction simplified.[38,39] Here we review only CVD and PECVD synthesis methods in detail.

B. Catalytic thermal chemical-vapor deposition

1. Thermal CVD and catalytic thermal CVD

Chemical-vapor deposition involves the adsorption, desorption, evolution, and incorporation of vapor species at the surface of a growing film. Since heat is the main energy source for reactions to occur, the CVD process is also often referred to as thermal CVD (TCVD). Process temperatures for TCVD production of carbon nanostructures typically lie in the range from 400 to 1000 °C. Catalytic CVD (or C-CVD) differs from CVD by involvement of a catalyst in the decomposition of vapor species on the catalyst surface and requires process temperatures similar to TCVD. Accordingly, the catalytically controlled thermal CVD will be abbreviated as C-TCVD. In addition to thermal excitation, methods include photoexcitation and electrical glow discharge (or plasma).

In a catalytic growth the deposition of carbon usually occurs on one side of the surface of a catalyst particle. Thus, two of the dimensions of the growing "film" are limited by the size of the particle, while the third dimension is not bound, leading to quasi-one-dimensional growth. In many synthesis processes, the diameter of the resultant carbon filament is approximately equal to that of the nanoparticle in the range from 5 to 500 nm. However, there is evidence that, for example, single-walled carbon nanotubes originate on catalyst particles that are significantly larger in size than the nanotubes themselves (1 nm).

The apparatus for C-TCVD usually consists of a quartz tube inside a furnace with a controllable source gas flow (Fig. 6). There are two common methods of introducing the catalyst into the system: supported catalyst and floating catalyst. In the supported catalyst method, the catalyst is deposited onto a substrate which is then placed inside the tube furnace (e.g., Ref. 40). In the floating catalyst method, the

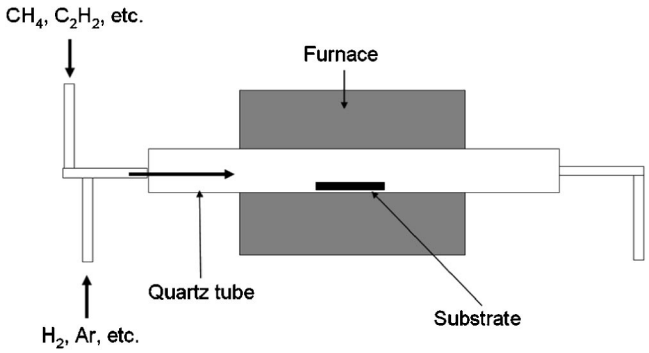

FIG. 6. Schematics of a tube-furnace-type TCVD apparatus.

catalyst particles form from a source gas and are not attached to a substrate. For example, the high-pressure carbon monoxide (HiPco) process, which allows a high volume production of carbon nanotubes, is one such floating catalyst method.[41]

C-TCVD has been successfully used to synthesize a whole range of carbon nanostructures. Carbon nanofiber synthesis using C-TCVD has been observed since the late 1950s.[2,3] Recently, C-TCVD has been optimized for the growth of multiwalled carbon nanotubes (MWCNTs),[42] and even single-walled carbon nanotubes (SWCNTs).[40,43] It is believed that SWCNTs are favored in CVD if the catalyst particles are small and the carbon supply is low, with sufficient energy in the system ($T > 900$ °C).[44] The catalyst particle preparation was found to be crucial in control of the structure of nanotubes.

By combining an efficient trilayer catalyst thin film (supported catalyst), developed by Delzeit *et al.*,[45] with introduction of ferrocene (floating catalyst) in addition to acetylene, Eres *et al.* produced dense arrays of vertically aligned multiwalled nanotubes by C-TCVD that are 3.5 mm tall.[46] Recently Eres *et al.* reported that after optimization, the maximum length of the nanotube achieved by this method was 9.25 mm.[47]

2. C-TCVD growth mechanisms

The catalytic nature of the carbon filament growth process was established by Tesner and co-workers[48,49] who showed that carbon filaments had metal particles associated with them. The growth mechanism leading to the formation of carbon nanofibers has been studied by many different groups. Baker *et al.* used *in situ* electron microscopy techniques to directly observe the manner by which small metal particles generated carbon nanofibers during the decomposition of acetylene.[50] From an analysis of recorded image sequences they measured the rates of growth of the material and determined some of the kinetic parameters involved in the process. On the basis of these experiments, a growth mechanism was proposed that was later refined to include the following steps: (i) adsorption and decomposition of the reactant hydrocarbon molecule on a surface of catalyst, (ii) dissolution and diffusion of carbon species through the metal particle, and (iii) precipitation of carbon on the opposite surface of the catalyst particle to form the nanofiber structure. Figure 7 shows a schematic diagram that illustrates the key

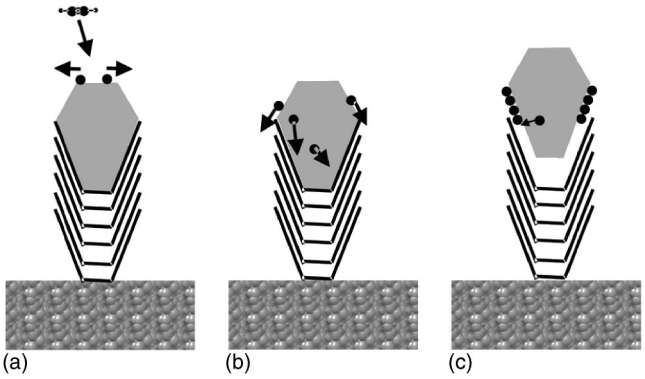

FIG. 7. Mechanism of carbon nanofiber formation. (a) Adsorption and decomposition of the reactant hydrocarbon molecule on the surface of catalyst, (b) dissolution and diffusion of carbon species through or around the metal particle, and (c) precipitation of carbon on the opposite surface of the catalyst particle and incorporation into graphene layers. (The drawing does not represent dynamic effects and transient effects on the initial stages.).

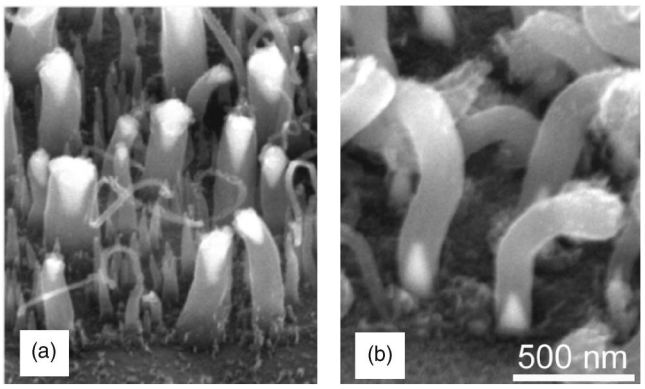

FIG. 8. Tip-type and base-type growth modes. SEM images of (a) tip-type and (b) base-type carbon nanofibers produced by dc C-PECVD. The bright triangles are the catalyst particles that are located at the tips in (a) and on the substrate in (b).

features of this growth model for a tip-type carbon nanofiber structure, where precipitation occurs on the bottom surface of the catalyst particle, thus elevating the particle, which remains at the tip throughout the growth. The chemical nature of the metal catalyst, the reaction temperature, and the composition of the reactant gas dictate the morphology and degree of crystalline perfection exhibited by the carbon nanofibers.

The kinetics of the three steps listed above determines the growth rate. The supply-limited process depends on the rates of arrival of different gas species to the catalyst surface, their adsorption rates, and their respective decomposition rates. It has been argued that diffusion of carbon through the metal catalyst particle is the rate-determining step, as supported by the close agreement between the measured activation energy for nanofiber growth and that for carbon diffusion through the respective metals used as catalysts. Initially, the driving force for the bulk diffusion of carbon through the metal particle was ascribed to a temperature gradient,[50,51] which was believed to develop due to exothermic reactions of decomposition on the surface of the catalyst. Later, it was proposed that concentration gradients drove the carbon diffusion through the catalyst particle, and there are several hypotheses about the processes involved in the formation of such concentration gradient. Nielsen and Trimm proposed that the carbon solubility at the gas/metal interface differs from that at the metal/carbon interface, since the activity of carbon in the gas phase may be much higher than one.[52] Sacco *et al.* suggested that the mass flux originates from the solubility difference between carbon at the alpha-iron/Fe_3C interface and that between alpha-iron and carbon itself.[53] Kock *et al.* proposed that the driving force for bulk carbon diffusion is the gradient of the carbon content of substoichiometric carbides, whereby the carbon content decreases in the direction of the metal/carbon interface.[54] Central to the model of Alstrup is the assumption that the carbon atoms entering the selvedge, which consists of subsurface layers that differ from the ideal structure of bulk crystal, create a "surface carbide" that forms the source of carbon atoms diffusing through the bulk of the metal particle.[55] In other words, the driving force for growth is a concentration gradient of carbon atoms from the metal-gas surface to the metal-graphite surface.[56] The validity of these models is still hard to assess due to the lack of direct *in situ* observations.

Recently, Helveg *et al.* presented what was described by Ajayan in an introductory article as "a long-awaited solution to the mystery of nanofiber growth."[57,58] They performed time-resolved, atomic-resolution *in situ* transmission electron microscope observations of the formation of carbon nanofibers from methane decomposition over supported nickel nanocrystals. Carbon nanofibers were observed to develop through a reaction-induced *reshaping* of the nickel nanoparticles. The nucleation and growth of graphene layers were found to be assisted by a dynamic, repetitive formation and restructuring of monoatomic step edges at the nickel surface. The authors proposed a mechanism, supported by density-functional theory calculations, that involves *surface* diffusion of carbon and nickel atoms. In their picture, the dissociative methane adsorption is facilitated at the step edges and C atoms adsorb preferentially at the step sites. The graphene layer forms at the terrace between the steps on the curved and dynamically changing catalyst nanoparticle surface. The process involves surface diffusion of C and Ni atoms from the step edge, and includes the breaking of the C bond to the Ni step on the free surface, incorporation under the graphene sheet, and diffusion at the graphene-Ni interface. Moreover their observations and calculations suggest that it is not necessary to include the bulk diffusion of C through the Ni particle, however, they do not eliminate such possibility.

a. Tip-type and base-type growth modes. Two different carbon nanofiber growth modes have been observed: (1) base-type [Fig. 8(a)], in which the catalyst particle remains on the substrate, and (2) tip-type [Fig. 8(b)], in which the catalyst is detached from the substrate and remains at the tip of the growing nanostructure. Baker *et al.* proposed that the growth mode depends on the interaction of the catalyst with its support.[3] Such interaction is believed to be related to wetting, which can be characterized by the contact angle of the catalyst with the support surface at a given growth temperature. A large angle corresponds to weak interaction, while a small angle is indicative of strong interaction. The strength of interaction must depend on the choice of catalyst materials

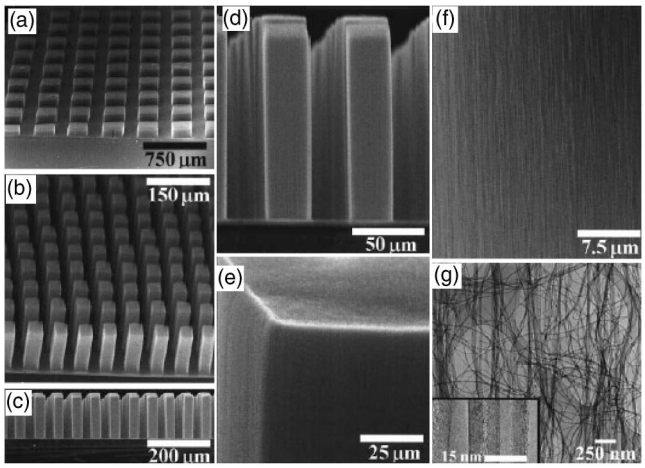

FIG. 9. Vertically aligned towers of dense nanotubes. Reprinted with permission from Ref. 60. Copyright 1999 AAAS. Electron micrographs of self-oriented nanotubes synthesized on *n*1-type porous silicon substrates. (a) SEM image of nanotube blocks synthesized on 250×250 mm^2 catalyst patterns. The nanotubes are 80 mm long and oriented perpendicular to the substrate [see (f)]. (b) SEM image of nanotube towers synthesized on 38×38 mm^2 catalyst patterns. The nanotubes are 130 mm long. (c) Side view of the nanotube towers in (b). The nanotubes self-assemble such that the edges of the towers are perfectly perpendicular to the substrate. (d) Nanotube "twin towers" a zoom-in view of (c). (e) SEM image showing sharp edges and corners at the top of a nanotube tower. (f) SEM image showing that nanotubes in a block are well aligned to the direction perpendicular to the substrate surface. (g) TEM image of pure multiwalled nanotubes in several nanotube blocks grown on an *n*1-type porous silicon substrate. Even after ultrasonication for 15 min in 1,2-dichloroethane, the aligned and bundled configuration of the nanotubes is still evident. The inset is a high-resolution TEM image that shows two nanotubes bundling together. The well-ordered graphitic lattice fringes of both nanotubes are resolved.

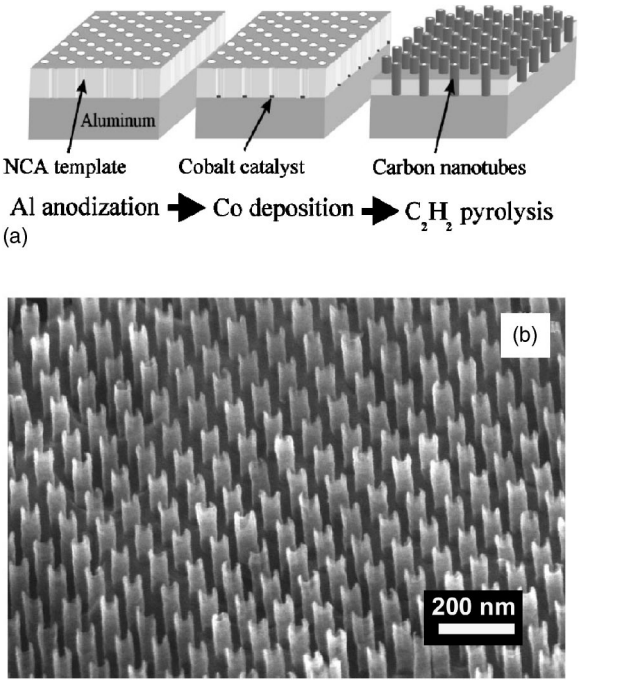

FIG. 10. Vertical alignment using a porous template. Adopted with permission from Ref. 65. (a) Schematic of fabrication process. (b) SEM image of the resulting hexagonally ordered array of carbon nanotubes fabricated using the method in (a).

and substrates. For example, it it has been reported that Ni on SiO_2 has a large contact angle at 700 °C and thus tip growth is favored in this system.[59] In experiments where Co or Fe were deposited on Si,[60–62] base-type growth was observed. However, the choice of materials does not completely control the growth mode. The kinetics of the growth process has a very strong influence as well. For example, using the same materials (Ni on a thin Ti layer deposited on Si), growth by PECVD (plasma) produces tip-type fibers, while growth by CVD (no plasma) produces base-type fibers. The PECVD process itself has a very large parameter space, and it is possible to choose growth parameters in such a way as to produce base-type or tip-type fibers for the same catalyst-substrate pair, depending on growth conditions.[22,63] We discuss this aspect further in a section devoted to the C-PECVD process.

b. Vertical alignment. Vertical alignment conventionally means that nanostructures are oriented perpendicular to the substrate. A variety of methods for production of aligned arrays of carbon nanostructures in C-CVD has been demonstrated and is reviewed, for example, in Ref. 17. Most frequently found in the literature are nanotubes or nanofibers grown in a very dense arrangement with alignment due to the crowding effect. Fan *et al.* used porous silicon substrates with a catalyst patterned by electron-beam evaporation through shadow masks to produce nanotube blocks that grew perpendicular to the substrate.[60] The high density of nanotubes within each block confined the nearest neighbors and attracted the outermost nanotubes to their neighbors via van der Waals forces, thereby producing oriented growth (Fig. 9). In addition, as described in a model by Li *et al.*, the nanotubes that initially grow in a direction that is not normal to the substrate eventually encounter their nearest neighbors and either stop growth or change the growth direction and become aligned.[64]

Another method of aligned growth of nanotubes is to use a nanoporous template. In this method, porous alumina produced in an aluminum anodization process is used as a template for nanotube growth. The anodic alumina has a porous structure with nanopores (30–50 nm) self-organized in a hexagonal pattern. Catalyst is electrodeposited into the nanopores and then nanotubes are synthesized by C-CVD. The porous template may be etched away after nanotube synthesis. An array of aligned nanotubes prepared using this fabrication process is shown in Fig. 10.[65]

C. Catalytic plasma-enhanced chemical-vapor deposition

1. Introduction to PECVD

Plasma-enhanced chemical-vapor deposition (PECVD) is similar to chemical-vapor deposition (CVD) which also uses gaseous sources. (See Ref. 66 for a review.) The important difference is that in CVD thermal energy is used to activate the gas, whereas in PECVD the molecules are activated by electron impact. The gas activation takes place in a nonequilibrium plasma, generally referred to as a glow discharge. As in the case of C-CVD, the growth of carbon nanofibers occurs through a catalyst (not by direct surface deposition). The main purpose of using plasma enhancement is to reduce the activation energy for a deposition process.

Thus, the first step in the proposed growth model described in Sec. II B 2, namely, decomposition of carbonaceous species on the surface of a catalyst, should benefit from plasma assistance. However, it is not clear how the next step, diffusion through the catalyst, would be facilitated by plasma excitation. In a recent review, Meyyappan *et al.* questioned whether plasma-enhanced CVD provides any facilitation of the growth process at all compared to thermal CVD in catalytically controlled processes.[13] They pointed out that in most of the reported PECVD growth the temperature was as high as in the thermal CVD growth, indicating the absence of apparent benefits. It has been recognized, however, that one of the most important and unexpected benefits of PECVD growth is the alignment of nanofibers due to interaction with the electric field.[24]

However, exploration of PECVD's potential for growth temperature reduction is far from over. For many applications low substrate temperature growth of carbon nanostructures is highly desirable. For example, integration with standard semiconductor integrated circuit technology requires reduced fiber-growth temperature and time, since metal contacts to shallow diffusion regions of the substrate can only withstand temperatures up to 450 °C for a limited time without significant degradation of electronic performance. Similarly, for field-emission display production the growth temperature must be lower than the soda lime glass substrate melting temperature of 500 °C. Recently, there have been several reports of growth at temperatures as low as room temperature.[67–70] It must be noted that Boscovic *et al.* proposed that a radio frequency (rf) field could selectively heat the catalyst particle while the substrate temperature remains low. If true, this speculation could be one of the most important revelations in the effort to allow a lower substrate temperature during nanofiber growth. All the evidences indicate that the growth of carbon nanotubes and nanofibers *requires* a catalyst particle temperature high enough to provide a high carbon diffusion rate. However, there seems to be no such requirement for the substrate temperature, as long as growth occurs at the tip. It has been demonstrated that small metal particles can be heated in high-frequency fields,[71] and magnetic particles have additional mechanisms for high-frequency field heating.[72] This brings to attention the unexploited potential of PECVD synthesis and the opportunity for further exploration. Certainly caution must be taken in measurements of the growth temperature in PECVD experiments. Power transfer to the substrate from the generated electromagnetic field via the plasma, or simply by resistive heating by induced current, in addition to dedicated temperature control of the substrate holder (or its absence), can be very significant. Plasma heating effects in the case of a dc system have been investigated by Teo *et al.*[73]

In order to understand the mechanisms involved in carbon nanofiber formation in a PECVD reactor, we briefly review some basic processes that occur in plasmas. In the simplest case of a dc diode-type reactor, a dc voltage is applied across a space filled with a low-pressure gas (a few torrs). The glow discharge that is initiated can be divided into four visible regions arranged from cathode to anode: (1) cathode dark space, (2) negative glow, (3) Faraday dark space, and (4) positive column. The positive column region is not used in PECVD processes. The dc discharge is maintained by the processes at the cathode and in the dark space. The ions are accelerated by the applied voltage and some of them bombard the cathode. This impact generates secondary electrons that accelerate away from the cathode. The collisions excite molecules and energetic electrons ionize some of them. The negative glow is the result of this excitation process. The thickness of the dark space is related to the electron mean free path.[74] The current in the dark space is carried primarily by ions, while in the negative glow it is carried by electrons. Thus, the negative glow is a low impedance region and the applied voltage drops mostly over the dark space. Since the dark space varies from a few hundred micrometers to a few millimeters, application of several hundred volts can create electric fields on the order of 10^4 V/cm.

2. C-PECVD experimental systems and results

A PECVD system consists of a vacuum chamber, vacuum pumps, and a pressure control system; a gas flow control system that includes gas manifolds, mass flow controllers, and a showerhead for uniform gas mixing and distribution over the substrate; one or two power supplies for plasma excitation with corresponding power coupling systems; and a substrate heater with a temperature control system. A variety of plasma sources, successfully used for the deposition of dielectric thin films for semiconductor circuits[75] and carbon-based thin films,[76] has been utilized for CNT and CNF growth. These sources include direct-current (dc PECVD), hot-filament dc (HF-dc PECVD), magnetron-type radio frequency (rf PECVD), inductively coupled plasma (ICP PECVD), microwave (M-PECVD), electron cyclotron resonance (ECR PECVD), hollow cathode (HCGD), and corona discharge plasma. Examples of different systems, growth conditions, and results are summarized in Table I.

a. Direct-current plasma-enhanced chemical-vapor deposition. In the case of a direct-current PECVD system, the substrate is placed on a substrate heater that serves also as a cathode (Fig. 11), making it crucial that the substrate is electrically conductive.[9,24,59,77–82] If growth on insulating substrates is desired, a thin metal film may be deposited under the catalyst film to establish contact between the cathode and the metal surface. The gas showerhead, used to produce a uniform gas flow distribution over the entire substrate surface, also serves as the anode.

Preparation of the growth catalyst is essential to the production of isolated VACNFs. Many different catalyst preparations can be found in the literature that include physical vapor deposition (evaporation or sputtering), electro- and electroless plating, and preparing nanoparticles from solution, etc.[83] For example, to synthesize isolated VACNFs patterned nickel (Ni) catalyst dots 100 nm in diameter and 40 nm thick can be prepared on Si substrates using conventional electron-beam lithography.[9] A 10-nm-thick Ti layer is deposited between the Ni catalyst and the Si substrate to prevent nickel silicide formation at the moderately high growth temperature of 700 °C. Following the preparation of the catalyst, the sample is mounted directly onto a heated cathode [Fig. 12(a)]. The vacuum chamber is evacuated be-

TABLE I. PECVD growth conditions.

Type of plasma system	Frequency	Catalyst/ substrate	Growth conditions: *F*-gas flow (SCCM)[a], *P*-pressure (Torr), *E*-power (W), *T*-temperature (°C), *U*-substrate bias (V)	Results	References
dc HF					8
dc	0 Hz			VACNF	121
Microwave	2.45 GHz		$F_{methane}=10-20$, $F_{hydrogen}=80-90$ $P=1.8-2.2$ $E=500$ $U=250$ $T=650$	Nanofibers	112
Microwave	2.45 GHz	Ni(30–40 nm)/Si	$F[(2\%)CH_4/(98\%)H_2]=$undefined $P=0.3$ $E=$undefined $T=900-1000$	Nanofibers (nonaligned)	99
Microwave	2.45 GHz	Co	$F_{total}=200$, $F_{acetylene}/F_{ammonia}=10\%-30\%$ $P=20$ $E=1000$ $T=825$	Dense forests of VACNF	61 and 102
ICP (dual power supplies)	13.56 MHz		$F_{ethylene\ in\ H2(20\%)}=100$ $P=3$ $E_{ICP}=100$, $E_{capacitive}=150$ $T=900$	MWCNF	22
ICP (dual power supply)	13.56 MHz	Ni	$F_{acetylene}=20-50$, $F_{hyrdogen}=30-150$ $P=5\times10^{-2}$ $E=1000$ $T=700$	VACNF	98
Corona discharge	ac (not specified)	Co AAO			117

[a]Denotes standard cubic centimeter per minute.

fore growth to an acceptable base pressure (e.g., 1×10^{-5} Torr). After reaching the base pressure, ammonia (NH_3) is introduced into the chamber, and the sample is pretreated with the NH_3 plasma and temperature. As a result of this treatment, discrete catalyst nanoparticles are formed from the deposited catalyst dots [Fig. 12(b)]. For Ni catalyst dots with the diameter and thickness mentioned above, only a single nanoparticle is formed from each catalyst dot. These

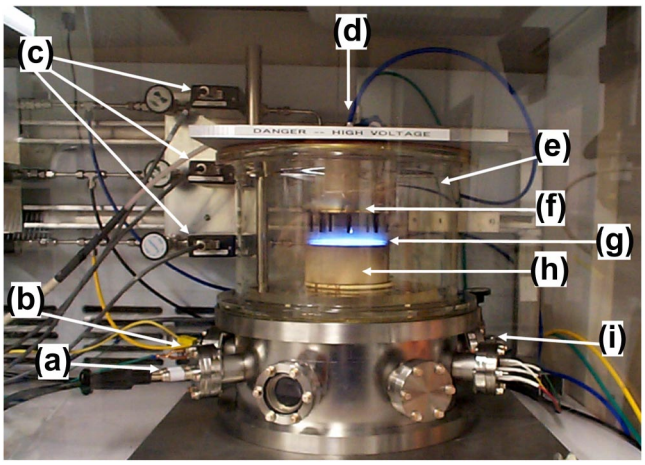

FIG. 11. (Color online) dc PECVD reactor for the growth of vertically aligned carbon nanofibers. (a) High current heater wiring; (b) thermocouple wiring; (c) mass flow controllers for acetylene, ammonia, and other gases (e.g., H_2); (d) gas inlet; (e) glass cylinder vacuum chamber; (f) gas showerhead and anode; (g) cathode glow of acetylene/ammonia plasma above a 100-mm diam Si wafer; (h) substrate heater and cathode; and (i) pressure transducer.

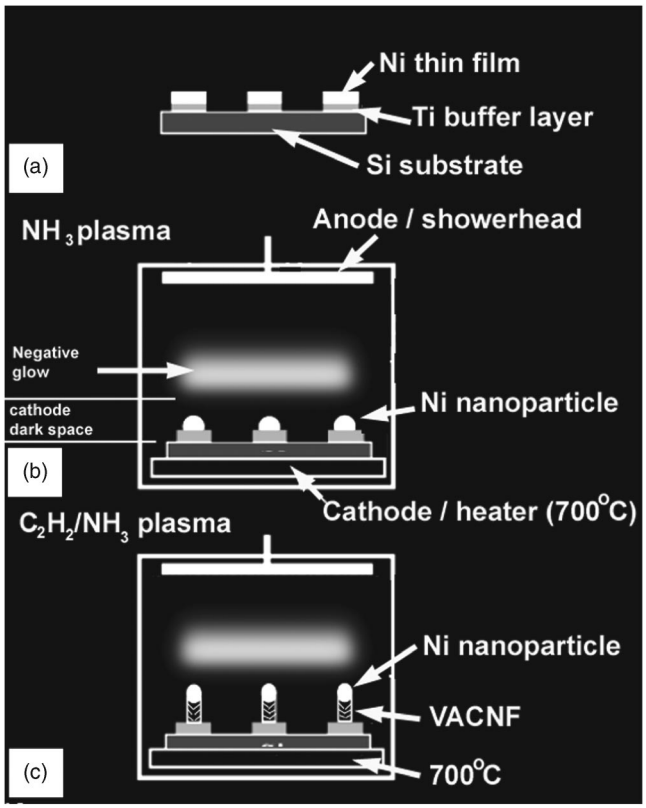

FIG. 12. Schematic representation of the PECVD process for growing vertically aligned carbon nanofibers. (a) Catalyst deposition, (b) catalyst pretreatment/nanoparticle formation, and (c) growth of carbon nanofibers.

nanoparticles act as the necessary seeds for the catalytic growth of isolated VACNFs. After the pretreatment step, acetylene (C_2H_2) is introduced into the chamber while maintaining the NH_3 plasma, immediately initiating the growth of the VACNF [Fig. 12(c)]. The VACNF tip diameter is approximately equal to that of the nanoparticle. The *initial* diameter of the nanoparticles, d, is roughly determined from mass conservation of the catalyst, that is, $1/6\pi d^3 = 1/4\pi D^2 t$ or $d=(3/2tD^2)^{1/3}$, where D is the diameter of the catalyst dot and t is its thickness. However, it has been observed that d decreases as the growth proceeds.[30] The NH_3 gas flow in Merkulov's experiments was maintained at a constant level of 80 SCCM (standard cubic centimeter per minute), and the C_2H_2 gas flow was varied to produce different gas mixtures. The total gas pressure during growth was maintained at 3 Torr. Typical scanning electron microscope (SEM) and TEM images of the resulting nanofibers are shown in Figs. 2, 4, and 5.

dc PECVD growth reactors possess a number of limitations when used in the growth of carbon nanostructures. The requirement that the substrate be electrically conductive in order to maintain a glow discharge limits the choice of substrate materials. One way around this obstacle is to deposit a layer of metal that, if undesired, can be etched away after the growth.[84] Alternatively, a radio frequency (rf) plasma system, in which the polarity of the electrodes changes fast enough to avoid surface charging, can be used. Also, in dc PECVD the power delivered into the plasma and the substrate bias are inextricably coupled, which limits the process control. One solution to this was offered by Cruden *et al.*, involving the introduction of graphite spacers into the electrode to vary the power input to the reactor while holding the voltage constant.[85] Plasma instability is another drawback of a dc discharge. Nonuniformity of the substrate surface may cause the formation of so-called "hot spots" and localized power dissipation through arcs instead of the glow discharge. The stability of the plasma depends on the substrate surface and the output of secondary electrons forms the substrate. The latter is obviously dependent on the substrate material and the condition of the substrate surface.

b. Hot-filament direct-current PECVD systems. PECVD growth of carbon nanofibers was first done in a HF-dc PECVD reactor in 1997 by Chen *et al.*[7,86] Their work was followed by the more well-known work of Ren *et al.*[8] who also used a hot-filament PECVD reactor. In HF-dc PECVD, which is commonly used for diamondlike carbon production, a filament is needed for the activation and decomposition of hydrogen gas into atomic hydrogen.[87] Recently, Hash *et al.* modeled processes in a HF-dc PECVD reactor[88,89] and showed that introducing a tungsten filament in the dc plasma produced a negligible influence on the system characteristics.[88] Cruden *et al.* demonstrated that the filament wire is important in the pretreatment of the substrate, but has a minor impact on the resulting nanofibers when combined with a dc plasma.[85]

HF-dc PECVD, as in the case of dc PECVD without a hot filament, allows synthesis of freestanding vertically aligned carbon nanofibers[10] if sufficiently small diameter catalyst patterns are prepared on the substrate. This type of reactor has been used to study different aspects of carbon nanofiber synthesis such as dependence on growth parameters (pressure, plasma power, gas composition, etc.), electron field-emission properties of the resulting material,[90] orientation of alignment control,[91] and effects of different buffer layers between the catalyst and the substrate.[92]

c. Radio-frequency (capacitively coupled) PECVD. Direct-current reactors have many drawbacks that include plasma instability and limitations on the choice of substrate material. In fact, for these reasons, the semiconductor industry has moved away from dc PECVD reactors and toward higher-frequency plasmas. There are many commercially available rf reactors suitable for carbon nanofiber growth. Most of these reactors have a radio-frequency source coupled to the plasma via a parallel-plate capacitor with the substrate placed on one of the electrodes. Boskovic *et al.* used a standard industrial rf (13.56 MHz) PECVD system (Plasma Technology) to produce nonaligned carbon nanofibers on powdered Ni catalyst using methane and hydrogen mixtures.[69] Ho *et al.* used a modified commercial rf PECVD reactor (Plasma quest) to grow, reportedly, carbon nanotubes using acetylene on Ni-coated quartz at 650 °C.[93] The fact that a commercially available system can be used for this purpose means that a custom-made system is not necessary and the growth of carbon nanofibers can be as much as a part of the microfabrication process as, for example, deposition of silicon dioxide or silicon nitride thin films.

Vertically aligned carbon nanofibers similar in structure to the fibers obtained by dc PECVD were produced by Hirata *et al.* using a magnetron-type rf plasma.[94] In their reactor, a magnetic field ($0<B_z<340$ G) was externally imposed parallel to a powered cylindrical rf electrode using solenoid coils. This allowed them to achieve lower plasma sheath voltages and higher plasma densities. In this work the authors studied the influence of a dc self-bias, V_{dc}, on the alignment of nanofibers, which in this case can be changed independently of other plasma parameters. Poor alignment was observed at V_{dc} as low as −180 V, fairly good alignment was observed at −235 V, and the nanofibers were damaged due to sputtering at $V_{dc}=-570$ V. These voltages were estimated to correspond to electric-field strengths at the nanofiber of 63, 68, and 86 mV/μm, respectively.

Ikuno *et al.* used a dual power supply rf system in which one power supply drove one electrode to maintain the plasma, while the other rf power supply was used to control the substrate bias.[95] This system configuration is commonly used to control film stress in Si_3N_4 PECVD processes. Similar to the configuration used by Hirata *et al.*, it offers control of the plasma power independently of the bias.

d. Radio-frequency inductively coupled PECVD. Relatively high-density plasmas can be achieved in ICP reactors. ICP sources are attractive because they are fairly simple in construction (no external magnets) and have been demonstrated to be applicable to large-area processing (>300 mm),[96] which is desirable for large scale manufacturing. In such a system a coil is connected to the rf power source as a part of a high Q network. Resonance currents circulating through the coil produce an alternating magnetic

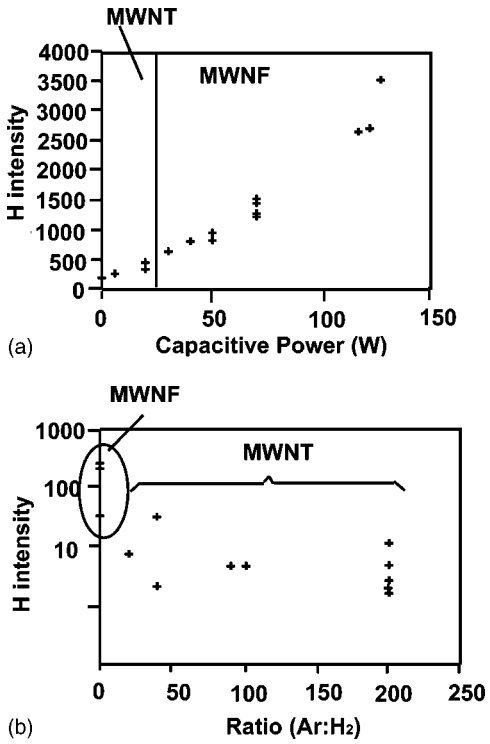

FIG. 13. Atomic hydrogen intensity from emission spectroscopy. (a) Variation with substrate power and (b) effect of argon dilution. Adopted with permission from Ref. 22.

field that induces electron currents in the plasma. Practical ICP sources usually utilize a combination of capacitive and inductive couplings.

Delzeit *et al.* used an ICP system for the growth of carbon nanofibers and carbon nanotubes.[22] They found that it is possible to produce either MWCNTs or nanofibers depending on the growth conditions. It was determined that the regimes producing the nanofibers coincide with the availability of large amounts of atomic hydrogen, which is common in hydrocarbon discharges with H_2 as a source gas. They showed that replacing H_2 with Ar favored the production of MWCNTs. Emission spectroscopy was used to explore the intensity of atomic hydrogen emission during the growth runs. These data are plotted in Fig. 13 and provide an interesting correlation to the observed transition. The growth of nanotubes is accompanied by a low intensity peak of atomic hydrogen. As the hydrogen emission intensity increases, nanofibers are obtained. The observation is consistent with the analysis of Nolan *et al.*[97] These observations are also supported by a simple zero-dimensional (0D) model[88,89] that suggests that the discharge produces large amounts of atomic hydrogen along with a variety of C_xH_y radicals. Stable species such as CH_4, C_2H_2, C_2H_4, etc., account for about 5% in a 20:80 CH_3/H_2 discharge at 3 Torr.

Caughman *et al.* synthesized arrays of freestanding VACNFs using an ICP system.[98] Their reactor operated at a much lower total pressure—approximately 50 mTorr—compared to other methods. They note that low-pressure operation is potentially advantageous because of the improvement in plasma uniformity as the pressure is decreased. In this PECVD system, the ICP source was operated at 13.56 MHz. The source coil consisted of a 15-cm-diameter flat spiral coil (6 turn) separated from the chamber vacuum by a 20-cm-diameter, 2.5-cm-thick fused-quartz window. The chamber was made from stainless steel and was 30 cm in diameter. A 4.4-cm-diameter substrate heater, equipped with rf biasing at 13.56 MHz, was located 20 cm below the window. Typical rf-induced self-biases of −50 to −200 V were used during growth.

Honda *et al.* used an ICP reactor to grow vertically aligned carbon nanofibers at 500 °C using CH_4 as the sole source gas.[67] They found that dc bias is essential for growth and possibly plays a critical role in the etching of carbon deposits. This work also explored a variety of growth temperatures lower than those typically used to grow VACNF. The nanofibers obtained at 500 °C displayed a herringbone-type structure. When the temperature was reduced to 400 °C no crystalline structure was observed in the nanofibers and their alignment deteriorated.

Lee *et al.* produced crystalline VACNFs at temperatures as low as 200 °C using ICP-CVD with a mixture of CH_4 and H_2 as the source gases.[68] The crystallinity of the VACNFs was measured by TEM, electron difraction, and Raman spectroscopy. In the latter technique, the intensity ratio of the *G* (1590 cm^{-1}) and *D* (1350 cm^{-1}) bands, attributed to CNFs and carbonaceous particles, respectively, was observed to change as a function of the hydrogen-to-methane volume ratios. The intensity of the *D* band, often referred to as the defect or disorder band, decreased with increasing hydrogen-to-methane volume ratio. The intensity of the *G* band displayed a maximum around the ratio of 30%. These results indicate that carbonaceous particles are etched by increased hydrogen dosing. However, upon excessive hydrogen dosing, not only the carbonaceous particles but also the CNFs were damaged, resulting in highly defective structures.

e. Microwave PECVD. In the high-frequency fields used in microwave discharges (typically 2.45 GHz) the plasma takes on the character of a free-electron gas. This leads to an increase in the density of high-energy electrons and increases the chemical activation efficiency of gases with high dissociation energies (e.g., N_2 and H_2). These types of reactors are frequently used for diamond film synthesis because the efficient dissociation of H_2 produces atomic H that preferencially etches graphitic forms, leaving diamond.

Kuttel *et al.* grew carbon nanofibers on silicon substrates using a microwave plasma under conditions that are normally used for the growth of CVD diamond films.[99] The films were grown on silicon substrates in a tubular geometry system. Except for a slightly increased substrate temperature (see Table I), the growth parameters were standard for CVD of diamond films. For catalyst material, they used both sputter-deposited Ni films on silicon substrates and Fe clusters, formed by reduction of $Fe(NO_3)_3$, in a hydrogen atmosphere at high temperature. The resulting films contained nonaligned 100-μm-long nanofibers 20–60 nm in diameter and onionlike structures (quasispherical particles composed of concentric graphitic shells synthesized and observed by Ugarte.[100] The catalyst remained at the base of the growing structures. The best growth conditions were found on the substrate in a position where the plasma was well above the

sample. At substrate locations more proximal to the plasma, the high concentration of atomic hydrogen etched the growing film. In another early use of M-PECVD, Qin *et al.* obtained entangled bundles of nanotubes.[101] They used an alumina substrate and the catalyst was deposited from a ferric nitrate solution. The nanotubes were grown at 850–900 °C in a mixture of CH_4 and H_2.

The M-PECVD system used by Bower *et al.* consisted of a 2.45-GHz, 5-kW microwave power supply with a rectangular waveguide that is coupled to a 6-in. inner diameter stainless-steel cylindrical growth chamber and a molybdenum substrate stage with a rf graphite heater that allows control of the substrate temperature independent of the plasma power.[61,102] Dense forests of carbon nanostructures were synthesized using this technique. The nanotube orientation was influenced by the self-bias potential (estimated to be −10 V) established on the immersed substrate surface in the high-frequency plasma, the field of which is invariably terminated perpendicular to the surface. Bower *et al.* claimed that electrostatic force alone would force these one-dimensional tubular structures to align with the field direction, the energetically most favorable orientation. The difference in alignment during PECVD and CVD was also observed in this work.[102]

Many other groups have used this type of growth system for the synthesis of carbon nanostructures.[101,103–110] Even though towers of nanofibers and nanotubes vertically aligned by crowding and van der Waals force have been produced,[61,102,106,111] to date the growth of individual free-standing nanostructures (i.e., single tubes or fibers) has not been demonstrated by microwave discharge. Tip-type herringbone-structured nanofibers were synthesized by Okai *et al.* utilizing M-PECVD.[112] They used a quartz reactor with flowing methane and hydrogen gases. A voltage of −250 V was applied to the substrates during the growth. Unfortunately alignment characteristics were not reported in this work. The nanofibers M-PECVD-synthesized by Cui *et al.* had a bamboo-type structure.[106]

Other studies of M-PECVD growth of carbon nanostructures include measurements of chemical species by *in situ* optical emission spectroscopy (OES) and quadruple mass spectroscopy (MS),[104] the effect of substrate bias,[105] and the influence of catalyst choice (among Fe, Ni, and Co).[111]

f. Electron cyclotron resonance. The main distinguishing characteristic of electron cyclotron resonance (ECR) sources is their ability to produce higher fluxes of low-energy ions than other sources. The ratio of ions to neutrals is much higher for ECR-PECVD than for other types of PECVD.

Lin *et al.* synthesized VACNFs using ECR-CVD producing various bamboo and herringbone structures, and conducted a comparative study of different catalysts (Fe, Ni, and Co) and of different gas mixtures (CH_4/H_2 and CH_4/N_2).[113] They also compared M-PECVD and ECR-CVD. They found that a nitrogen-containing mixture was more effective in the production of bamboolike nanofibers, suggesting that bombardment with nitrogen ions provides a more efficient sputtering agent that keeps the catalyst surface active.

g. Hollow cathode PECVD. A hollow cathode glow discharge (HCGD) is another version of a dc source in which a cathode is shaped in the form of a cylinder so that the secondary electrons are self-contained in the negative glow. The plasma densities are one to two orders of magnitude higher than in a diode discharge.[114] A hollow cathode system was used by Huczko *et al.* for synthesis of a dense forest of vertically aligned carbon nanofibers[115] by decomposition of $Fe(C_5H_5)_2$ in He at 200 °C (determined from optical emission spectrum). In their experiments the substrate [anodic aluminum oxide AAO] was not biased and was placed inside the cathode both perpendicular and parallel to the cathode axis. They report that the nanofibers were arranged in bundles with apparent Fe particles at the tips and were not in registry with AAO pores. However, the alignment mechanism was not suggested by the authors. It is worth noting that their spectroscopic analysis of the generated plasma revealed that the strongest emission peaks were those generated by C_2 and CH radicals. They went on to speculate that the C_2 radicals constitute the key intermediate phase in nanofiber formation, referring to molecular-dynamics simulations by Xia *et al.*,[116] in which C_2 species were suggested to be responsible for the formation of open-ended nanotubes in the absence of catalyst. Consequently, Huczko *et al.* concluded that the plasma-generated C_2 species, together with the catalytic Fe, produce nanofibers at a fairly low "effective" temperature of 200 °C.

h. Corona discharge. Li *et al.* used a corona discharge plasma combined with template-controlled growth to produce aligned carbon nanotubes at atmospheric pressure and temperatures below 200 °C.[117] However, it has to be noted that the reported temperature is the temperature of the gas estimated from the measurement of the temperature of the outer walls of the reactor. In order to explain the successful growth at such a low temperature the authors note that nonequilibrium plasmas, such as corona discharges, are characterized by high electron energy and low gas temperature, and the energetic electrons usually can decompose molecules to reactive species without additional heat energy. The corona discharge plasma reactor used in these experiments consisted of a quartz tube and two axially centered electrodes—a tungsten wire electrode and lower circular plate stainless-steel electrode.[118]

3. C-PECVD specific aspects of carbon nanostructure growth control

a. Basic processes at the catalyst particle in a dc plasma environment. So far the majority of the works on the growth and applications of vertically aligned carbon nanofibers were done using dc and HF-dc systems. As the simplest of the PECVD reactors, the dc systems can be used to understand most of the fundamental processes involved in C-PECVD growth of carbon nanofibers. For clarity of discussion in this section we focus on dc discharges.

Developing control over catalytically grown nanostructures can only be achieved through a detailed understanding of the behavior of the catalyst nanoparticle. Figure 14 presents a very simplified schematic of the processes that occur in this fascinating nanoscale environment. Many of these processes are present in thermal CVD, namely, arrival of excited species to the surface (A), catalytic dissociation (B), departure of undissociated molecules (C), solution of carbon

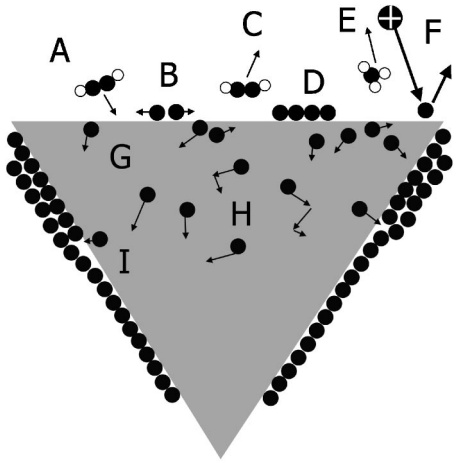

FIG. 14. Processes at the nanoparticle in a PECVD environment.

into the catalyst particle (G), formation of carbon film on the surface (D), diffusion of carbon through or around the catalyst particle (H), and incorporation of carbon atoms into a growing graphene layer (I). PECVD introduces a few additional processes due to application of electrical field and partial ionization of the gas, such as sputtering due to ion bombardment (F), chemical etching (E), and mechanical force due to interaction of a conducting cylinder with high electric field. In fact, the coupling of the latter to the rates of carbon incorporation into graphene layers around the particle, via stress distribution, is believed to be the mechanism of vertical alignment.[24]

b. Growth-parameter space. Compared to thermal CVD, plasma excitation provides an additional level of control while simultaneously introducing an additional level of process complexity. Unlike TCVD reactors in which temperature, total gas pressure, and flow govern the nanostructure growth process, in the PECVD process, parameters specific to the glow discharge must be considered. The voltage, current, power, and resultant field distributions within the discharge all play a critical role in shaping the outcome of the growth process. It is important to note that plasma is usually used for both the deposition of thin conformal films and for etching, depending on the choice of conditions. Counter intuitively, in order to "deposit" carbon nanostructures a PECVD reactor must be operated in the etching, rather than deposition, regime to avoid thin-film formation. Special consideration must be given to finding the balance between etching and deposition to prevent detrimental formation of carbon films and at the same time avoid damage to the sidewalls of growing nanofibers.[119]

The C-PECVD process involves a host of parameters variable over a multidimensional space, leading to extraordinary changes in the structure and morphology of the resultant carbon deposit, from amorphous carbon films to nanofibers and nanotubes. The parameters that constitute this multidimensional parameter space include (1) total pressure (P), (2) total gas flow (F), (3) carbon source to etchant gas flow ratio (e.g., C_2H_2/NH_3) (R), (4) substrate temperature (T), and (5) plasma power [current (I) and voltage (U)]. A slice of the phase diagram along the T-R axis, with all other parameters

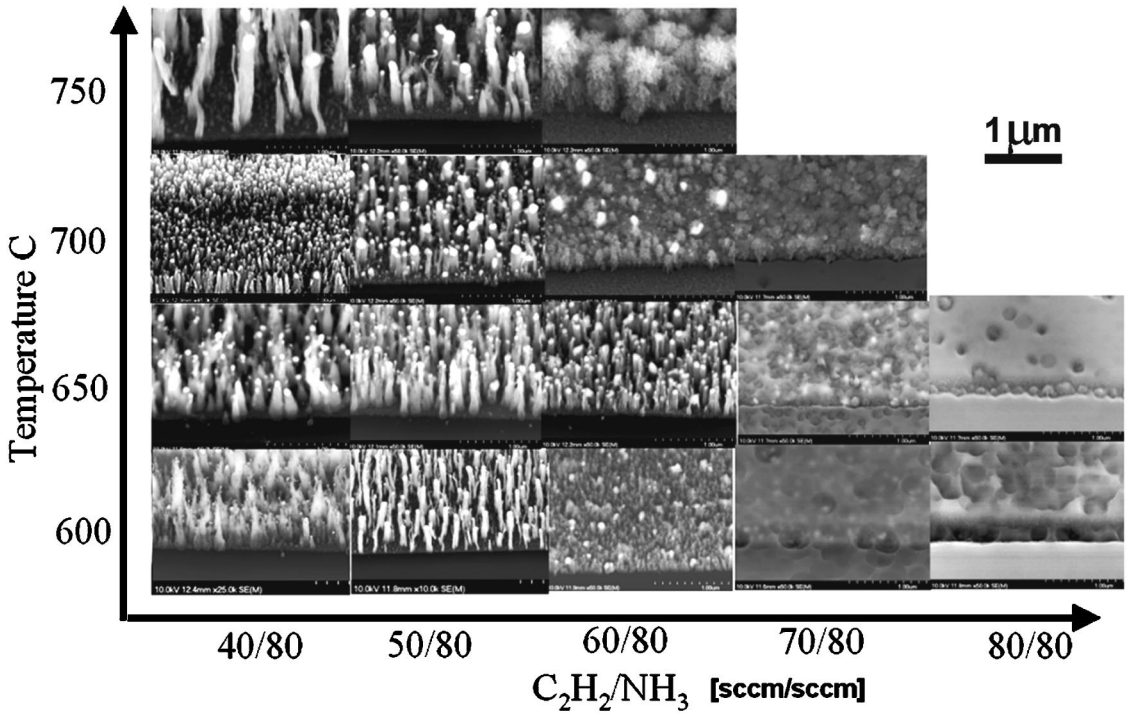

FIG. 15. A slice of growth parameter space. SEM images of VACNFs tiled to illustrate a phase diagram of the VACNF in a T-R slice of the multidimensional parameter space. The other parameters were the same (I=100 mA, P=2 Torr, F_{NH3}=80 SCCM, and growth time=10 min). The substrate was Si, the catalyst was 10 nm of NiFe alloy (50%: 50%) a top of 10 nm Ti buffer layer. The areas of the "good" VACNFs are (T,R) =(750,40/80),(700,50/80),(650,60/80),(600,50/80). The (750,60/80) are peculiar "fluffy" nanofibers. The part of the diagram to the right of the good VACNFs represents the sample coated with a graphitic film that prevented the VACNF growth. The VACNFs on the left [e.g., (600,40/80)] are damaged and contained a considerable amount of nitrogen.

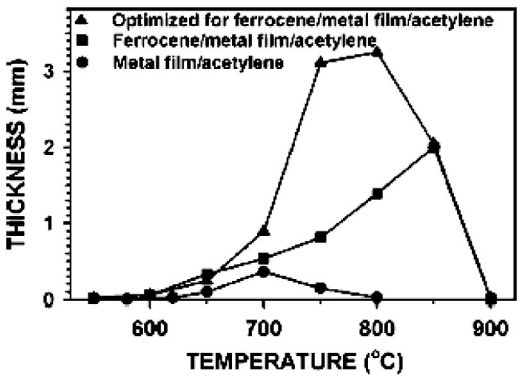

FIG. 16. Temperature dependence of CNT growth rates (film thickness). Adopted with permission from Ref. 46. The solid dots correspond to CVD on the Al/Fe/Mo multilayer film using a 100 SCCM/2.9 SCCM hydrogen/acetylene ratio. The solid squares represent the CVD growth with addition of 4 mg/h of ferrocene. The filled triangles represent the CNT growth for an optimized ratio of 4 mg/h of ferrocene to 12.4 SCCM of acetylene.

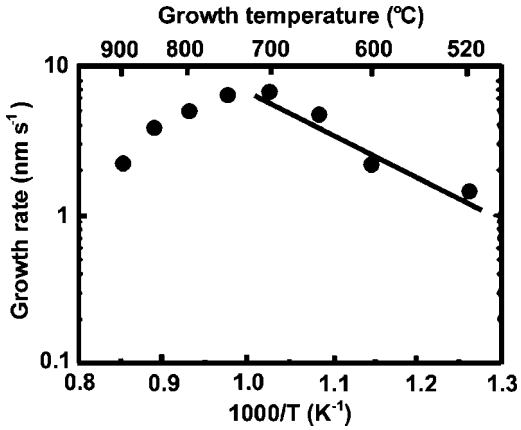

FIG. 17. Average nanofiber length vs inverse deposition temperature after growth at all conditions constant in a dc PECVD process. Adopted with permission from Ref. 59.

kept constant, is presented in Fig. 15. There are specific bounded regions where the resultant material possesses the characteristics of the high-quality VACNFs shown, for example, in Figs. 5 and 6. In general, for a given T, there is a particular range of R values for which favorable growth occurs. At higher R, a graphitic carbon film forms on the substrate and prevents fiber growth. At small values of R the fibers are chemically etched during growth, producing heavily damaged fibers. Taken to an extreme, the fibers can be etched down to the substrate leaving nothing but stublike remnants. At higher plasma power, the regions for which high-quality VACNF growth occurs are shifted toward higher R values.

The selection of the parameters used to perform VACNF growth is dependent upon the combination of catalysts, substrates, carbon source and etchant gases, the presence of a dilution gas, and the catalyst pattern. Several studies were devoted to the discovery of trends and interrelationships between parameters.[59,63,78,120–122] These trends are discussed below.

A typical growth rate versus temperature curves for C-TCVD growth of carbon nanostructures is usually similar to the one displayed in Fig. 16 as solid circles (lower curve).[46] On the low-temperature side, the slope and curvature of the plot can be attributed to a diffusion-limited growth process. The growth rate reduces abruptly on the high-temperature side of the curve, which can be interpreted as a supply-limited growth regime as a consequence of the drastic reduction in the sticking rate of the species impinging onto the catalyst surface. Chhowalla *et al.* have observed similar behavior in dc PECVD growth, as shown in Fig. 17.[59] However, the activation energy of 0.56 eV, determined from the slope in the growth rate versus inverse temperature plot, is significantly lower than the activation energy of C diffusion through Ni of 1.5 eV. This suggests either enhanced diffusion of C through the Ni particle or, as was proposed by Helveg *et al.*,[58] of C along the Ni particle surface. Such low activation energy also suggests the possibility of true room-temperature growth.

The gases used for carbon nanofiber growth from a supported catalyst include carbon monoxide and hydrocarbons, such as acetylene, methane, benzene, etc. However, as described above, if carbon source gases are used alone, carbon films (amorphous or graphitic) are formed and no carbon nanofiber growth occurs. Thus the selection of operating parameters must be made such that etching, rather than deposition, is the dominant process. This is achieved in part by selection of an appropriate etchant gas such as hydrogen or ammonia.

The optimal value of R depends on several operating parameters. Teo *et al.* studied the dependence of amorphous carbon film formation during VACNF growth as a function of acetylene-to-ammonia ratio using Auger electron spectroscopy.[79] The chemical composition of species near the substrate surface, i.e., at the catalyst particle level, depends on the diffusion of active species from the plasma sheath. By changing the operating voltage, the size and shape of the characteristic regions of the plasma can be altered. This is ultimately reflected in the distance that the activated species must diffuse through to reach the catalyst surface. A direct relation between plasma power and R has been established by Merkulov *et al.*[121] In these experiments the gas ratios were adjusted at different current values to obtain identical nanofibers (Fig. 18), showing a linear dependence between R and the discharge current I. This relationship can be used interchangeably to control the composition of species near the substrate surface. It has been reported that different species participate in the PECVD VACNF and CVD CNF growth.[122] Free radicals are involved in PECVD growth while C_2H_2 is the dominant species in CVD processes.

The VACNF growth rate is proportional to the number of radicals impinging on the catalyst surface and to the decomposition rate of these radicals at the surface. (Here, by decomposition we mean a complex process involving adsorption and fragmentation of the radicals at the catalyst surface as well as desorption of the reaction byproducts from the surface.) Different types of radicals are expected to have different decomposition rates. One way to increase the growth rate is to change the gas mixture and plasma power to create more radicals or to shift the radical distribution towards those with higher decomposition rates. Simply in-

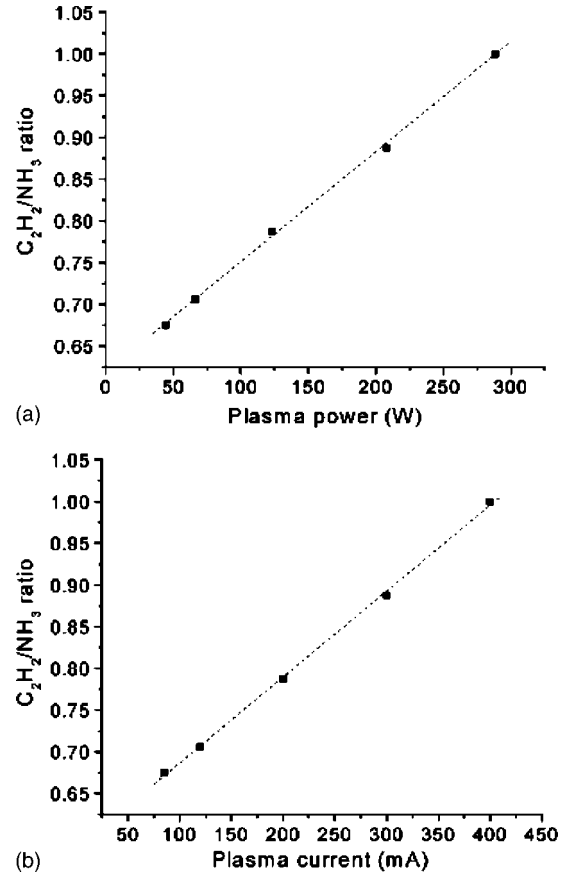

FIG. 18. Relationship between plasma power and gas flow ratio in a dc PECVD process, showing the C_2H_2/NH_3 ratio required to produce a VACNF with similar geometry as a function of (a) plasma power and (b) plasma current. Adopted with permission from Ref. 121. Copyright 2002 American Chemical Society.

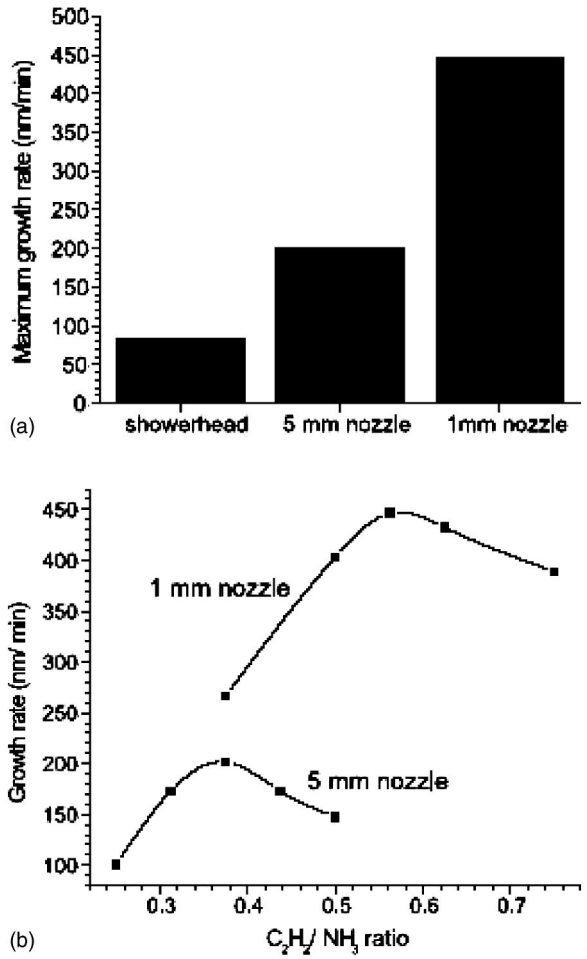

FIG. 19. Influence of gas flow rates on the growth of carbon nanofibers in a dc PECVD process. (a) Maximum VACNF growth rates for different experimental setups and therefore different gas flows to the substrate surface. (b) VACNF growth rate as a function of C_2H_2/NH_3 gas ratio for two nozzle diameters of 1 mm (upper curve) and 5 mm (lower curve). Adopted from Ref. 122 with permission from Elsevier.

creasing the C_2H_2 content increases the growth rate only up to a certain value (still substantially lower than that for thermal CVD), after which the growth rate begins to decrease.[59] Above a critical C_2H_2 content, which depends upon a particular set of experimental conditions such as plasma power, pressure, temperature, etc., more radicals with lower decomposition rates and fewer radicals with higher decomposition rates are produced. Moreover, the radicals with lower decomposition rate may start forming a shell encapsulating the catalyst particle, thereby limiting the carbon supply available for VACNF growth, and may permanently attach to the substrate surface. This results in a reduced growth rate and, if the C_2H_2 content is increased even further, leads to the formation of a thick carbon film covering the entire substrate. This phenomenon has been experimentally observed in several studies.[79,119]

Since some applications may require very long VACNFs, it is highly desirable to develop controllable ways to further increase the growth rate. One way of accomplishing this was explored by Merkulov *et al.* and involved increasing the gas flow directed towards the substrate.[122] This was achieved by replacing the flat showerhead typically used in PECVD reactors with a capillary-type gas nozzle featuring a variable orifice. These experiments were carried out using two different orifice diameters: 1 and 5 mm. Figure 19(a) shows that the maximum growth rates increase significantly as smaller nozzle sizes, generating higher local gas flows, are used. The maximum growth rate for the 1-mm nozzle is more than twice than that for the 5-mm nozzle and about five times higher than that for the showerhead. Another salient point of these experiments is that the gas chemistry, i.e., mutual interactions among the gas species, plays an important role in determining the growth rate. This is demonstrated in Fig. 19(b), which shows the growth rate for the 1- and 5-mm nozzles as a function of the C_2H_2/NH_3 gas ratio. Clearly, the growth rates in both cases depend strongly upon the gas mixture and each exhibits a well-defined maximum. Moreover, the maximum growth rates for the two nozzle sizes correspond to different values of the C_2H_2/NH_3 gas ratio. This probably occurs because orifices with different diameters produce different gas flow velocities, which affects the interaction among the gas species within the flow. This results in modification of the chemical composition of the resultant species that reach the sample surface and consequently changes the growth rate. In addition to empirical approaches to understand how to create the most favorable conditions for the synthesis of a nanofiber, some modeling effort has been applied to this complicated system. Hash *et*

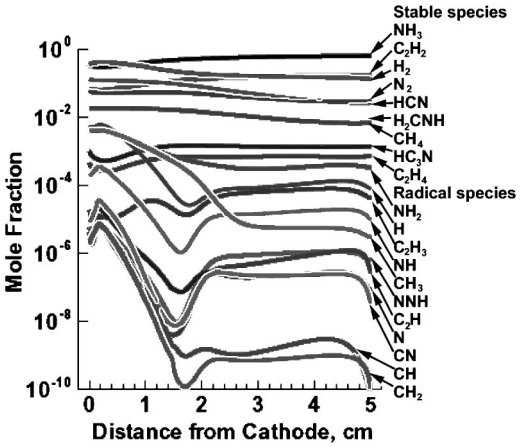

FIG. 20. Simulated distribution of the concentration of various neutral species with distance from the cathode in a dc PECVD system using one-dimensional kinetic model. It is for a 9-Torr, 200-W dc plasma with a 677-V negative bias using 54:200 SCCM C_2H_2:NH_3 with a cathode at 700 °C heated solely by the plasma. Courtesy of D. B. Hash *et al.* See also Ref. 88.

al., in order to understand what species are actually involved in this processes, simulated the growth conditions using a one-dimensional model[88] of hot-filament dc PECVD. Figure 20 shows the concentration of the neutral species along the axis of a dc reactor simulated for an $Ar/C_2H_2/NH_3$ gas mixture without involvement of the filament.

The total pressure is related to the total number of species near the catalyst surface. For the glow discharge there are more excited species involved causing an increase in the deposition rate. This was also demonstrated for dc PECVD by Chhowalla *et al.*, as shown in Fig. 21.[59] This plot represents almost the full range in which a dc glow discharge can be maintained. It is worth noting that at higher pressure, fewer ions reach the surface due to collisions, thus the etching is reduced. This work demonstrates that selecting the proper gas flow ratio is essential for avoiding the deposition of a carbon film which, as discussed above, can deactivate the catalyst and inhibit growth.

c. Tip-type and base-type growth modes. As in C-TCVD, two growth modes have been observed in PECVD (Fig. 22) in which the catalyst particle is located either at the tip of the growing fiber or at its base. It has been suggested that the growth mode depends on the interaction of the catalyst with its supporting substrate.[3,12] However, Melechko *et al.* showed that the kinetics of the growth process also plays a

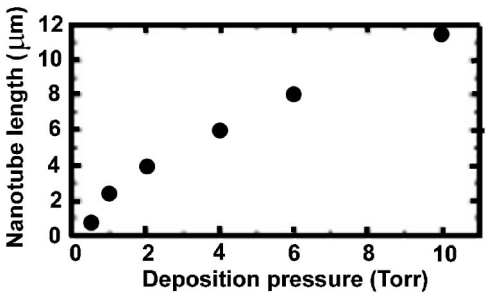

FIG. 21. Dependence of growth rate on total gas pressure in dc PECVD process. Adopted with permission from Ref. 59.

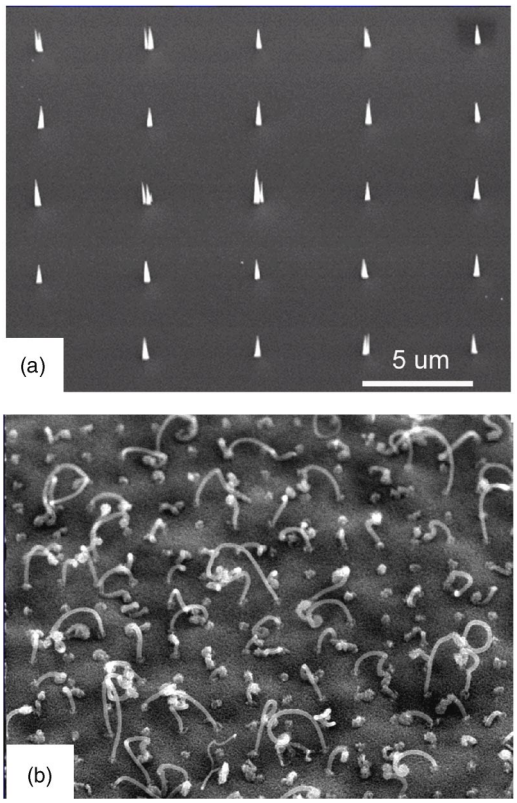

FIG. 22. SEM images of (a) vertical alignment of carbon nanofibers in a tip-type growth mode, and (b) nonaligned growth of base-type carbon nanofibers by dc PECVD process.

role in the selection of the growth mode and it is possible to grow base-type or tip-type fibers on the same substrate and using the same catalyst material by changing the gas flow ratio.[63]

d. Vertical alignment. A direct correlation between the alignment of CNFs and the growth mode (base or tip) has been observed in a PECVD process.[24] In the case of tip-type fiber growth, the catalyst particle undergoes a process where it lifts from the substrate, eventually detaching from it completely. Once this occurs, the particle follows the path of the electric-field lines present in the plasma sheath. This type of growth leads to field alignment irrespective of the density of CNF on the substrate, i.e., without the need for crowding for CNF to grow vertically. In contrast, it has been established that base-type CNFs tend to grow in random orientations unless the density of the fibers is so great that vertical alignment occurs due to crowding or van der Waals forces (Fig. 10).

A model to describe the alignment mechanism of tip-type CNF growth was proposed by Merkulov *et al.* describing the alignment as the result of a feedback mechanism associated with a nonuniform stress (part tensile, part compressive) created across the interface of the catalyst particle with the CNF by the electrostatic forces (Fig. 23).[24] The axis of a CNF growing perpendicular to the substrate coincides with the direction of the applied electrostatic force, resulting in a uniform tensile stress across the entire nanofiber/catalyst particle interface, as shown in Figs. 23(a) and 23(b). Consequently, carbon uniformly precipitates across the interface

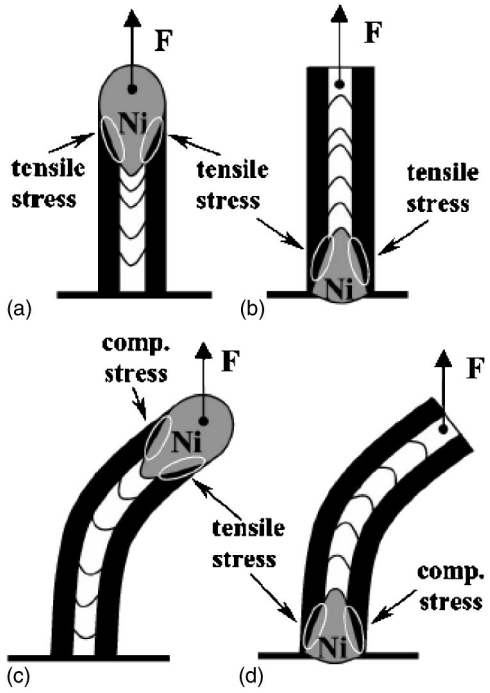

FIG. 23. Alignment mechanism based on stress-dependent growth rate and stress distribution caused by interaction of nanofiber with electric field. Adopted from Ref. 24.

and the fiber continues to grow vertically (perpendicular to the substrate). However, if there were a spatial fluctuation in the carbon precipitation at the interface, CNF growth would deviate from vertical alignment, as shown in Figs. 23(c) and 23(d). In the case of nanofibers growing from the tip (catalyst particle at the tip), the electrostatic force produces a compressive stress at the part of the particle/nanofiber interface where the greater rate of growth is seen [Fig. 23(c)]. Likewise, a tensile stress is produced at the part of the particle/nanofiber interface where the lesser rate of growth is seen. It is proposed that these opposing stresses favor subsequent carbon precipitation at the interface experiencing tensile stress. The net result is a stable, negative feedback that acts to equalize the growth rate around the entire periphery of the particle/nanofiber interface, leading to vertically aligned CNF growth. The difference in the growth rates at the two boundaries may be caused by stress-induced diffusion[123] due to the stress gradient in the catalyst particle and possibly by the variation in the stress-dependent sticking of diffusing C atoms to the C side of the Ni–C interface. In any case, the exact mechanism may be quite complex and a detailed study of the stress-induced C diffusion and precipitation in the C–Ni system is needed. When the catalyst particle is located at the base of the CNF, however, the situation with the preferred location of carbon precipitation is different. Since the nanofiber base is attached to the substrate, the stress created at the particle/nanofiber interface with the greater growth rate is tensile [Fig. 23(d)] and acts to continue the increased growth rate, thus causing the CNF to bend even further.

Understanding the e-field mechanism of tip-type nanofiber alignment allows control of the orientation. Usually in a planar geometry the field is perpendicular to a metallic substrate. However, field direction can be changed by placing the substrate close to the edges of the substrate holder, and this effect was exploited to grow nanofibers at a variety of angles other than perpendicular to the surface (Fig. 24).[124] To distinguish from the alignment by using porous templates or the crowding effect, carbon nanofibers aligned by the e-field present in the plasma sheath of a PECVD system should be called field aligned rather than vertically aligned. However, because the field direction is usually perpendicular to the substrate these nanofibers are referred to as vertically aligned in the current literature, and we often retain this terminology in this review.

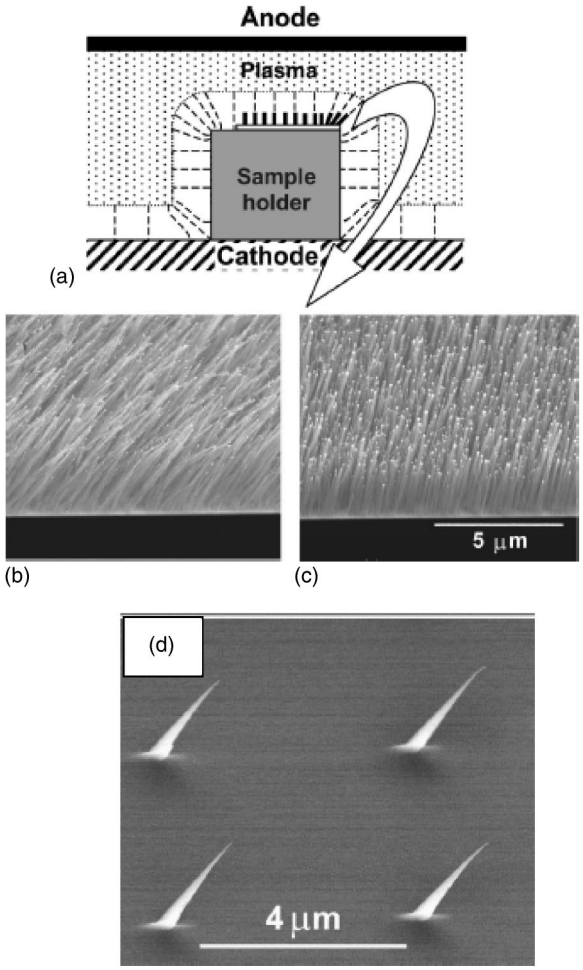

FIG. 24. Control of electric field and alignment direction of carbon nanofibers in a dc PECVD process. (a) A schematic representation of the experimental setup during the PECVD process, in which the substrate is located close to the sample holder edge, and scanning electron microscopy images showing the resultant CNF forests located at (b) 100 and (c) 1000 μm away from the edge and aligned at 38° and 12° angles to the substrate normal, respectively. (d) SEM image taken at a 45° tilt angle of an array of individual CNFs grown in the vicinity (10 μm) of the substrate/the sample holder edge. Adopted from Ref. 124.

D. Substrates and catalysts

1. Substrates

The substrate plays a crucial role in carbon nanostructure synthesis especially in PECVD processes. The substrate not only acts as a medium for support but it also interacts with

the catalyst and growth environment. Silicon and silicon dioxide are two of the most common substrates for obvious reasons of application in silicon-based technology, however, the choice is practically unlimited. There are several issues that have to be considered when choosing a substrate.

In dc-PECVD systems, with the substrate as a cathode, it is necessary to have an electrically conductive surface, so insulating substrates such as SiO_2 must be covered in a metal layer, which can later be removed, as in Ref. 84. Furthermore, substrates also contribute to the radical species in the plasma. During PECVD growth on Si substrates silicon species can be etched, sputtered, and redeposited onto the sidewalls of the fibers, creating an insulating sheath,[125] which may or may not be desirable. To avoid Si incorporation into the fiber walls, a metal overlayer can be used to cover the substrate.

In addition, there has been some concern about depositing Ni catalyst directly onto Si substrates. Several research groups claimed that nickel silicide formation prevents nucleation of the catalyst particles from thin films and inhibits growth.[59,126] Recently, however, Nihei *et al.* proved the opposite by showing that nanotubes can be synthesized directly from nickel silicide.[127] Furthermore, there have been related debates as to whether CNTs prefer Si or SiO_2 surfaces. Some say that CNTs will selectively grow on Si over SiO_2,[128] while others affirm the opposite.[126,129] Due to incompatibilities of substrates with catalyst materials and the growth environment, buffer layers, underlayers, and adhesion layers have come into widespread use. Buffer layers such as Ti, W, and SiO_2 have often been used to prevent diffusion or intermixing of catalyst and substrate, as in the case of nickel silicide mentioned above. The significant effect of underlayer materials on carbon growth is mostly attributed to wetting and particle formation. First of all, it has been shown that multilayered catalysts, i.e., metal underneath and sometimes on top of the catalyst material, drastically influence the CVD carbon nanotube growth. Aluminum, for example, is often put underneath the Ni and Fe catalysts because it promotes the small particle formation needed for CNT growth; in fact, without it no growth is observed.[45,46] The thicknesses of both the underlayer and catalyst are crucial to the success of nanotube growth.[45,130] Christen *et al.* studied the dependence of nanotube growth rates on thicknesses of both the catalyst and overlayer in a trilayer system of Mo/Fe/Al.[131] They used pulsed laser deposition to create orthogonally overlapping metal film gradients of Fe and Mo on top of 10 nm of Al on a Si wafer. In a C-CVD process using $C_2H_2/Ar/H_2$ mixture they achieved growth rates exceeding 17 μm/min for a specific thickness ratio of Fe/Mo that correspond to an atomic ratio of 16:1. In addition, an underlayer can help to "glue" the catalyst to the substrate and act as an adhesion layer for base-type nanotube growth.[45] An extensive list of substrate and underlayer materials, their uses, and references can be found in Table II.[239–245]

2. Catalysts

The growth of carbon nanostructures is catalytically controlled, thus the choice of catalyst plays an imperative role in determining the outcome.[45,132] The catalyst particle is responsible for breaking bonds and adsorbing carbon at its surface, then diffusing carbon through or around an interface where the carbon reforms in graphitic planes.[133] The properties of the catalyst can therefore determine the rate of each of these steps as well as the degree of crystalline perfection and geometric structure of the resulting carbon fiber.

A variety of metals and their alloys are catalysts for the production of carbon nanostructures. A list of all known carbon catalysts, their uses, and references are compiled in Table II. The most commonly used and studied are Fe, Ni, and Co, whose physical properties and solubility with carbon are shown in Table III.[246–248] Included in this list are several binary or multimetal alloys, which have been shown in some cases to provide certain advantages over single-element catalysts for the growth of filamentous carbon.[134] Whereas the trusted transition metals Fe, Ni, and Co are known to be very active in their ability to break and reform carbon–carbon bonds, other noncatalytic metals such as Al or Cu, when combined with a promoter catalyst, can enhance carbon diffusion and reaction rates.[133] In some cases, alloy catalysts have resulted in higher activity,[135] low-temperature growth,[136] and branched nanostructures.[55,135,137–143]

Recently there have been efforts to investigate a battery of catalyst and substrate combinations by high throughput methods. Ng *et al.* came up with an efficient methodology for evaluating underlayer material compatibility with various catalysts for CVD nanotube growth;[144] Cassell *et al.* published a similar approach for exploring nanofiber PECVD growth.[145] In their experiments strips of several different metal contact layers were deposited onto a Si wafer, then the wafer was turned 90° and the strips of different catalysts were deposited on top. This created an underlayer-catalyst grid, which was then used to grow carbon nanostructures either by CVD or PECVD. Ng *et al.* concluded that Ti was the best underlayer in terms of low contact resistance and high growth density, however, Fe–Ni and Ni grew the most vertically organized on an Al underlayer.[144] Cassell *et al.* found that for their growth process Ni catalyst on a Cr underlayer yielded the highest-quality fibers on the basis of growth rate, alignment, and diameter uniformity.[145] It is efforts like these that will lead to rapid development and implementation of the best catalyst and substrate for a given application.

3. Methods of catalyst preparation

There are numerous ways to prepare catalyst particles for CNF growth including physical vapor deposition (PVD), electro- and electroless plating, and coprecipitation methods. The most common approach is to deposit a thin film of catalyst and then sinter it into discrete nanoparticles. In this approach, a thin film is deposited by electroplating, electroless plating, or most commonly by PVD. PVD can be accomplished either by sputtering or evaporating techniques, each of which has its pros and cons. A sputtered atom typically has tens of eV arriving at the substrate surface, in comparison to thermal energies of evaporated films, which are on the order of tens of eV. Thus sputtering leads to better mixing at the interface and adhesion relative to evaporated films. In addition, substrate heating and substrate bias capabilitiy can

TABLE II. Catalysts and substrates.

Catalyst	Underlayer and substrate	Growth method	Carbon structure	References
Al–Fe, Cu–Fe, Fe–Ni–Al	Quartz tube	CVD	CNF, MWCNT	239
Alumina–Ni, Alumina–Ni–Cu	Quartz tube	CVD	CNF, multidirectional	142
Co	Al oxide	Corona discharge PECVD	CNT	117
Co	MgO	CVD	*y*-junction CNF	140
Co	Nanochannel alumina	CVD	CNT, *y*-junction CNT	65 and 240
Co	Si	M-PECVD	CNF	61
Co, Co–Cu alloy	Si	PECVD CVD	VACNF CNF	241
Co, Co–Cu alloy powder	Ceramic boat	CVD	CNF, multidirectional	138
Co, Co–Ni alloy, Fe, Fe–Ni alloy, Ni	Cr, Ir, Ta, Ti, and W on Si	PECVD	VACNF	145
Co, Fe, Fe–Ni alloy, Ni	ITO, Ir, Al, Ti, Ta, and W on Si	CVD	CNT	144
Co, Fe, Ni	Si	M-PECVD	VACNF	111
Co, Fe, Ni	Si	ECR-PECVD	VACNF	113
Co, Ni	SiO_2 on Si	PECVD	VACNF	59
Co, Ni	W wires	PECVD	VACNF	82
Cu–Ni alloy	Quartz tube	CVD	CNF	135
Cu–Ni alloy	SiO_2	CVD	CNF, multidirectional	141
Cu–Ni alloy, Ni powder	Quartz tube	CVD	CNF, multidirectional	133
Cu–Ni, Fe–Ni, Pd–Se alloys	Si	CVD	CNF	136
Fe	Al_2O_3	HCGD	CNF	115
Fe	Alumina	M-PECVD	CNF	101
Fe	Fe foil	CVD	CNF	53
Fe	Mesoporous Si	CVD	VA-MWCNT	42
Fe	Porous Si	CVD	VA-MWCNT	60
Fe	Porous Si	CVD	CNF	62
Fe	Si	CVD	CNF	129
Fe	Si, quartz, ceramic	M-PECVD	CNF	108
Fe	SiC on Si	CVD	CNT	201
Fe	SiO_2	CVD	CNF	129
Fe	SiO_2 on Si	M-PECVD	VACNF	106
Fe	SiO_2 on Si	CVD	CNT	77
Ni	Si	PECVD	VACNF	
Fe, Fe–Ni alloy, Fe–Tb alloy, Ni	Silica, alumina	CVD	CNF, MWCNT	134
Fe, Mo/Fe-layered film	Ir, Al, Nb, and Ti on Si	CVD	SWCNT	130
Fe, Ni	Al on Si, fused quartz, mica, HOPG	CVD	MWCNT	219
Fe, Ni	Si	M-PECVD	CNF	99
Fe–Mo, Mo powder	Alumina	CVD	SWCNT	242
Fe–Ni alloy	Cr, Ti, Ta, and W on Si	HF CVD	CNF	92
Fe–Ni alloy	Si	CVD rf PECVD	CNF VACNF	95
Fe–Ni alloy	SiO_2 on Si	CVD	SWCNT	128
Fe–Ni–Cr, Ni	Si	M-PECVD	CNF	112
Mo/Fe-layered film	Al on Si	ICP PECVD	MWCNT	22

TABLE II. (*Continued.*)

Catalyst	Underlayer and substrate	Growth method	Carbon structure	References
Mo/Fe-layered film	Al on Si	CVD	VA-MWCNT	46
Ni	Al	ICP PECVD	VACNF	68
Ni	Brass, bronze	ICP PECVD	VACNF	154
Ni	Cr on glass	M-PECVD	CNF	104
Ni	Cr on Si	PECVD	VACNF	189
Ni	Cr on SiO_2 on Si	PECVD	VACNF	193
Ni	Glass	PECVD, HF PECVD	VACNF	90
Ni	Glass, Si	HF PECVD	VACNF	8 and 10
Ni	Graphite, Si, plastic	rf PECVD	CNF	69
Ni	$MgAl_2O_4$	CVD	CNF	58
Ni	Ni wafer	PECVD	CNF	86
Ni	Pt crucible	CVD	CNT, CNF	97
Ni		CVD	CNF	50
Ni	Si	PECVD	CNF	126
Ni	Si	CVD PECVD	CNT VACNF	91
Ni	Si	M-PECVD	VACNF ropes	94
Ni	Si	ICP PECVD	VACNF	67
Ni	Si	M-PECVD	MWCNT	109 and 110
Ni	Si	M-PECVD	VACNF ropes	94
Ni	Si, PDMS	CVD	MWCNT	243
Ni	SiO_2 on Si, Cr on polyimide foil	PECVD	VACNF	70
Ni	Ti on Si	PECVD	VACNF	121
Ni	W–Ti alloy and Ti on Si	ICP PECVD	VACNF	98
Ni silicide	Si	PECVD	CNF	127
Pd	Quartz tube	CVD	CNF	231
Pd powder	Quartz tube	CVD	CNF	244
Pt	Si	M-PECVD	Carbon nanostructures	107
Ru	Silica, alumina titania	CVD	CNF multidirectional	245

have a profound effect on the film properties such as crystal structure, orientation, density, and grain size. Choi *et al.* reported on the controlling of the grain size of sputtered Ni films by varying the rf power, which in turn affected the diameter, length, and purity of the CNTs grown from the film.[109] Sputtering also allows for alloy depositions from an alloy target, whereas alloys cannot be directly evaporated accurately due to differences in the vapor pressure of each element. Evaporation does have its advantages, though, mostly attributed to its highly directional deposition, which enables patterns to be easily transferred to the substrate by resist lift-off methods outlined below.

If catalyst patterning is required, it can be done before or after the catalyst film is deposited. Commonly, the pattern is defined beforehand and a lift-off process is employed. First, the resist is applied to the substrate and the desired catalyst pattern is exposed and developed. A PVD method is then used to deposit the catalyst material onto the substrate. Following the deposition, the substrate is immersed in a solvent capable of dissolving the resist, causing the metal to be removed from the remaining resist-covered areas. Conversely, the film can also be patterned following catalyst deposition by coating it with a resist suitable for either photo or e-beam lithography. The pattern is then exposed and developed such that resist remains in the areas where catalyst is desired. The exposed metal is then removed by wet etching,[146] ion-beam sputtering, or reactive ion etching.

In order to grow carbon nanotubes or nanofibers from a thin-film catalyst, the film must first be sintered into islands or discrete nanoparticles.[45] While the sintering temperature is typically well below the bulk melting temperature for the catalyst metal, the reflow of metal indicates that surface diffusion is at work.[147] The formation of catalyst nanodroplets can also be explained by a stress buildup in the film due to

TABLE III. Physical properties of Fe, Ni, and Co. (bcc refers to body-centered-cubic structure, hcp refers to hexagonal close-packed structure, and fcc refers to face-centered-cubic structure.)

Element	Atomic number	Density of solid at 20 °C (g/cm^3)	Melt temp (°C)	Eutectic with carbon (°C)	Crystal structure	Lattice spacing (A)	Electronic configuration
Fe	26	7.87 (Ref. 169)	1538 (Ref. 169)	727 (Ref. 169)	(α) bcc	2.8 665 866 (Ref. 246)	$[Ar]3d^64s^2$
Co	27	8.90 (Ref. 169)	1495 (Ref. 169)	1320 (Ref. 247)	hcp	2.5071 4.0 696 514 4.105 (Ref. 248)	$[Ar]3d^74s^2$
Ni	28	8.91 (Ref. 169)	1455 (Ref. 169)	1326.5 (Ref. 247)	fcc	3.524 540 (Ref. 246)	$[Ar]3d^84s^2$

different expansion coefficients from the substrate.[9] In some cases, though, heat alone is not enough to break up the catalyst film and additional techniques are required. As was mentioned in the substrate section, underlayers are often used to increase surface roughness or wetting capabilities.[45] Nanoparticle creation can also be encouraged by pretreatment of the catalyst film with an etchant gas or ion bombardment in a plasma environment. For example, the research group at Cambridge heats the substrate in H_2 for 15 min at 750 °C (Ref. 59) before initiating PECVD growth. Lee *et al.* found that they could control the diameter of Fe particles for CVD growth by adjusting the condition of ammonia pretreatment.[129] Oak Ridge does a combination of heating in an ammonia environment and then initiating an ammonia plasma for up to 2 min before introducing the carbon source gas.[121] In any case the outcome is the same, the catalyst thin film breaks into nanoparticles, which grow fibers when the carbon source gas is introduced.

The size of the catalyst particles is ultimately determined by the thickness of the film, in addition to the wetting properties of the catalyst and substrate materials as well as the method of catalyst preparation and pretreatment. Since nanotubes are of such small dimensions, the size and uniformity of the nanoparticles become increasingly important. Chhowalla *et al.* and Wei *et al.* reported a direct correlation of Ni nanoparticle size increasing with the thickness of the original film.[59,77] However, Chhowalla *et al.* only observed this phenomenon on SiO_2 substrates and found that the Ni film failed to sinter on clean Si substrates, which they attributed to nickel silicide formation. Cobalt, on the other hand, has been found to wet well on both Si and SiO_2 substrates, showing the same correlation of particle size to original film thickness.[59,61] Bower *et al.* also verified that thinner Co films, leading to smaller particles, determined the diameter and length of the resulting nanotubes.[61] Wei *et al.* found that for Fe films there was a critical thickness over which no nanotubes would grow. In addition, below this critical film thickness, there appeared to be no correlation between film thickness and CNT diameters, which may be a characteristic of CVD systems.[77] It can generally be said that for PECVD growth, thinner films lead to smaller particles, which in turn lead to denser arrays of smaller diameter fibers.

If periodic arrays of VACNFs are desired, the amount of material deposited for each catalyst dot is crucial in determining if single or multiple fibers form. It was shown previously that catalyst film thickness relates to fiber array density and particle size. Likewise, the diameter and thickness of a lithographically defined catalyst dot influence whether one droplet or thus one fiber forms from each dot. In fact, Merkulov *et al.* found that there was a critical dot size resulting in single fibers (Fig. 25), which was dependent upon several parameters including the choice of buffer layer, the substrate, and the type and thickness of the catalyst used.[9]

4. Catalyst particle evolution

Nanoparticles formed by sintering a thin-film metal generally have a disklike hemispherical shape due to a large contact area with the substrate before the growth is initiated. A succession of "stop-action" images shows that after an initial few seconds of growth, the particle is pushed upward by the flux of carbon and becomes elongated. As growth continues the bottom surface of the particle begins to slope upward until it has a conical or teardrop shape, with the tip of the cone directed toward the growing carbon nanostructure and pointing in the direction of carbon diffusion.[148] This has been found in both tip-type and base-type growths.[63]

Most of the characterization of catalyst particles by SEM and TEM is performed *ex situ* once the substrate has cooled down. The particle in this final state can show an elongated conical end or remain spherical. Some particles have a faceted shape on top. This has been repeatedly observed for particles involved in tip-type growth. An example of Ni particles displaying this feature is shown in Fig. 26. The faceting might have occurred during the cooling process, however, this cannot be stated conclusively. There are still many mysteries regarding the behavior of the catalyst particle during growth. One interesting phenomenon is the repeated stretching or "lurching" behavior of the particle inside the body of the growing nanostructure. Thanks to recent technological advances, there have been a few accounts that capture the catalyst's evolution and the growth phenomenon *in situ*.[58,149] The invoked stretching-retracting mechanism of the catalyst nanoparticle could explain the periodic formation of horizontal graphene planes characteristic of a bamboo structure.

Another interesting phenomenon is the decrease and subsequent exhaustion of the catalyst material during

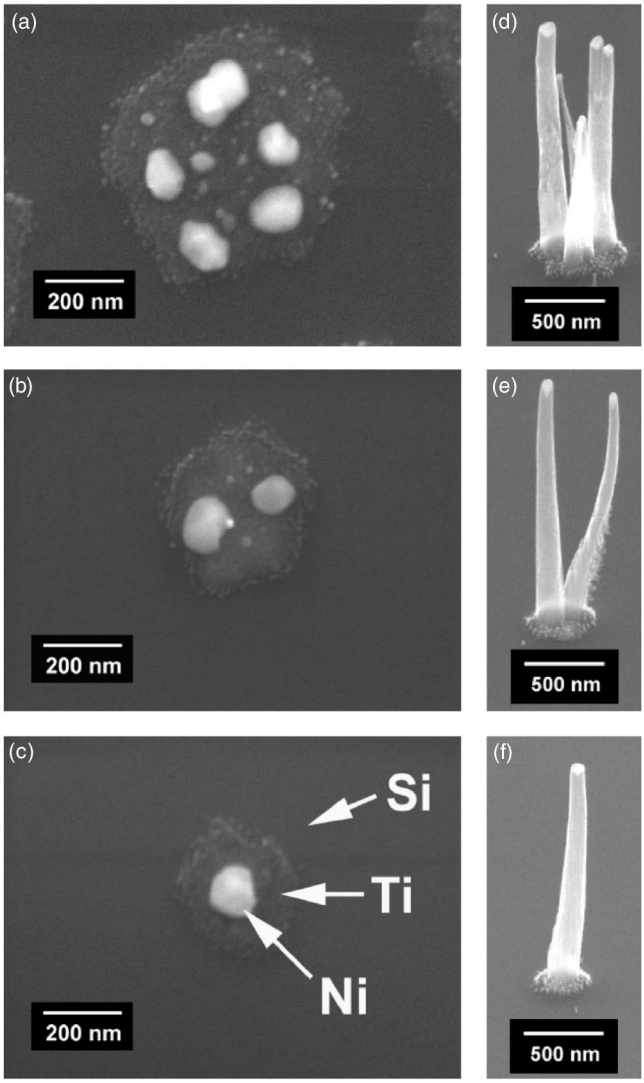

FIG. 25. Formation of multiple (a), (b), and single (c) Ni droplets on the patterned evaporated dots (15 nm Ni/10 nm Ti on Si) and subsequent growth of multiple (d), (e), and single (f) VACNFs. The Ni droplets were formed during NH_3/He plasma preetching and heating up to 600–700 °C. The SEM images were taken at 15 kV and 0° tilt (a)–(c) and at 50° tilt (d)–(f). Adopted from Ref. 9.

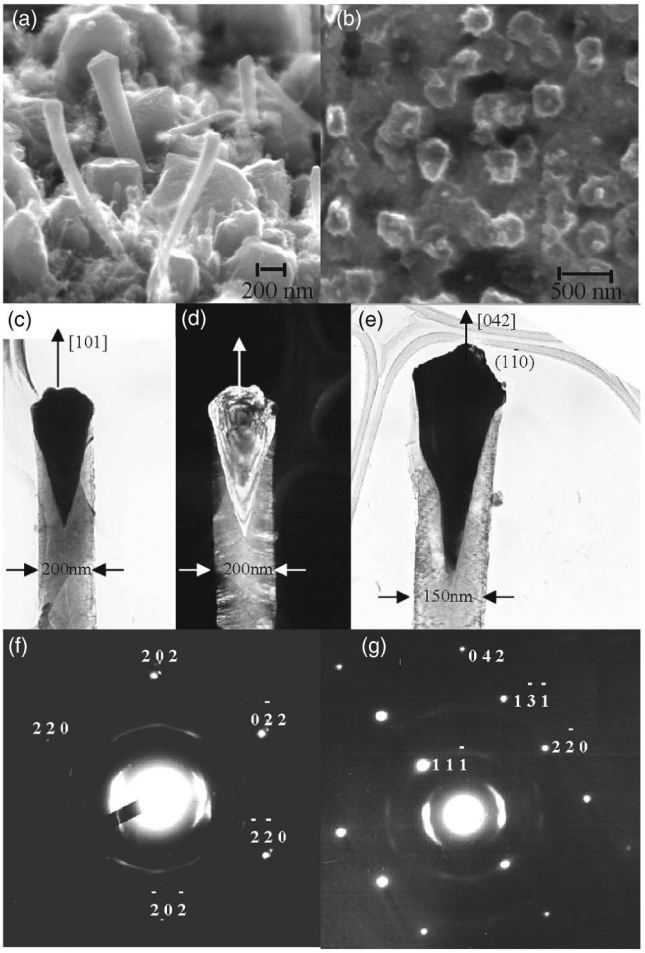

FIG. 26. An example of one of the possible faceting of Ni catalyst nanoparticles on the tips of VACNFs grown by PECVD. (a) TEM image of a VACNF at 400 kV, (b) electron diffraction pattern from the Ni nanoparticle, and zone axis [0 0 1]. Adopted with permission from Ref. 155.

growth. It has been reported that the size of the catalyst particle decreases continually during the PECVD synthesis process.[30] The diminishing of the catalyst material could be due to ion-beam sputtering or by loss of Ni along the nanofiber body. Since particle size correlates to fiber diameter,[9] with the particle size reduction the fiber diameter also reduces. This trend can be used to sharpen the tips of the nanofibers for use in such applications as field emission and intracellular probes. However, this size reduction simultaneously creates a limitation on the maximum obtainable length of the freestanding isolated nanofiber due to the loss of catalyst material. In order to achieve a desired final length the amount of metal contained in the catalyst particle must be sufficient to last the duration of the growth process. This is stipulated by the role the catalyst particle plays in protecting the core of the growing nanostructure from physical and chemical etchings. In other words, the nanoparticle functions as an etch mask. Should the nanoparticle disappear before the nanofiber achieves the targeted length, the fiber core would no longer be masked and would be etched back.

III. PROPERTIES

A. Structure

Carbon-based materials have unique mechanical, electrical, and chemical properties that relate to the various bonding arrangements or possible electronic configurations that a carbon atom can form with its nearest-neighbor carbon atoms.[150] Each carbon atom has six electrons which occupy $1s^2$, $2s^2$, and $2p^2$ atomic orbitals. The $1s^2$ orbital contains two strongly bound core electrons. Four more weakly bound electrons occupy the $2s^2 2p^2$ valence orbitals for the free-carbon atom. In the crystalline phase, the valence electrons give rise to $2s$, $2p_x$, $2p_y$, and $2p_z$-orbitals which are important in forming covalent bonds in carbon materials. Since the energy difference between the higher-energy $2p$ levels and the lower-energy $2s$ level in carbon is small compared with the binding energy of the chemical bonds, the electronic wave functions for these four valence electrons can readily mix with each other (hybridize), thereby changing the occupation of the $2s$ and three $2p$ atomic orbitals so as to enhance the binding energy of the carbon atom with its neighboring

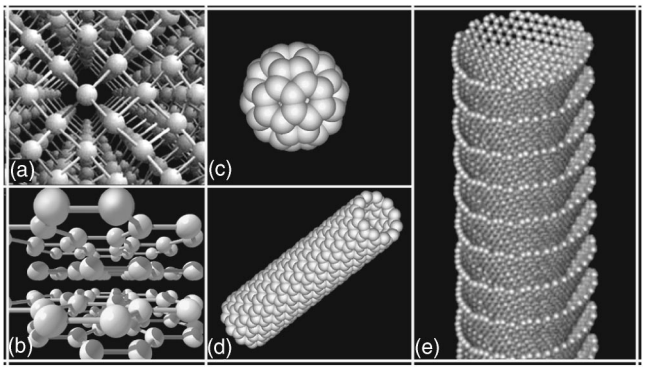

FIG. 27. Carbon structures: (a) diamond, (b) graphite, (c) buckminster fullerene, (d) single-walled carbon nanotube, and (e) stacked cone carbon nanofiber (Adopted with permission from Ref. 20.)

atoms. Three possible hybridizations occur in carbon: *sp*, sp^2, and sp^3. The various bonding states are associated with certain structural arrangements, so that *sp* bonding gives rise to chain structures, sp^2 bonding to planar structures, and sp^3 bonding to tetrahedral structures. The major bulk phases of carbon are sp^2-bonded graphite [Fig. 27(b)] and sp^3-bonded diamond [Fig. 27(a)]. The existence of nanostructured phases, all based on the sp^2-bonded hexagonal network of atoms (graphene sheets)—such as fullerenes [Fig. 27(c)], nanotubes [Fig. 27(d)], and nanofibers [Fig. 27(e)]—is attributed to the energetically favored elimination of dangling bonds, even at the expense of increasing strain energy, thereby promoting the formation of closed cage structures.

There is an abundance of literature devoted to the structure of carbon nanotubes and a full description will not be repeated here. In addition to the definitions given in the introduction it is worth noting that a nanotube can be formed by rolling a graphene sheet into a cylinder and merging its opposite edges. The open edge structure—a scroll—has also been observed and has been confirmed by unrolling them in an electric explosion.[151] One of the distinctions of nanofibers from nanotubes is that for nanofibers the edges of different

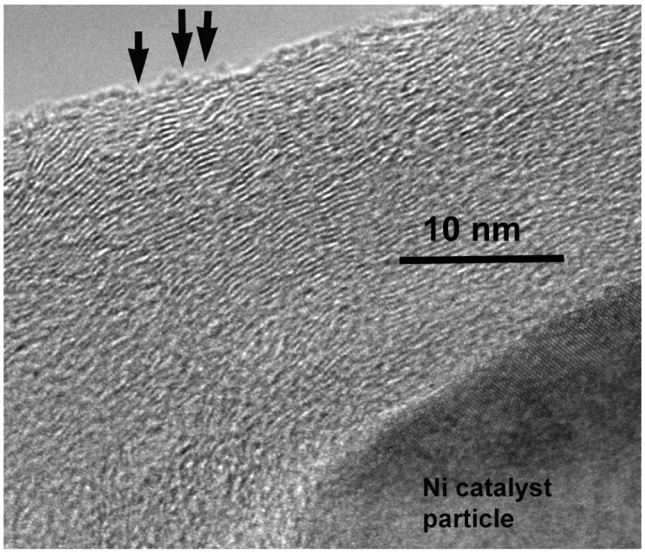

FIG. 28. TEM image of an edge of a nanofiber, displaying the free graphene-sheet ends (indicated by arrows).

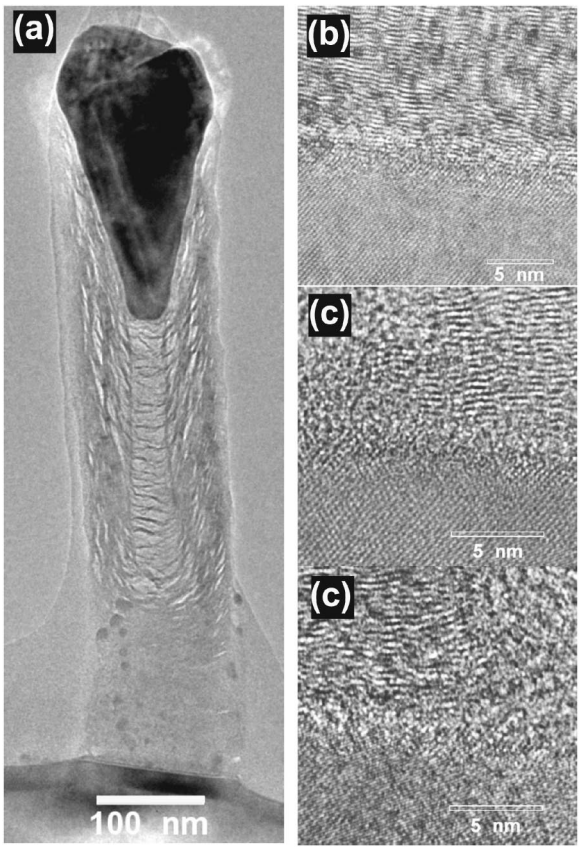

FIG. 29. Transverse TEM images of a VACNF after 5-min growth: (a) complete TEM image of the VACNF on the silicon substrate; (b) high-resolution transmission electron microscopy (HRTEM) image of the interface between the VACNF and the silicon substrate; (c) interface images of the left edge of the VACNF, silicon substrate, and amorphous resin; (d) of the right edge; (e) a void in the sidewalls; and (f) a void between the cup bottoms. Note that (e) and (f) are taken from a different VACNF from (a). Due to sputtering during the VACNF growth, the silicon substrate around the VACNF is etched, producing the protruding appearance of the silicon substrate immediately under the VACNF in (a). The dotted lines indicate how the wall angle is measured with the assistance of the voids in the sidewalls. To guide the reader's eyes, circular dots are used to mark the transition between the cup bottoms and cup walls. (b) shows a clear boundary between the VACNF and the silicon substrate with an interface layer of only two graphitic planes. The interface layer that appears in (a) is thus caused by these graphitic planes. Adopted with permission from Ref. 148.

graphene sheets end at the sidewalls, for example, as shown by Chen *et al.* (Fig. 28).[152] The annealing experiments conducted by Endo *et al.* showed that when the "stacked cup" nanofibers are subjected to temperatures as high as 3000 °C these open edges are removed by formation of closed-loop structures.[153]

The structure of VACNFs has been studied by many groups using TEM. However, in all cases the reported structure was from either the middle of the nanofiber or from its tip. Recently Cui *et al.* concentrated on the base of the VACNF.[148] They showed that the area in the vicinity of the nanofiber-substrate interface is a telltale of the initial stages of its growth. Figure 29 shows TEM images of the area near the base of the nanofiber. It can be seen that at first the graphene layers are formed parallel to the substrate and subsequent layer edges bend upward as the nanoparticle bottom changes its shape from a flat surface to a conelike structure. This fact has serious implications for electrical and mechani-

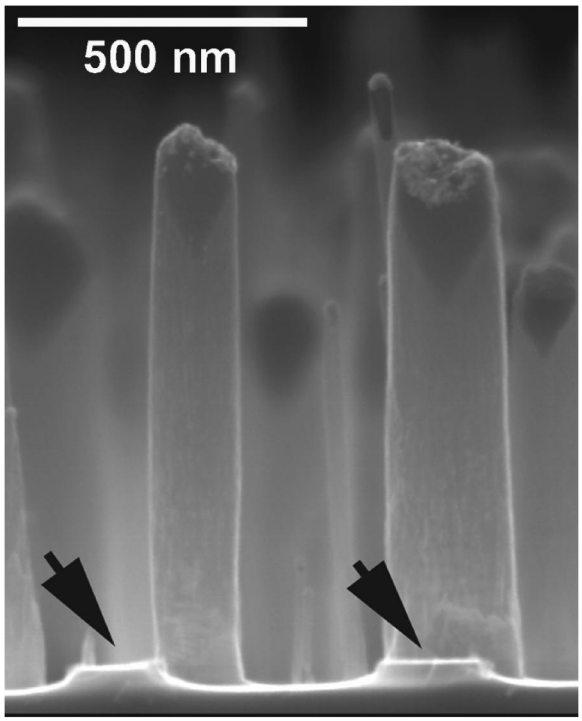

FIG. 30. SEM images of VACNFs mechanically sheared from their bases. The arrows indicate the stumps of VACNFs demonstrating that nanofibers are weakest to lateral shearing near the substrate.

cal properties of the VACNFs. For example, this explains why when lateral force is exerted on nanofibers they typically break at their bases by a horizontal shear along graphite planes (Fig. 30).

Catalyst particle crystallographic orientation and shape have been identified as two of the factors that govern the structure of carbon nanofibers. Recently, Kiselev *et al.* have reported on their studies of the relation of the structure of VACNFs to the orientation and faceting of Ni catalyst particles.[154] VACNFs were grown in acetylene/ammonia atmosphere by ICP PECVD from Ni 10-μm-thick film electroplated onto bronze plates. TEM and diffraction observations showed that Ni catalyst particles are faceted single crystals. They found that {100} facets preferentially decompose carbon while {031} facets deposit carbon. Kuang *et al.* showed that the axial direction of the VACNFs grown by dc PECVD on Ni wafers is mainly parallel to the ⟨110⟩ and ⟨042⟩ directions of Ni.[155] The graphene cone angle varied around 30° which they concluded to be not matching {110} planes and thus corresponding to high-index crystal planes of Ni. From these experiments it appears that the graphene cone angle is not completely governed by the nanoparticle shape and orientation. At the same time, the *in situ* video recordings by Helveg *et al.* clearly show the formation of graphene layers on the step edge of a [111] surface of Ni. It is interesting to note that in their work two different types of nanofibers are presented that are herringbone and bamboo in our definitions are possibly the result of different orientations of Ni nanoparticles. Another set of observations that might connect the nanofiber structure with the crystallography of catalyst nanoparticles is the difference in the nanofiber structure produced by different catalysts. Fe, Ni, and Co have different crystal structures (Table III). Dong *et al.*, for example, showed that at the same CVD conditions Fe and Co produced nanotubes, while Ni resulted in herringbone nanofibers.[156] It is not clear at the moment how to control the catalyst nanoparticle orientation and shape but it might be a key factor to be able to control the structure of the nanofibers. However, catalyst control alone might be not sufficient for that because the growth conditions influence structure formation as well. Nolan *et al.*, based on their observations, asserted that the cone angle is controlled by the amount of atomic hydrogen present during CVD process.[97] Specifically, the cone angle increases with the increase of atomic hydrogen concentration.

B. Electrical properties

Lee *et al.* have investigated the electrical characteristics of individual nanofibers by measuring the $I-V$ characteristics of suspended nanofiber bridges.[157] The nanofibers exhibited linear $I-V$ characteristics at low positive and negative applied voltages. Note that this two-contact measurement provides a resistance that is the sum of the contact and the nanofiber resistances. For this particular section of the nanofiber the resistance was 622 Ω, which corresponds to 1 kΩ/μm of nanofiber length. Using the assumption that conduction was through the entire cylindrical cross-sectional area of the nanofiber, the range of resistivity was estimated to be between 10^{-6} and 10^{-5} Ω m. These values compare very well to arc discharge multiwall nanotubes,[158] for which the resistivity was calculated to be 9×10^{-6} Ω m for a 350-nm-long section of a 20-nm-diameter nanotube whose resistance was 10 kΩ. In general, the resisitivities of multiwall nanotubes are comparable to those of arc-grown graphite fibers and ropes of single-wall nanotubes whose resistivities are $\sim10^{-6}$ Ω m.[159] Schonenberger *et al.* also demonstrated that electrical breakdown occured at current densities of $10^{7}-10^{8}$ A/cm^2, which is much higher than the typical current density of $\sim10^{6}$ A/cm^2, (CRC Handbook) at which metal wires undergo electromigration, demonstrating the advantage of covalently bonded conductors.

While two-probe measurements provide an estimate of the resistivity of a CNF, precise measurements should be done using a four-point probe technique to exclude the contact resistance contribution. Such measurements were recently performed by Zhang *et al.* using multiple Ti/Au ohmic contacts patterned on top of the nanofibers using electron-beam lithography (Fig. 31). These fibers were harvested from a VACNF forest and deposited onto an insulating substrate, and the contacts on individual fibers exhibited resistances of a few kilohms.[160] These four-point probe measurements demonstrate that VACNFs exhibit linear $I-V$ behavior at room temperature, with a resistivity of approximately 4.2×10^{-5} Ω m. Zhang *et al.* propose that this value is consistent with a dominant transport mechanism of electrons traveling through intergraphitic planes in the VACNFs.

C. Electron field emission

Field emission involves the extraction of electrons from a solid by tunneling through the surface-potential barrier, typically equal to the work function of the material, ϕ. An

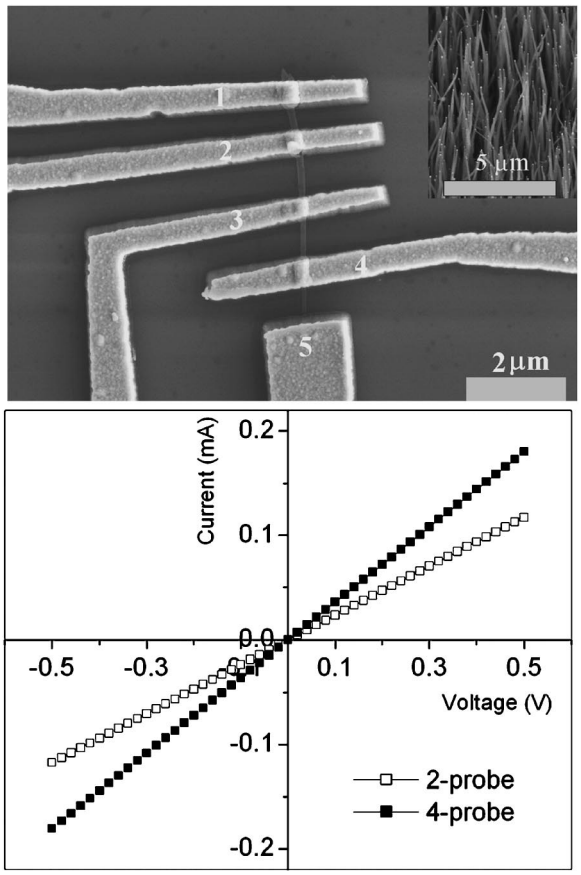

FIG. 31. Four-probe measuremnts of VACNF resistivity. (a) A SEM image of a completed VACNF structure with five metal electrodes (200 nm each of Ti/Au) contacting the nanofiber. The inset is a SEM image of the as-grown VACNF forest. (b) $I-V$ curves for the four-probe [electrodes 1, 2, 3, and 4 of the device in (a)] and two-probe (electrodes 2 and 3) measurements. Adopted from Ref. 160.

applied electric field, E, lowers the barrier height by an amount $\Delta\phi$ described by the following relation:

$$\Delta\phi = \left(\frac{qE}{4\pi\varepsilon_0}\right)^{1/2}. \tag{1}$$

The emitted current depends on the local electric field at the emitting surface, E, and on ϕ. A model offered by Folwer and Nordheim based on early experimental evidence, shows that the dependence of emitted current on E and ϕ should be exponential,[161]

$$I = \frac{q^3E^2\alpha}{8\pi h\phi t^2(y)} \exp\left[\frac{-8\pi(2m)^{1/2}\phi^{3/2}}{3hqE}\nu(y)\right], \tag{2}$$

where α is the emission site area in units of cm^2, h is Planck's constant, m is the electron mass, $y=\Delta\varphi/\varphi$ and $t(y)$ and $\nu(y)$ are the Nordheim elliptic functions.

The local electric field strongly depends on the shape of a surface and can be significantly enhanced at the apex of sharp features. Such influence can be expressed as a geometric field-enhancement factor, β. This leads to the following simple relation for the field at the tip, E_{tip}, of a field-emitting surface:

$$E_{tip} = E\beta. \tag{3}$$

For a thin cylinder, β is roughly proportional to the height-to-diameter ratio, or aspect ratio.[162] For electron emission to occur, the electric field at the emitting surface must be on the order of 1–3 V/nm, which at reasonable applied voltages requires large values of β.

Carbon field-emission cathodes have some distinct advantages compared to other materials. It has been shown by Baker *et al.* and Lea that graphitic carbon microfibers can be operated continuously in ambient gas pressures two decades higher than conventional tungsten field emitters without observation of degraded performance.[163,164] Graphitic carbon also possesses the lowest sputter yield of any material. This stems from the covalent bonding present in graphite. Consequently, carbon is far more resistant to sputtering from ionized residual gas molecules than conventional field-emission cathodes composed of refractory metals.

Field emission from nanostructured graphitic materials including single- and multiwalled CNTs and CNFs has been an area of intense investigation in recent years. This body of research indicates that these materials possess the environmental robustness inherent to microscopic carbon fiber field emitters while offering high β values as a consequence of their nanoscale dimensions and intrinsically high aspect ratios.[165,166] Almost every publication on the synthesis of carbon nanostructures contains data on electron field emission from the material that is presented. The main impetus for this focus is the potential use of such materials in applications that involve electron field-emission sources. This topic is discussed in detail in the *Applications* section of this article.

There are many reports with measurements of field emission from thin films or mats of carbon nanostructures.[167,168] In such arrangement it is difficult to determine the contribution of individual nanofibers or nanotubes to the observed experimental data. Moreover, a dense arrangement of nanostructures marginalizes the geometric field enhancement due to the screening of the electric field by the neighboring nanostructures. In order to determine the actual field-emission properties of individual nanotubes or nanofibers they should be isolated. For this purpose Merkulov *et al.* prepared arrays of conical VACNFs with average base diameters of 200 nm, average tip diameters of 25 nm, and average heights of 2 μm, spaced at 50-μm intervals on *n*-type Si substrates.[168] Field-emission properties of individual VACNFs were measured with a movable current probe capable of positioning a 2-μm-diameter probe tip above an individual VACNF with submicron accuracy. Field-emmission (FE) measurements revealed that isolated nanofibers are good field emitters with emission threshold fields between 15 and 50 V/μm. Isolated VACNFs displayed stable emission for 175 h (the longest test period) of continuous 10-nA operation at vacuum levels of 10^{-6} Torr. FE current versus voltage ($I-V$) analysis has shown a maximum measured FE current exceeding 5 μA without any degradation to the VACNF tip. This corresponds to a current density of approximately 500 kA/cm^2. The FE $I-V$ characteristics of isolated VACNFs display Fowler–Nordheim-like tunneling behavior (Fig. 32).

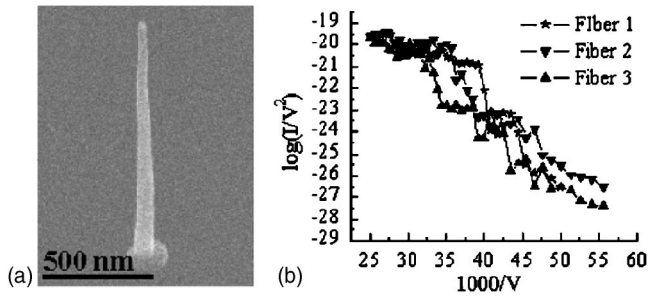

FIG. 32. Electron field emission from a VACNF. (a) SEM image taken at 45° of an individual VACNF grown from an electron-beam lithography (EBL)-patterned catalyst site. (b) Fowler–Nordheim plots of scanned-probe FE measurements from three individual fibers. Maximum field-emission currents exceeding 5 μA were observed corresponding to a current density of approximately 500 kA/cm^2 for a nominal VACNF tip diameter of 30 nm. Adopted from Ref. 195.

D. Mechanical properties

It is well known that nanoscale structures exhibit different mechanical properties than their bulk counterparts. Furthermore, an important characteristic of most materials is that a small diameter fiber is much stronger than the bulk material[169] due to the diminished probability of critical surface flaws with decreasing specimen volume. The vast majority of engineering forms of carbon have more or less disordered graphite microstructures. The microstructure of the crystalline layers within the fiber influences properties such as strength, stiffness, deformation modes, fracture behavior, and toughness.[170] The literature shows great variance in the mechanical properties of carbon forms such as carbon nanotubes and carbon fibers. Table IV[249–259] gives some general ranges for the strength and modulus of engineering carbons.

The high volumetric density of short, strong sp^3 bonds gives diamond the highest stiffness of any known materials (Young's modulus ~1 TPa). Similarly, the high areal density of short, strong sp^2 bonds in the basal plane of graphite results in a Young's modulus that is comparable to that of diamond.[170] The sp^2 graphite bond is the strongest of all chemical bonds, but the weakness of the interplanar bonding means that an ordinary graphite is of little value as a structural material.[171] One way the great in-plane strength of graphite can be exploited is in the development of high-modulus carbon fibers that have basal planes preferentially oriented along the fiber axis. Even so, we cannot neglect the graphite's highly anisotropic mechanical properties. Single-crystal graphite has a Young's modulus over 28 times higher in the direction parallel to the basal planes than in the perpendicular direction.[170] Thus, while there is a preferred orientation of basal planes parallel to the fiber axis, this creates poor transverse properties. Carbon fibers can also have as high as 100 times more stiffness along the fiber axis than perpendicular to it.[170]

Single-crystal carbon nanotubes have extremely large length-to-diameter (aspect) ratios, with diameters as small as only a few nanometers. They are the strongest known material, with a specific tensile strength as high as 100 times that of steel.[172] CNTs also have high stiffness and ductility. For SWCNTs, tensile strengths range between 50 and 200 GPa, Young's modulus is on the order of 1 TPa and fracture strains are between 5% and 20%.[169] As a consequence of their size and high degree of crystalline perfection, CNTs are virtually flaw-free, which contributes to their exceptional strength.[169] However, in spite of their incredible mechanical properties, SWCNTs are not utilized extensively as a reinforcement medium because they are expensive to produce and purify.

On the other hand, MWCNTs are easier to produce since they do not require as stringent catalyst particle preparation. MWCNTs are composed of concentric graphene sheets and have diameters on the order of tens of nanometers depending on the number of graphite layers. One drawback is that these layers can slide past each other easily, often failing by the

TABLE IV. Mechanical properties of carbon-based materials.

Material	Density (g/cm^3)	Tensile strength (GPa)	*E* Young's modulus (GPa)
Diamond	3.52 (Ref. 249) 3.20–3.52 (Ref. 169)	0.800–1.4 (Ref. 169)	1054 (Ref. 249) 700–1200 (Ref. 169)
Graphite	2.26 (Ref. 250) 1.71–1.78 (Ref. 169)	0.0138–0.069 (Ref. 169) 0.01–0.08 (Ref. 251)	1060 in plane (Ref. 252) 1020 parallel to basal, 36.3 perp. (Ref. 250) 11 (Ref. 169)
C60	1.72 (Ref. 253)		16 (Ref. 253)
SWCNTs		50–200 (Ref. 169)	1000 (Ref. 169) 900–1700 (Ref. 254)
MWCNTs		6.2–2.2 (Ref. 252) 11–63 (Ref. 173)	1800 average (Ref. 255) 690–1870 (Ref. 252) 270–1280 (Ref. 171) 270–950 (Ref. 173)
Graphite whiskers	2.2 (Ref. 169)	20 (Ref. 169) 20 (Ref. 256)	700 (Ref. 169)
Carbon fibers	1.78–2.15 (Ref. 169)	2–5 (Ref. 257) 0.3–8 (Ref. 170) 1.5–4.8 (Ref. 169) 0.6–3.7 (Ref. 258)	~80–700 (Ref. 170) 228–724 (Ref. 169) 680 average (Ref. 259)

"sword-in-sheath" mechanism.[173] This failure and the increased probability of defects with greater mass make MWCNTs less desirable than SWCNTs, but their strength still surpasses that of steel and they have a high modulus.

Carbon whiskers are very thin single crystals that have high aspect ratios. As a result of their small size and crystalline perfection they, too, have very desirable mechanical properties, including a Young's modulus of 700 GPa and tensile strength of 20 GPa.[169] In spite of these appealing properties, again whiskers are extremely expensive to produce and can be impractical to incorporate into a matrix.[169]

Carbon fibers, composed of polycrystalline and amorphous carbon, have diameters ranging from hundreds to thousands of nanometers and can be grown thousands of micrometers long. For carbon fibers, tensile strengths are about an order of magnitude lower than for CNTs, ranging from 1.5 to 4.8 GPa and the Young's modulus is between 228 and 724 GPa.[169] Carbon fibers retain their high tensile modulus and strength at elevated temperatures and are not affected by water, solvents, acids, or bases at room temperature. Even though their mechanical properties are not as astounding as those of carbon nanotubes, carbon fibers are relatively easy to produce as well as economical.

In order to measure the mechanical properties of individual carbon nanofibers produced by C-CVD, Gao *et al.* observed electromechanical resonance in TEM.[174] A nanofiber was excited by applicaton of a periodic voltage with respect to a counterelectrode. The bending modulus of bamboo-type nanofibers with point defects was $\sim$30 GPa and that of nanofibers with volume defect was 2–3 GPa. The time-decay constant of nanotube resonance in a vacuum of 10^{-4} Torr was $\sim$85 ms. Such *in situ* TEM method provides a powerful approach to study the mechanics of high aspect ratio nanostructures.

One of the applications for which the mechanical properties of carbon fibers are of high importance is in composite materials.[175] Fibers have relatively low densities, making them attractive for lightweight applications. Most importantly though, carbon fiber and composite manufacturing processes have been developed that are relatively cost effective. In fact, carbon fibers are the most commonly used reinforcement in advanced polymer-matrix composites.[169]

Recently, Weisenberger *et al.* showed that the mechanical properties of polyacrylonitrile fibers could be enhanced by creating a composite fiber reinforced with MWCNTs. They reported a 36% initial modulus increase and a 46% yield strength increase.[176]

E. Chemical properties

McCreery provides an excellent overview of both the chemical and electrochemical properties of carbon-based materials, including "carbon fibers" that correspond to the vertically aligned, catalytically synthesized fibers of this review.[177] In general, nanofibers are chemically and mechanically resistant to many standard microfabrication etch and deposition processes including nitric acid (used for Ni catalyst dissolution), HF and buffered HF, photoresist spin casting, exposure and development, fluorine-based dry etch processing, and a variety of PVD, CVD, and PECVD coating processes, including metal, oxide, and nitride depositions. Calcination, electrochemical oxidation, and oxygen-containing plasma processing can be used to etch a nanofiber material or to provide oxygen-rich moieties on the nanofiber surface.

Carbon electrode functionalization strategies are a vast topic in the literature, ranging, for example, from direct immobilization of materials to the carbon surface to entrapment of materials in polymer films or nucleated islands on the surface of the electrode. Noncovalent modification has been widely used, specifically for nanotubes for which the aromatic nature of the sidewalls provides for strong adsorption of aromatic compounds.[178] These noncovalent strategies are often preferred when the nanotube's sp^2 structure is to be preserved. Bahr and Tour provide an overview of covalent functionalization strategies specifically for carbon nanotubes, but all are likely applicable to nanofiber modification as well.[179] Due to lack of defect sites, covalent functionalization of nanotubes is often preceeded by mechanical and oxidative treatments, such as sonication in sulfuric and nitric acid, pirhanna etch (sulfuric acid and hydrogen peroxide), electrochemical oxidation, or exposure to air or oxygen plasmas. Resultant defect sites are predominantly formed on the ends of nanotubes. The sidewalls of nanotubes, due to their aromatic nature, are far less reactive, although several sidewall functionalization strategies have been developed.[180] In contrast, the edge planes of the stacked structure of nanofibers provide convenient covalent functionalization along their entire length, particularly if these surfaces are oxidatively pretreated.

Carbodiimide chemistries are some of the most widely used functionalization strategies for both carbon nanotubes and nanofibers with surfaces activated by oxidative treatment. Peptide bonding, i.e., condensation of primary amines to carboxylic acids, is perhaps one of the more commonly employed techniques. Amine-containing materials, including proteins and DNA, can be covalently coupled to generated carboxylic acid sites by use of, for example, 1-ethyl-3-(3-dimethylaminopropyl) carbodiimide (EDC) which forms a reactive intermediate at the carboxylic acid site that can couple with available amines to form amides, or to sulfhydryls forming thiol ester linkages.[181] *N*-hydroxysuccinimide (NHS) is often used to stabilize the reactive intermediate, *o*-acylisourea in these reactions.

Lin *et al.* have demonstrated the direct immobilization of functional enzymes (glucose oxidase, GO_x) on the tips of the vertical nanostructured carbon elements for the purpose of mediatorless electrochemical sensing of glucose.[182] Here carboxylic acid sites were generated by electrochemical pretreatment in 1N NaOH (1.5 V for 90 s). NHS-stabilized exposure to EDC (2 h) was then followed by a 2-h incubation in 2 mg/mL glucose oxidase in 100-mM phosphate- buffered saline (PBS), resulting in condensation of primary amines of the GO_x with activated sites on the carbon elements. Also, using EDC/NHS carbodiimide chemistry, Nguyen *et al.* have demonstrated the immobilization of amine- and dye-terminated single-stranded oligonucleotides on the opened ends of the aligned forests of carbon nano-

structures, ultimately for hybridization and detection of DNA.[183] McKnight *et al.* have employed EDC condensation of whole plasmids (5031 bp pGreenlantern-1) to carboxylic acid groups on nanofiber scaffolds and demonstrated transcriptional activity of the bound DNA in nanofiber-penetrated live cells.[184] As opposed to using amine-terminated DNA constructs, double-stranded plasmid DNA was bound putatively at base amines on cytosine, guanine, and adenine.

F. Electrochemical properties

Carbon materials have been used extensively as electrodes in chemical production and in measurement equipment. In general, carbon-based electrodes feature relatively wide potential windows in aqueous media, are low cost, have low chemical and electrochemical reactivity, and provide reproducible responses following appropriate surface treatments. Various conventional carbon-based electrode systems include glassy carbon, carbon paste, highly ordered pyrolytic graphite (HOPG), and wax-impregnated graphites, as reviewed in Refs. 177 and 185. In line with the intent of this review, we focus on the literature aimed directly at vertically aligned carbon-based nanomaterials.

Several research groups have investigated forests of closely packed vertical nanofibers and nanotubes as electrodic material. Li *et al.* characterized densely packed multiwalled nanotube towers (MWNTT) grown by thermal CVD and aligned by the crowding effect.[186] Individual nanostructured elements within the electrode matrix featured lengths from 30 to 100 μm and diameters ranging from 15 to 80 nm at a densely packed spacing of 100–200 nm. Compared to "paper-film" electrodes prepared from laser ablation synthesized and acid-treated SWCNT in the same study, the three-dimensional MWNTT matrix featured lower volumetric capacitance (2.0 F/cm^3 vs 6.25 F/cm^3) but a redox response to the $Fe(CN)_6^{3-/4-}$ couple that scaled with the thickness of the MWNTT film. Heat treatment of 450 °C in air for 10 h was found to increase the volumetric capacitance to 4.7 F/cm^3, perhaps due to removal of amorphous carbon within the three-dimensional matrix. This scaling of redox with the thickness (lengths) of the vertical electrode material demonstrated that electron transfer was occurring within the matrix along the lengths of the nanostructured elements. Peak separation of the $Fe(CN)_6^{3-/4-}$ couple was larger than for the prepared SWCNT material (170 mV vs 100 mV) and increased with heat treatment to 230 mV.

Murphy *et al.* studied the electrochemical behavior of less aligned, more crowded nanostructured carbon, grown also by thermal CVD using Fe_2O_3 as catalyst.[187] For the $Ru(NH_3)^{2+/3+}$ couple, slightly wider peak separation was observed than that obtained with a conventional glassy carbon electrode, with some peak separation being attributed to the resistive drop in the electrode material. It was recognized that volumetric redox of analyte within the nanotube matrix was occurring. In the same study, oxidation of hydroquinone resulted in significantly higher charge transfer than that expected from the material within the electrode matrix and this was attributed to strong adsorption. Thorough rinsing of the electrode in 1-M phosphate buffer did not remove the adsorbed hydroquinone-benzoquinone analyte, but 30-min soaking in ethanol could remove these materials.

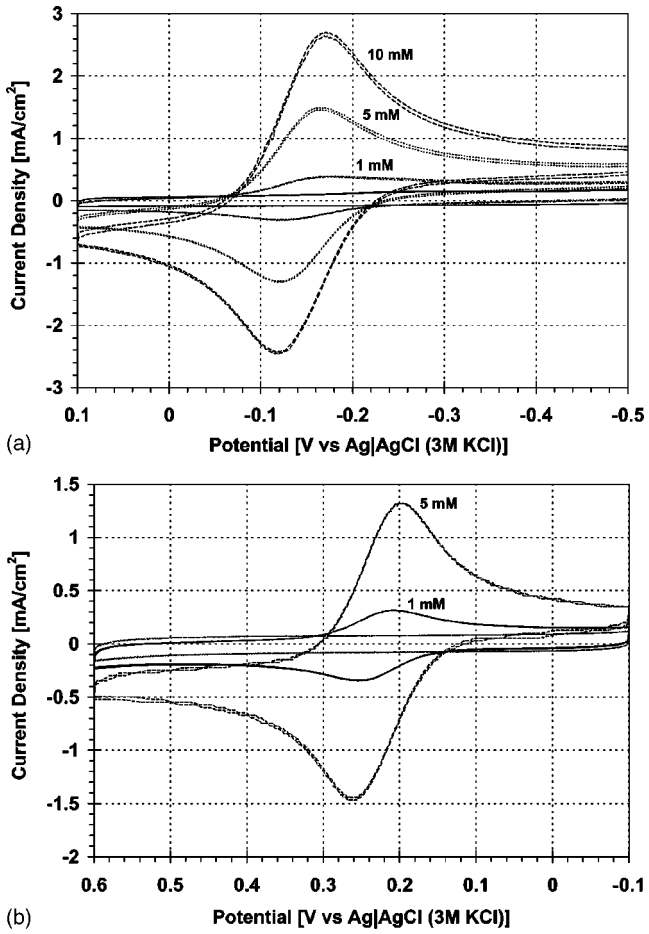

FIG. 33. Cyclic voltammogramms of VACNF forests. Responses of 5-mm-diameter nanofiber forest electrodes to varying concentrations of (a) ruthenium hexamine trichloride and (b) potassium ferrocyanide. These voltammograms are IR compensated to account for resistive losses in the interconnect/fiber-substrate junction/solution, which are pronounced due to the relatively large currents from the high-concentration analytes. All subsequent voltammograms are not IR compensated. Reprinted with permission from Ref. 191, Copyright 2003 American Chemical Society.

McKnight *et al.* characterized the electrochemical properties of as-grown as well as treated VACNF forest electrodes of different dimensions, which were grown using dc-PECVD and nickel catalyst.[188] Various electrode configurations were evaluated using a variety of outer sphere, quasireversible analytes including $Fe(CN)_6^{3-/4-}$ and $Ru(NH_3)_6^{2+/3+}$ at 0.5-, 1-, and 5-mM concentrations in 100 -mM KCl. Figures 33(a) and 33(b) provide representative cyclic voltammograms (CV: 100 mV/s) for a large surface area (5-mm diameter) VACNF forest corrected for resistive drop of the electrode, interconnects, and solution. For these as-grown electrodes, which can be described as stacked funnel-type carbon nanofibers, the quasireversible couples exhibited rapid electron-transfer kinetics, with cathodic and anodic peak separations at sweep rates of 100 mV/s very near the ideal 59 mV for a single electron-transfer reaction, and the anodic/cathodic peak ratio near unity. As with the Li and Murphy study, the CVs in Fig. 33 indicate the diffusion-

limited electrode responses with peak currents of 10%–15% greater than those expected from a 5-mm-diameter planar electrode where analyte access is limited to the electrode surface by semi-infinite planar diffusion. The additional charge transferred can be explained by redox of the analyte adsorbed to and within the free volume of the porous electrode matrix.[186]

Tu *et al.* reported on the use of sparse arrays of vertical nanostructured carbon as electrode material.[189] Low site-density arrays were grown by PECVD from randomly electrodeposited Ni on a Cr-coated silicon substrate. Magnetron-sputtered SiO_2, followed by thick layers of a two-component solvent-thinned epoxy (M-Bond 610), were used to insulate and fill the substrate and interfiber spaces. The potted structure was then polished to expose sparse nanofiber tips in a planar format on the electrode surface. This sparse array of electrodes acted effectively as the sum of many $(10^6/\mathrm{cm}_2)$ individual ultramicroelectrodes, providing a redox response to the $Fe(CN)_6^{3-/4-}$ couple that indicated radial diffusive transport to the active nanofiber sites. Li *et al.* generated polished planarized electrodes of Ni-catalyzed PECVD-grown nanofibers insulated and tip exposed from thick layers of tetraethoxysilane CVD SiO_2.[190] In this case, individually addressed pads of closely packed forests of fibers presented planar diffusion-limited redox responses to $Fe(CN)_6^{3-/4-}$, while lower-density nanofiber spacing (achieved via electron-beam lithography) produced the sigmoidal response of radial diffusion. Using ac and differential pulse voltammetry, low-density electrodes provided higher sensitivity (versus high density) of response to surface-immobilized ferrocene.

Guillorn *et al.* demonstrated the ability to electrically connect with an individually addressed nanofiber by using a multistep microfabrication process.[84] Here dc-PECVD-synthesized nanofibers were grown from electron-beam patterned nickel dots on tungsten interconnects. This work was continued by McKnight *et al.* as the electrochemical properties of photolithographically defined, individually addressed nanofiber elements (typical lengths of $4-10\ \mu$m) and nanofiber tips (<250-nm-diameter semihemisphere) were characterized against $Fe(CN)_6^{3-/4-}$, $Ru(NH_3)_6^{2+/3+}$, and $IrCl_6^{2-/3-}$.[191] The redox response of electrodes was dependent on the surface area of the exposed nanofiber material, thus indicating that electron transfer occurs along the entire length of these vertically aligned structures. Electrode interfacial capacitance was evaluated at $\sim 140\ \mu\mathrm{F/cm}^2$ by performing voltammetry of various length fibers $(2-12\ \mu\mathrm{m})$ at multiple scan rates in 100-mM KCl. The potential window of these electrodes was evaluated in several aqueous solvents, including 100-mM KCl and phosphate-buffered saline [1.2 to −1.3 V vs Ag/AgCl(3-M KCl)], methanol (1.2 to −0.6 V), 1-N sulfuric acid (1.5 to −0.5 V), and sodium hydroxide (0.8 to −1.5 V). Tip exposed (semihemispherical) and electrodes with an overall surface area $<10\ \mu\mathrm{m}^2$ adhered well to classic ultramicroelectrode steady-state response. Longer electrodes (fibers with lengths $>10\ \mu$m and surface areas $>10\ \mu\mathrm{m}^2$) began to indicate a quasisteady-state response of cylindrical ultramicroelectrodes, with slight diffusion-limited peaking of the oxidation and reduction curves at scan rates of 200 mV/s for ruthenium hexamine trichloride in 100-mM KCl.

Recent work with vertically aligned structures exploits some of the classic electrochemical modifications performed with other carbon-based electrode systems to provide specific modification of the electrode response. Chen *et al.* have demonstrated the electrodeposition of polypyrrole (pPy) films over well-aligned vertical nanostructured carbon.[192] Conformal polypyrrole films were electropolymerized onto each individual element of vertical forests of carbon fibers from 17.3-mM pyrrole monomer in 0.1-M $LiClO_4$ at anodic potentials [>0.4 V versus standard calomel electrode (SCE)]. As an electronically conductive polymer film, pPy can be used to immobilize redox mediators, including enzymes, to provide specificity to nanostructured carbon-based electrodes. Direct immobilization of enzymes to the nanofiber material has also been demonstrated by Lin *et al.* (see previous section) to provide probing specificity to glucose. Similarly, direct immobilization of oligonucleotides has been demonstrated by Li *et al.* and Koehne *et al.* for detection of hybridization of subattomole DNA targets by using $Ru(bpy)_3^{2+}$-mediated guanine oxidation.[190,193]

G. Postsynthesis processing

There are many applications of carbon nanofibers that require the integration of their synthesis process into the overall device microfabrication process. Very often synthesis is not the first or the last step, which generates an issue of compatibility of the processes and materials. First of all, the integration of the growth process requires use of large-scale reactors for substrates compatible with microelectronic device manufacturing equipment (e.g., 100 mm or larger diameter round Si and quartz wafers). Second, multilevel processing requires the ability to synthesize high-quality VACNF in precisely defined locations, as subsequent fabrication processes need to be performed in registry with defined patterns. This can be achieved by deposition of catalyst in areas defined by lithography. Third, the nanofibers must be able to withstand the conditions to which they are exposed during standard microfabrication processing used in the production of integrated circuits and microelectromechanical systems (MEMS). Fortunately, in many cases this compatibility has been demonstrated.[26,28,30,31,33,39,190,194] As in any process engineering, there are still many issues that need to be resolved for each specific application and set of materials. We briefly describe some of the more useful processing steps below.

Perhaps the most fundamental operation is the deposition of thin films on VACNF arrays. The effect of SiO_2 and amorphous Si deposition onto VACNF using rf PECVD has been investigated.[195] The layers could be uniformly deposited onto the fibers resulting in a conformal coating. Thermal CVD using tetraethylorthosilicate (TEOS) at 700 °C in a quartz tube furnace was also employed for conformal SiO_2 coating of VACNFs.[190,193] Physical vapor deposition techniques including sputtering and electron-beam evaporation have also been used successfully for this purpose, providing a mechanism to modify the surface of the VACNF. Of par-

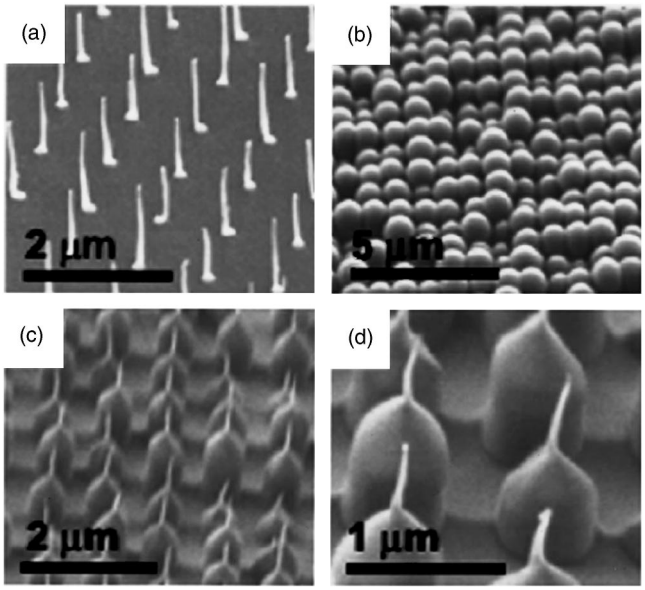

FIG. 34. Deposition and removal of conformal PECVD SiO_2 on VACNF arrays. (a) VACNF array on Si as grown (b) following the deposition of a 1-mμ-thick PECVD SiO_2 layer (c), (d) after 40 min of reactive ion etching (RIE) using a CHF_3/O_2 plasma. All micrographs were taken in a SEM at a 45° angle. Adopted from Ref. 195.

ticular interest was the coating onto the VACNF of dielectric layers that could be selectively removed from the regions of the fiber with subsequent microfabrication processes. Figure 34 shows the VACNFs conformally coated with and subsequently directionally emancipated from SiO_2. This provides the ability to control the amount of the fiber body participating in electron transport independent of the aspect ratio or geometry of the fiber. The detailed studies of controlled removal of insulator coating from the tips of the nanofibers were performed by Ikuno *et al.*[196]

Once the material has been deposited onto a substrate, typically some sort of patterning is performed. Photolithography has long been established as the standard workhorse technique used in the microelectronics industry for this purpose. This process involves the patterning of ultraviolet (UV) sensitive polymer layers (photoresists). Photoresists are typically spin-cast onto substrates at speeds ranging from 1000 to 6000 rpm. Simple experiments involving the deposition of photoresist layers between 200 nm and 2-μm thickness demonstrated that even high aspect ratio VACNFs survive this processing. Not only can photoresist be applied to substrates with VACNF on them, but it can also be exposed and developed using well-established techniques. Moreover, photoresist can be stripped from substrates containing fibers by using a combination of organic solvents and ultrasonic agitation with no damage to the structural integrity of the VACNF. Furthermore, brief exposure to an oxygen rf plasma, usually used to remove remains of photoresist, does not significantly affect nanofibers. Once a pattern has been exposed in a layer of photoresist and developed, it is transferred onto the substrate by either the addition or removal of material, referred to as additive or subtractive pattern transfer, respectively. In the case of subtractive pattern transfer, some form of etching is used to remove the desired layer or layers from the patterned area. These processes include various forms of plasma-based etching along with wet chemical etching. Material deposited onto VACNF can be removed using several combinations of these techniques without significantly damaging the fiber. The fact that the VACNF is composed of graphitic carbon provides it with a relatively robust body that can withstand bombardment of ions during plasma-based processes and any sort of chemical reaction with the exception of those designed to attack carbonaceous materials. The tolerance of VACNFs and CNTs to HF provides an isotropic method of SiO_2 removal. This property was also used for the removal of CNT from a SiO_2 substrate for successive use or transfer to another substrate, e.g., one that cannot withstand CNT growth temperatures.[197]

The processing techniques described above have resulted in the fabrication of several microscale structures that exploit the unique nanoscale properties of the VACNF.[26–28,30,32,33,35,39,190,194] A process for passivating the body of the fibers with an insulating thin film while leaving the tips electrically and electrochemically active was developed for the fabrication of electrochemical probes with high spatial resolution. This technology was then combined with a process for creating individually electrically addressable VACNF on an insulating substrate to produce arrays of high aspect ratio electrochemical probes.[84] The changes in the electrochemical activity of the carbon nanofiber-based electrodes, due to exposure to different microfabrication processes, are reviewed in Ref. 188.

Chemical mechanical polishing (CMP) is frequently used in microelectronic circuit manufacturing to planarize substrate morphology, and can be applied to films deposited onto VACNF. Deep layers of SiO_2 have been successfully planarized without damaging the buried VACNF. Continuation of this process has been shown to remove sections of the VACNF at the same rate as the SiO_2, leaving the exposed fiber core coplanar with the surrounding oxide topography.[190,193] This strategy has enabled the synthesis of coplanar electrode arrays for electrochemical applications where many fibers perform transduction in a parallel fashion.

All of the above show the ability of carbon nanostructures to withstand numerous processing conditions but methods of CNF modification or removal are also important for device fabrication. For example, a VACNF can be used as a sacrificial template for the creation of vertically oriented nanofluidic devices.[33,63] In this process, arrays of VACNFs are grown on either Si or Si_3N_4 membranes and are coated with a thin conformal film using PECVD or low-pressure chemical-vapor deposition (LPCVD). The tips of the fibers are liberated using the process described above for the individual electrochemical probes. Following the removal of the remaining photoresist, the substrates are subjected to a brief etch in concentrated nitric acid to remove the Ni catalyst particle at the tip, and an O_2 reactive ion etch is then used to remove the body of the fiber from within the thin-film SiO_2 tube encasing it. Once the body of the fiber has been entirely removed, the bottom of the tube can be opened to create a nanometer-sized pipe structure, or nanopipe (Fig. 35).

The accessibility of the catalyst particle allows for its easy removal from the VACNF. When Ni is used as a cata-

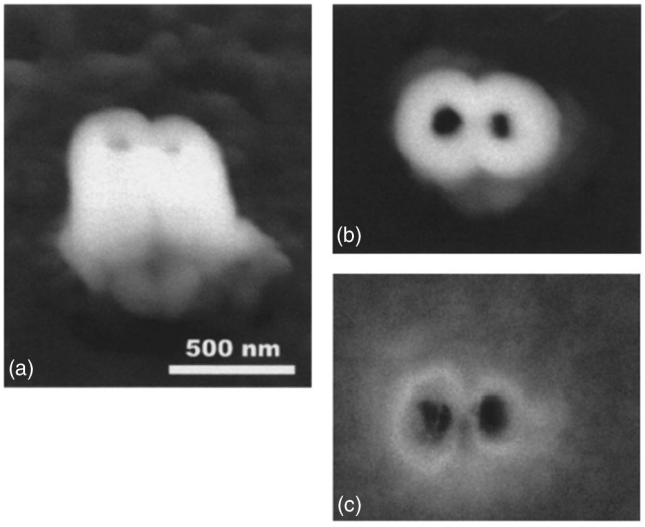

FIG. 35. Nanopipes made using VACNFs as nanotemplates. Adopted from Ref. 33.

lyst, the catalyst particle can be removed by nitric acid etch that is preceded by a brief oxygen plasma, as described above. A simple purification process for the removal of iron catalyst particles at the tip of VACNFs synthesized using C-PECVD is reported by Nguyen *et al.*[38] In this process, the first step involves thermal oxidation in air, at temperatures of 200–400 °C, resulting in the physical swelling of the iron particles due to formation of iron oxide. Subsequently, the complete removal of the iron oxide particles is achieved with diluted acid (12% HCl). The purification process appears to be very efficient at removing all of the iron catalyst particles. Electron microscopy images and Raman spectroscopy data indicate that the purification process does not damage the graphitic structure of the nanofibers.

In addition to thermal oxidation in oxygen atmosphere and using an oxygen plasma etch, carbon nanostructures can be removed electrochemically. MWNTs were etched at potentials more positive than 1.7 V vs Ag/AgCl (3-M NaCl) in an aqueous 0.1-M KCl electrolyte solution.[198] Hinds *et al.* used this same method to tailor the length of CNTs.[199]

IV. APPLICATIONS

A. Microfabricated field-emission electron sources

The design and fabrication of vacuum microelectronic devices based on field-emission cathodes of various types have proven to be a fruitful area of research for many groups over the last three decades.[200] Recently, the construction of devices using various forms of nanostructured graphitic carbon has received a significant amount of attention.[195,201,202] Xu and Brandes presented data on the operating CNT-based gated cathode device in 1998 by employing disordered mats of multiwalled CNTs (MWNT) grown within electrostatic gating structures by thermal CVD.[203] Several other groups have fabricated similar devices using a variety of different techniques, all achieving similar results. Due to the multiplicity of CNTs in the cathodes of these devices, numerous emission sites are present, yielding devices capable of delivering high emission currents at relatively low operating voltages. However, it has been demonstrated that this feature may be the source of significant device-to-device nonuniformity.[27]

Devices using mats of CNTs for the field-emission cathode possess no way to precisely control the location or density of the emission sites. This significantly complicates the construction of field-emission devices that produce well-focused emitted electron beams. While focused beams are not required for every application of microscale field-emission guns, beam focusing is essential for more demanding uses such as electron sources for electron-beam lithography or electron microscopy. In these applications, VACNFs offer some additional advantages over other nanostructured graphitic carbon-based cathodes. In particular, the ability to construct devices with single VACNF cathodes greatly simplifies the design of integrated focusing and deflection optics and has a significant impact on the minimum achievable beam diameter. This stems from the fact that the location of the VACNF can be precisely controlled within the device structure, at least within the dimensional tolerances of the VACNF themselves. It follows that the emission site, presumed to be at or near the tip of the VACNF, can also be controlled with accuracy of probably a few nanometers. This cannot be said of devices employing ensembles of nanotubes or nanofibers, for which multiple active emission sites are spread out over an entire micron-scale cathode.

In situ growth of VACNF into prefabricated electrostatic gating structures was demonstrated by Guillorn *et al.*[32] While this approach is capable of realizing device structures, there are some disadvantages to this process. Primarily, the dc plasma discharge used to grow the VACNFs was found to cause charge-induced damage to the gating structure. Nevertheless, Pirio *et al.* have used a variant of this process to fabricate gated cathode structures with multiple VACNF emitters on each cathode.[202] This work demonstrated that arrays of such devices displayed field-emission characteristics that agreed with the Fowler–Nordheim model with field-emission threshold voltages as low as 10 V. However, the presence of multiple VACNF withinin the cathode negates the point of using VACNF for this type of device, and provides no advantage over CNT-based devices. In a later work, the ability to fabricate devices with single, low-quality VACNF cathodes was demonstrated using this technique.[204] The operation of these devices has not been published at this time.

A robust process for fabricating integrated field-emission electron sources using single VACNF cathodes was demonstrated by Guillorn *et al.*[29,195] This process utilized the ability already noted of the VACNF to withstand microfabrication processing to synthesize functional devices in a wafer-scale fabrication technology. Tested devices displayed behavior consistent with the Fowler–Nordheim model[161] of field emission, and operated with very high efficiency with less than 2% of the emitted current being collected by the gate electrode. This process was later improved upon by forming the gate electrode using a self-aligned process.[31] This eliminated the need for definition of the gate electrode by an aligned

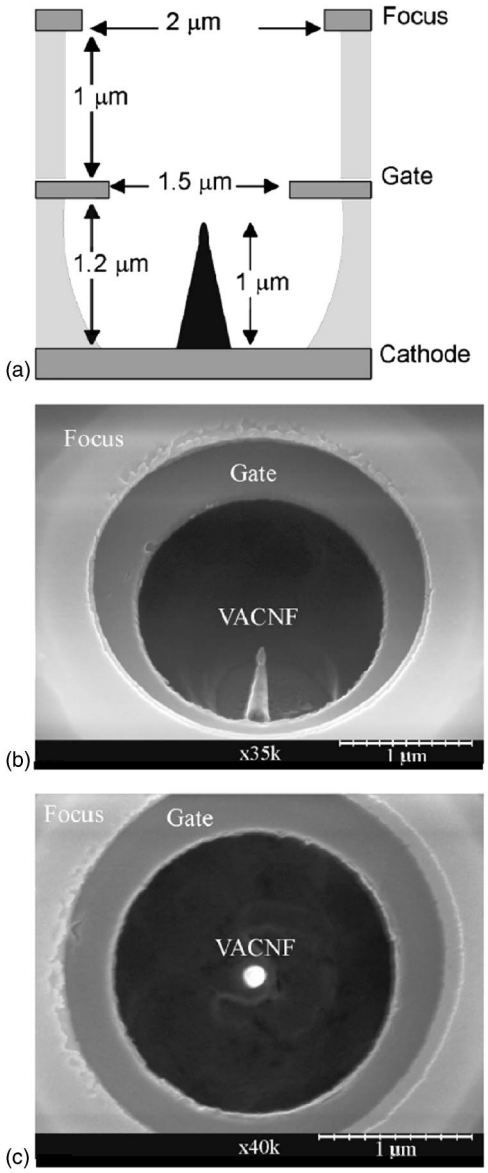

FIG. 36. Microfabricated structure with a single VACNF as a cathode and integrated focusing electrode. Adopted from Ref. 205.

lithographic exposure step, thus significantly simplifying device construction without compromising the operational performance.

A microfabricated electron gun structure with an integrated electrostatic focusing electrode using a single VACNF as the field-emission cathode was reported by Guillorn *et al.* in 2004 (Fig. 36).[205] This device was fabricated using a variant of the device processing techniques reported in their earlier works, with the addition of an out-of-plane focusing electrode that is aligned coaxially with the VACNF cathode and gate electrode apertures. The performance of the integrated focusing electrode was investigated by modulating the potential on this electrode while projecting the image of the emitted electron beam onto a phosphor screen. This was found to have a significant impact on the beam diameter. The observed experimental results were also in good agreement with numerical simulations of the device performance, thereby revealing that true refocusing of the electron beam had occurred. Devices of this design were used to image submicron lines in an electron-beam resist to demonstrate their potential use in a massively parallel electron-beam lithography system.[206]

B. Microfabricated x-ray sources

X-ray sources are widely used in industrial, medical, and scientific instruments. X rays are usually generated by bombardment of a metal target with energetic electrons. The properties of the x-ray source, such as beam size, crucially depend on the electron source. Cold electric-field enhanced (EFE) sources with carbon nanostructure cathodes show improved performance and have lead to portable and miniature x-ray sources for industrial and medical applications.[207] Sugie *et al.* used carbon nanotubes grown by C-CVD on a W wire as a primary electron source.[208] They showed at a moderately low pressure of 2×10^{-7} Torr, the CNT had a stable operation for more than 1 h and enabled the acquisition of clear x-ray images. The intensity of the x rays passing through a beryllium window was measured as a function of the target potential from 10 to 60 kV at a constant current of 10^{-7} A. The x-ray intensity increased approximately exponentially with the linear increase in the target potential: 0.005 mSv/h at 20 kV and 4 mSv/h at 50 kV.

Yue *et al.* fabricated a device that can readily produce both continuous and pulsed x rays with a programmable wave form and repetition rate.[209] A total emission current of 28 mA was obtained from a 0.2-cm^2-area CNT cathode. The x-ray intensity is shown to be sufficient to image a human extremity at 14 kVp and 180 mA s. Pulsed x-ray generation with a repetition rate greater than 100 kHz was readily achieved by programming the gate voltage.

The advantages of carbon nanofibers for a point x-ray source have been demonstrated by Matsumoto and Mimura.[210] A point x-ray emission was obtained from a diode configuration composed of a graphite-nanofiber cold cathode and a conical-shaped copper metal anode. When combined with a highly sensitive charge coupled device (CCD) camera with a scintillator, this x-ray source was then used to obtain x-ray transmission images of a tungsten mesh and an x-ray test chart. The spatial resolution of this x-ray radiography system was on the order of 10 μm and the acquisition time for these images was less than 10 s. This combination of the point x-ray source and the sensitive detection system offers a high-resolution x-ray radiography system.

C. Electrochemical probes

The incorporation of micro- and nanoscale carbon materials into electrodes has long served to augment electrode performance for specific applications. Modification of carbon paste electrodes with nanotubes is frequently employed, for which the nanoscale structure of the incorporated nanotubes enables improved coupling of the bulk electrode with the redox center of, for example, immobilized redox mediating enzymes. Bundles of nanotubes have also been incorporated into individual microscale probing elements, and in this configuration serve as a material of choice for a variety of microelectrophysiological measurements and electroanalytical detection techniques and applications, including electro-

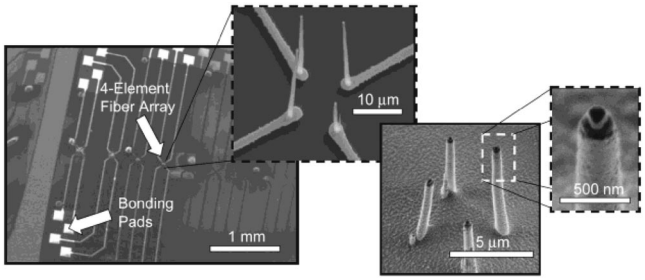

FIG. 37. Microarrays of electrochemical nanoprobes. Scanning electron micrographs of an individual chip of 40 nanofiber probing elements. At far left, image taken following the oxide deposition step and prior to SU-8 passivation to facilitate imaging the underlying interconnect structure (first inset). At right, a four-element array is shown following device completion. Individual fibers feature oxide and some SU-8 passivation, with only the extreme tip being exposed for electrochemical activity. SU-8 on the substrate hides the underlying interconnect structure in these images. Reprinted with permission from Ref. 191, Copyright 2004 American Chemical Society.

chemical detection of microfluidic separations,[211] scanning electrochemical microscopy,[212] and dynamic electrophysiological measurements in and around excitable cells.[213] Advances in the ability to incorporate vertically aligned nanoscale carbon electrodes into multielement devices, such as arrays of individually addressable probing elements, should provide unique platforms that will introduce a high level of parallelism into these well-established electrophysiological and electroanalytical techniques (Fig. 37).

D. Intracellular gene delivery devices

Methods to introduce genetic material into cells have remained a central theme in molecular biology, biotechnology, and medicine. While many methods exist, including target-specific viral vectors, electroporation,[214] liposome fusion,[215] and microprojectile bombardment,[216] it is perhaps microinjection that provides the most effective mechanism across a broad range of cell types. In this application, individual microscale needles are used for the direct injection and delivery of genetic material to the intracellular domain and to the nuclear domain of eukaryotes. Recently, a parallel microinjection-based method termed *impalefection* has been demonstrated using vertical aligned arrays of carbon nanofibers (Fig. 38).[184,217] In this technique, arrays of nanofibers are either coated with DNA or covalently modified with DNA and are directly inserted into many cells simultaneously using a variety of techniques, including centrifugation of cells onto the nanofiber array or direct pressing of the DNA-modified array into tissue matrices. The size scale and morphology of the vertically aligned nanofibers provide effective penetration into cells, including into the nucleus of mammalian cells, where the DNA is either released from the nanofiber and expressed by the cell, or transcribed even while tethered to the nanofiber scaffold. In either case, penetrated cells can recover from the procedure, with their plasma membranes effectively resealing around the penetrant nanoscale structure. Proliferation of cells occurs upon the nanofiber substrate and, often, these proliferating cells tend to maintain intracellular residence of the penetrant nanofibers for extended periods of time (weeks).

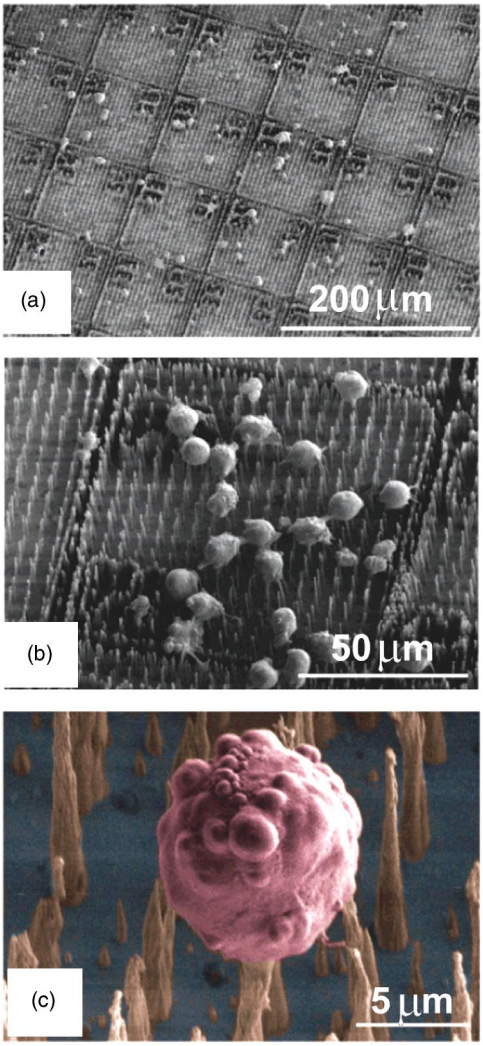

FIG. 38. (Color online) SEM images of VACNF arrays as gene delivery devices. Electron micrographs of mammalian cells (SP2/0-AG14; mouse myeloma13) following centrifugation at 600 G onto an indexed nanofiber gene delivery chip and culture for 3 days (viewing angle is 30°). The cells were fixed with 2% gluteraldehyde in PBS and dehydrated with methanol prior to electron microscopy. SP2 cells were used for this image as they are a suspension cell line and therefore do not attach and spread on the nanofiber platform, thus facilitating clearer images. Nonetheless, some material has clearly agglomerated onto the fiber surfaces, as seen in panel C (false color added). Reprinted with permission from Ref. 217, Copyright 2004 American Chemical Society.

In the course of impalefection experiments, the requirements for successful use of VACNF arrays as material delivery vectors have been identified: nanofibers are required to be sharp, sparse, considerably tall, rigid, and able to retain DNA during the insertion. For typical mammalian cells that have linear dimensions on the order of 10 μm it has been determined that conical 6–10-μm-long nanofibers with tip diameters of 100 nm or less, positioned in an array with 5-μm spacing between fibers, provide effective impalefection.

E. Scanning probe microscopy tips

The atomic force microscope (AFM) has emerged as a valuable tool for probing various surfaces in semiconductor metrology and profilometry, imaging of biological samples,

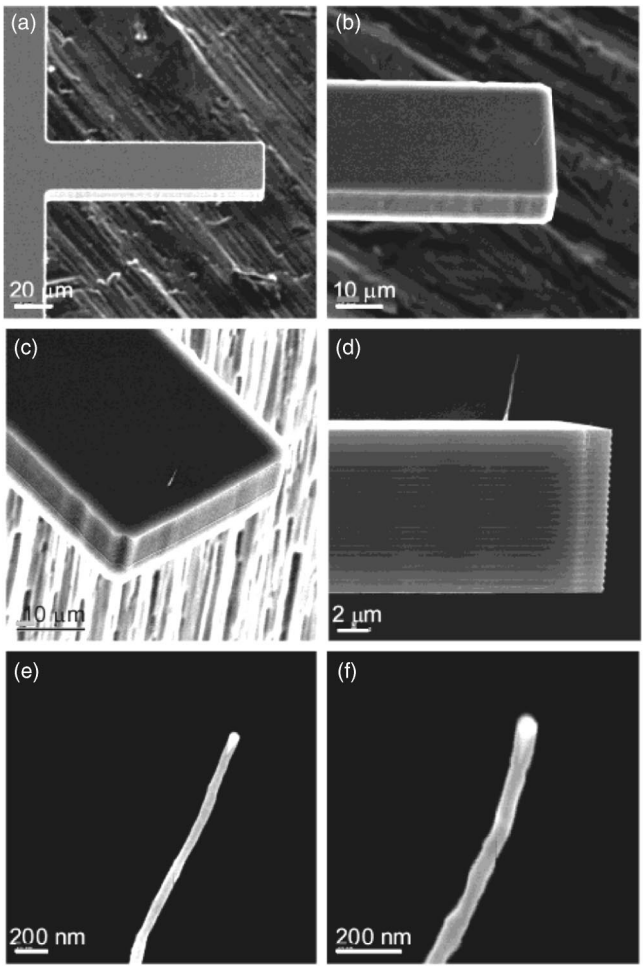

FIG. 39. VACNF as scanning probe tips synthesized on AFM cantilevers on the wafer scale. Adopted with permission from Ref. 35, Copyright 2004 American Chemical Society.

and numerous other surfaces since its inception.[218] Conventional AFM cantilevers have a pyramidal-shaped silicon probe, and advances in micromachining and fabrication technology allow this probe tip to be made as small as 10 nm. A small tip diameter is important for achieving high resolution, but a critical problem with the conventional silicon tips is their brittleness. As the tip wears out quickly, degradation of image resolution is unavoidable, resulting in the need to change the probe frequently. CNT probes, due to their small tip diameter (1–10 nm), offer very high resolution.[219,220] Their extraordinary strength and the ability to retain structural integrity during operation in contact or tapping mode make CNT tips very robust. Figure 39 shows an example of a CNT tip grown by thermal CVD at the end of a silicon cantilever. The ability to functionalize carbon nanostructures brings extended range of applications to scanning probe techniques.[221] Deterministic synthesis of vertically aligned carbon nanofibers by C-PECVD allows large-scale production of AFM tips on a wafer scale.[35]

F. Nanoelectromechanical devices (NEMS)

Nanoelectrochemical devices (NEMS) utilize geometrical, electrical, and mechanical properties of carbon nanostructures. Atomic force microscopy tips, discussed in the previous section, can also be classified as NEMS devices. In this case, CNTs and CNFs are parts of the AFM cantilever microelectromechanical device. Nanotubes themselves can be used as cantilevers as was demonstrated by Poncharal *et al.* who constructed a nanobalance that can be used for weighing nanoparticles.[222] Even though manipulation of single atoms has been demonstrated,[223] manipulation of nanoscale objects still remains a challenge. Kim and Lieber fabricated nanotweezers constructed using carbon nanotubes that may provide a universal means of nanomanipulation.[224] The integration of nanotweezers with AFM cantilevers brings an additional level of control over positioning and imaging.[225]

G. Nanoporous membranes

Membranes are used in a multitude of applications such as chemical separations, drug delivery, and waste water remediation, and membranes with nanometer-size pores are of special importance. Carbon nanotubes and carbon nanofibers can be used for this purpose in geometries parallel and perpendicular to the transport directions. Vertically aligned carbon nanotubes can be incorporated into a membrane by embedding into a polymer film.[199] In this case transport occurs inside the nanotubes perpendicular to the substrate. In another geometry the nanotubes or nanofibers can be placed perpendicular to the transport direction.[194] In this case the effective "pore size" is controlled by their density and size, which depends in turn on the catalyst particle preparation. Such membranes can be incorporated into microfluidic channels, for example, to mimic cell membrane functionality (Fig. 40).[226]

H. Other applications

There are many potential applications for carbon nanotubes and nanofibers that the research community continues to explore.[227] Some, such as composite materials, do not rely on deterministic synthesis.[175] In this case the bulk material is used as a filler of a polymer matrix, though directional alignment or alternating alignment may be needed to develop enhanced thermal or electrical conduction or great strength. Composite fibers produced by spinning CNTs with polymers can be made tougher than any natural or synthetic organic fiber. They can be used to make superstrong and superlight textiles.[228] They can also be used to make fiber supercapacitors that are suitable for weaving into textiles.

Hydrogen and energy storage are other areas in which carbon nanofibers can be of high importance, but there is much debate over the actual potential.[229–233] There is a continuous search for cleaner renewable energy sources, and hydrogen-based alternatives are being considered as attractive candidates. One of the main challenges for use of hydrogen is its storage, as currently there are no efficient and safe methods. Approaches now in use or under development include compressed hydrogen gas, liquid hydrogen, chemical storage in hydrides (e.g., metal hydrides), and gas-on-solid physisorption. Recently there were several reports on the perhaps extraordinary hydrogen storage ability of carbon nanostructured materials. For example, Chambers *et al.* re-

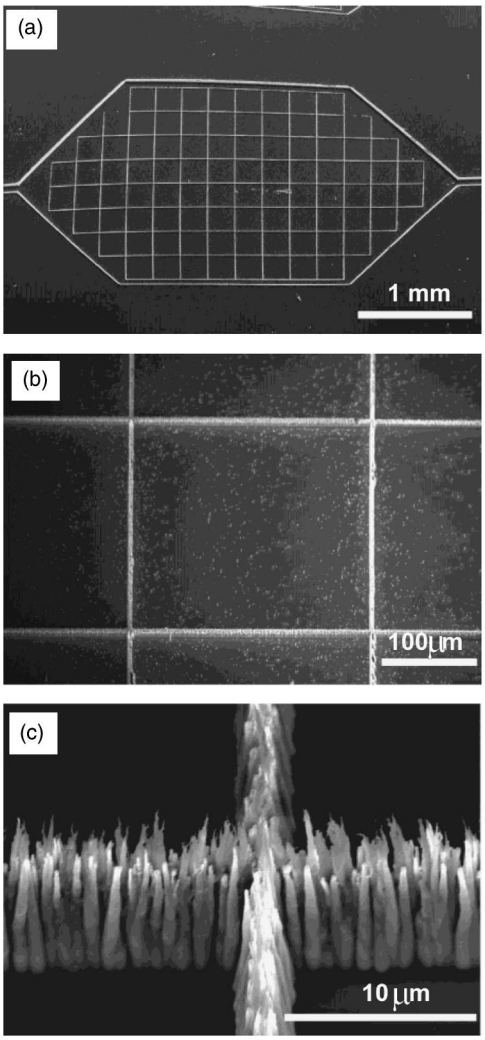

FIG. 40. VACNF forests as cell mimic membranes. Electron micrographs of the cell mimic structure. Panel A illustrates the overall design of the cell mimic device and the integrated microfluidic structure. The microfluidic inlet and outlet channels that allow fluid flow to the array of the cell structures are 50 μm wide and 10 μm deep. Panels B and C (30° viewing angle) show close-ups of a single cell and the component nanofibers, respectively. Reprinted with permission from Ref. 226, Copyright 2004 American Chemical Society.

ported that a material consisting of carbon nanofibers is capable of sorbing and retaining in an excess of 20 L (STP) of hydrogen per gram of carbon when the nanofibers are exposed to the gas at pressures of 120 atm at 25 °C,[21] which is an order of magnitude better than with the other means of hydrogen storage. They argued that this result, based on the measurements of pressure drop, is due to the unique crystalline arrangement existing within the graphite nanofiber structure, in which the graphene planes make a system of subnanometer pores with only the edge sites exposed. Since the interplanar distance within the material is 3.37 Å, sorption of molecular hydrogen, which possesses a kinetic diameter of 2.89 Å, is a facile process owing to the short diffusion path. Other reports with lower but still impressive values for the specific adsorption have also appeared. However, lately many of these results were disputed and much more moderate adsorption capacities in the range 0–2.5 wt % (at low temperatures and ambient pressures) were quoted. (See Ref. 234 and references within.)

VACNFs have been proposed for use in charge storage devices.[192] Ren *et al.* proposed to use VACNF electrodes coated with an electrically conducting polymer (such as polypyrrole) for electrical energy storage devices such as rechargeable batteries, fuel cells, and capacitors. For many such applications, a high charge capacity is required. In order to increase the capacity of a polymer battery without deteriorating the electrodic performance (charging/discharging rates) due to long ion diffusion time and migration length in the thick film, high surface area is required. The VACNF forest electrodes offer a high surface area conductive substrate.

The high surface area, size, hollow geometry, and chemical inertness of carbon nanotubes (CNTs) make them attractive for demanding applications in the field of gas sensing.[235] To date, studies on possible applications of CNTs have been focused either on individual single-walled carbon nanotubes (SWNTs) as sensitive materials for O_2, NO_2 and NH_3 sensing, or on multiwalled carbon nanotube (MWNT) mats as NH_3, CO, CO_2, humidity, and O_2 gas sensors.

Carbon materials have important advantages for use in catalysis including[236] (i) resistance to acid/base media, (ii) possibility to control, up to certain limits, the porosity and surface chemistry, and (iii) easy recovery of precious metals by support burning, resulting in low environment impact. In recent years, carbon nanofibers and carbon nanotubes have been shown to be promising candidates as catalyst supports. The major limitation for their extensive use so far remains high-ost and low-roduction volumes. Although a relatively high-yield process, CVD is a batch-type process and cannot be easily scaled up. There are many reports demonstrating that the characteristics of CVD-grown carbon nanofibers are promising for catalyst support. For example, Pesant *et al.* recently demonstrated that CNF-supported palladium catalyst showed higher conversion performance in liquid-phase hydrogenation of nitrobenzene into aniline, compared to palladium catalyst supported on high surface area activated charcoal.[237] They explain such increase by the higher surface-to-volume ratio of CNF material.

Another use of enhanced electron field-emission characteristics of carbon nanotubes is in electric lighting devices.[238] It is interesting to note that the proposed application for "carbon filaments" in 1889 was for a lighting device as well as filament of an electric light bulb.[1]

V. FUTURE DEVELOPMENTS AND CONCLUSIONS

Significant progress has been made to achieve controlled synthesis and directed assembly of carbon nanostructures. However, there is still a need for a process that operates at temperatures that can be tolerated by a larger variety of substrate materials, yet provides greater control of nanostructure properties. A better understanding of the fundamental mechanisms of nanostructure nucleation and growth points the way for future work. The key to the catalytic growth of carbon nanofibers is in the processes that occur at the surface of or within the catalytic particle. Plasma processing provides a way to control these processes via interaction with the electromagnetic field. The electric field plays a crucial role in the

alignment control of carbon nanofibers by the coupling of mechanical force to the synthesis process. High-frequency electromagnetic fields, augmented by field enhancement at the tip of a nanofiber, may be the way to control the temperature of the catalyst separately from the substrate. Another major challenge is the precise control of the nanofiber structure. The growth of isolated single vertically aligned carbon nanotubes, mulitwalled or singlewalled, is yet to be demonstrated. We are just beginning to gain an understanding of the processes that control the arrangement of graphene layers of a growing nanostructure. The relation of a carbon nanofiber structure and catalyst particle shape, crystallographic orientation, and their dynamics will eventually be understood and an additional level of control of synthesis will be achieved, bringing future possibilities for practical nanoscale devices due to improved characteristics.

ACKNOWLEDGMENTS

We would like to thank I. A. Merkulov and G. Eres for fruitful discussions. This work was sponsored by Material Sciences and Engineering Division Program of the DOE Office of Science under Contract No. DE-AC05-00OR22725 with UT-Battelle LLC, the Defense Advanced Research Projects Agency (DARPA) under Contract No. DE-AC05-00OR22725, and the Center for Nanophase Materials Sciences (CNMS) Research Scholar Program.

[1]T. V. Hughes and C. R. Chambers, *Manufacture of Carbon Filaments*, US Patent No. 405, 480, (1889).
[2]L. V. Radushkevich and V. M. Lukyanovich, Zh. Fiz. Khim. **26**, 88 (1952).
[3]R. T. K. Baker, Carbon **27**, 315 (1989).
[4]R. T. K. Baker and P. S. Harris, in *Chemistry and Physics of Carbon*, edited by P. L. Walker (Marcel Dekker, New York, 1978), pp. 83–165.
[5]H. W. Kroto, J. R. Heath, S. C. Obrien, R. F. Curl, and R. E. Smalley, Nature (London) **318**, 162 (1985).
[6]S. Iijima, Nature (London) **354**, 56 (1991).
[7]Y. Chen, Z. L. Wang, J. S. Yin, D. J. Johnson, and R. H. Prince, Chem. Phys. Lett. **272**, 178 (1997).
[8]Z. F. Ren, Z. P. Huang, J. W. Xu, J. H. Wang, P. Bush, M. P. Siegal, and P. N. Provencio, Science **282**, 1105 (1998).
[9]V. I. Merkulov, D. H. Lowndes, Y. Y. Wei, G. Eres, and E. Voelkl, Appl. Phys. Lett. **76**, 3555 (2000).
[10]Z. F. Ren *et al.*, Appl. Phys. Lett. **75**, 1086 (1999).
[11]K. P. De Jong and J. W. Geus, Catal. Rev. - Sci. Eng. **42**, 481 (2000).
[12]N. M. Rodriguez, J. Mater. Res. **8**, 3233 (1993).
[13]M. Meyyappan, L. Delzeit, A. Cassell, and D. Hash, Plasma Sources Sci. Technol. **12**, 205 (2003).
[14]H. J. Dai, Surf. Sci. **500**, 218 (2002).
[15]M. S. Dresselhaus and M. Endo, in *Carbon Nanotubes* (2001), pp. 11–28.
[16]K. B. K. Teo, C. Singh, M. Chhowalla, and W. I. Milne, in *Encyclopedia of Nanoscience and Nanotechnology*, edited by H. S. Nalwa (American Scientific Publishers, 2003), pp. 1–22.
[17]A. Huczko, Appl. Phys. A: Mater. Sci. Process. **74**, 617 (2002).
[18]L. M. Dai, A. Patil, X. Y. Gong, Z. X. Guo, L. Q. Liu, Y. Liu, and D. B. Zhu, ChemPhysChem **4**, 1150 (2003).
[19]A. Krishnan, E. Dujardin, M. M. J. Treacy, J. Hugdahl, S. Lynum, and T. W. Ebbesen, Nature (London) **388**, 451 (1997).
[20]M. Endo *et al.*, Appl. Phys. Lett. **80**, 1267 (2002).
[21]A. Chambers, C. Park, R. T. K. Baker, and N. M. Rodriguez, J. Phys. Chem. B **102**, 4253 (1998).
[22]L. Delzeit, I. McAninch, B. A. Cruden, D. Hash, B. Chen, J. Han, and M. Meyyappan, J. Appl. Phys. **91**, 6027 (2002).
[23]Y. Huang, X. F. Duan, Y. Cui, L. J. Lauhon, K. H. Kim, and C. M. Lieber, Science **294**, 1313 (2001).
[24]V. I. Merkulov, A. V. Melechko, M. A. Guillorn, D. H. Lowndes, and M. L. Simpson, Appl. Phys. Lett. **79**, 2970 (2001).
[25]J. Koehne, H. Chen, J. Li, A. M. Cassell, Q. Ye, H. T. Ng, J. Han, and M. Meyyappan, Nanotechnology **14**, 1239 (2003).
[26]X. J. Yang *et al.*, Nano Lett. **3**, 1751 (2003).
[27]M. A. Guillorn, M. D. Hale, V. I. Merkulov, M. L. Simpson, G. Y. Eres, H. Cui, A. A. Puretzky, and D. B. Geohegan, Appl. Phys. Lett. **81**, 2860 (2002).
[28]L. R. Baylor *et al.*, J. Vac. Sci. Technol. B **20**, 2646 (2002).
[29]M. A. Guillorn, A. V. Melechko, V. I. Merkulov, E. D. Ellis, C. L. Britton, M. L. Simpson, D. H. Lowndes, and L. R. Baylor, Appl. Phys. Lett. **79**, 3506 (2001).
[30]V. I. Merkulov, A. V. Melechko, M. A. Guillorn, D. H. Lowndes, and M. L. Simpson, Chem. Phys. Lett. **350**, 381 (2001).
[31]M. A. Guillorn, A. V. Melechko, V. I. Merkulov, D. K. Hensley, M. L. Simpson, and D. H. Lowndes, Appl. Phys. Lett. **81**, 3660 (2002).
[32]M. A. Guillorn, M. L. Simpson, G. J. Bordonaro, V. I. Merkulov, L. R. Baylor, and D. H. Lowndes, J. Vac. Sci. Technol. B **19**, 573 (2001).
[33]A. V. Melechko, T. E. McKnight, M. A. Guillorn, V. I. Merkulov, B. Ilic, M. J. Doktycz, D. H. Lowndes, and M. L. Simpson, Appl. Phys. Lett. **82**, 976 (2003).
[34]J. Moser, R. Panepucci, Z. P. Huang, W. Z. Li, Z. F. Ren, A. Usheva, and M. J. Naughton, J. Vac. Sci. Technol. B **21**, 1004 (2003).
[35]Q. Ye, A. Cassell, H. Liu, K.-J. Chao, J. Han, and M. Meyyappan, Nano Lett. **4**, 1301 (2004).
[36]Z. G. Mao, A. Garg, and S. B. Sinnott, Nanotechnology **10**, 273 (1999).
[37]W. Kratschmer, L. D. Lamb, K. Fostiropoulos, and D. R. Huffman, Nature (London) **347**, 354 (1990).
[38]C. V. Nguyen, L. Delziet, K. Matthews, B. Chen, and M. Meyyappan, J. Nanosci. Nanotechnol. **3**, 121 (2003).
[39]A. V. Melechko *et al.*, J. Vac. Sci. Technol. B **20**, 2730 (2002).
[40]A. M. Cassell, J. A. Raymakers, J. Kong, and H. J. Dai, J. Phys. Chem. B **103**, 6484 (1999).
[41]M. J. Bronikowski, P. A. Willis, D. T. Colbert, K. A. Smith, and R. E. Smalley, J. Vac. Sci. Technol. A **19**, 1800 (2001).
[42]W. Z. Li, S. S. Xie, L. X. Qian, B. H. Chang, B. S. Zou, W. Y. Zhou, R. A. Zhao, and G. Wang, Science **274**, 1701 (1996).
[43]A. Moisala, A. G. Nasibulin, and E. I. Kauppinen, J. Phys.: Condens. Matter **15**, S3011 (2003).
[44]H. Kanzow and A. Ding, Phys. Rev. B **60**, 11180 (1999).
[45]L. Delzeit, C. V. Nguyen, B. Chen, R. Stevens, A. Cassell, J. Han, and M. Meyyappan, J. Phys. Chem. B **106**, 5629 (2002).
[46]G. Eres, A. A. Puretzky, D. B. Geohegan, and H. Cui, Appl. Phys. Lett. **84**, 1759 (2004).
[47]G. Eres, A. A. Puretzky, D. B. Geohegan, and H. Cui, In situ Control of Catalyst Efficiency in Chemical Vapor Deposition of Long Vertically Aligned Carbon Nanotubes, in March Meeting of American Physical Society, Montreal, Canada, 22–26 March 2004 (unpublished).
[48]P. A. Tesner and I. S. Rafalkes, Dokl. Akad. Nauk SSSR **87**, 821 (1952).
[49]P. A. Tesner, R. Ey, I. S. Rafalkes, and E. F. Arefieva, Carbon **8**, 453 (1970).
[50]R. T. K. Baker, M. A. Barber, R. J. Waite, P. S. Harris, and F. S. Feates, J. Catal. **26**, 51 (1972).
[51]R. T. Yang and J. P. Chen, J. Catal. **115**, 52 (1989).
[52]J. R. Nielsen and D. L. Trimm, J. Catal. **48**, 155 (1977).
[53]A. Sacco, P. Thacker, T. N. Chang, and A. T. S. Chiang, J. Catal. **85**, 224 (1984).
[54]A. Kock, P. K. Debokx, E. Boellaard, W. Klop, and J. W. Geus, J. Catal. **96**, 468 (1985).
[55]I. Alstrup, J. Catal. **109**, 241 (1988).
[56]J. W. Snoeck, G. F. Froment, and M. Fowles, J. Catal. **169**, 240 (1997).
[57]P. M. Ajayan, Nature (London) **427**, 402 (2004).
[58]S. Helveg, C. Lopez-Cartes, J. Sehested, P. L. Hansen, B. S. Clausen, J. R. Rostrup-Nielsen, F. Abild-Pedersen, and J. K. Norskov, Nature (London) **427**, 426 (2004).
[59]M. Chhowalla *et al.*, J. Appl. Phys. **90**, 5308 (2001).
[60]S. S. Fan, M. G. Chapline, N. R. Franklin, T. W. Tombler, A. M. Cassell, and H. J. Dai, Science **283**, 512 (1999).
[61]C. Bower, O. Zhou, W. Zhu, D. J. Werder, and S. H. Jin, Appl. Phys. Lett. **77**, 2767 (2000).
[62]J. I. Sohn, S. Lee, Y. H. Song, S. Y. Choi, K. I. Cho, and K. S. Nam, Appl. Phys. Lett. **78**, 901 (2001).
[63]A. V. Melechko, V. I. Merkulov, D. H. Lowndes, M. A. Guillorn, and M. L. Simpson, Chem. Phys. Lett. **356**, 527 (2002).
[64]D. C. Li, L. M. Dai, S. M. Huang, A. W. H. Mau, and Z. L. Wang, Chem. Phys. Lett. **316**, 349 (2000).

[65] J. Li, C. Papadopoulos, J. M. Xu, and M. Moskovits, Appl. Phys. Lett. **75**, 367 (1999).
[66] F. Jansen, *Plasma Enhanced Chemical Vapor Depositon*, in AVS Monograph Series, edited by H. G. Tompkins (American Vacuum Society, New York, 1998).
[67] S. Honda, M. Katayama, K. Y. Lee, T. Ikuno, S. Ohkura, K. Oura, H. Furuta, and T. Hirao, Jpn. J. Appl. Phys., Part 2 **42**, L441 (2003).
[68] K. Y. Lee *et al.*, Jpn. J. Appl. Phys., Part 2 **42**, L804 (2003).
[69] B. O. Boskovic, V. Stolojan, R. U. A. Khan, S. Haq, and S. R. P. Silva, Nat. Mater. **1**, 165 (2002).
[70] S. Hofmann, C. Ducati, J. Robertson, and B. Kleinsorge, Appl. Phys. Lett. **83**, 135 (2003).
[71] K. Hamad-Schifferli, J. J. Schwartz, A. T. Santos, S. G. Zhang, and J. M. Jacobson, Nature (London) **415**, 152 (2002).
[72] R. Hergt, W. Andra, C. G. d'Ambly, I. Hilger, W. A. Kaiser, U. Richter, and H. G. Schmidt, IEEE Trans. Magn. **34**, 3745 (1998).
[73] K. B. K. Teo *et al.*, Nano Lett. **4**, 921 (2004).
[74] N. Mutsukura, K. Kobayashi, and Y. Machi, J. Appl. Phys. **68**, 2657 (1990).
[75] D. R. Cote, S. V. Nguyen, A. K. Stamper, D. S. Armbrust, D. Tobben, R. A. Conti, and G. Y. Lee, IBM J. Res. Dev. **43**, 5 (1999).
[76] M. Funer, C. Wild, and P. Koidl, Appl. Phys. Lett. **72**, 1149 (1998).
[77] Y. Y. Wei, G. Eres, V. I. Merkulov, and D. H. Lowndes, Appl. Phys. Lett. **78**, 1394 (2001).
[78] V. I. Merkulov, M. A. Guillorn, D. H. Lowndes, M. L. Simpson, and E. Voelkl, Appl. Phys. Lett. **79**, 1178 (2001).
[79] K. B. K. Teo *et al.*, Appl. Phys. Lett. **79**, 1534 (2001).
[80] K. B. K. Teo *et al.*, J. Vac. Sci. Technol. B **20**, 116 (2002).
[81] K. B. K. Teo *et al.*, Nanotechnology **14**, 204 (2003).
[82] M. Tanemura, K. Iwata, K. Takahashi, Y. Fujimoto, F. Okuyama, H. Sugie, and V. Filip, J. Appl. Phys. **90**, 1529 (2001).
[83] J. H. Yim, S. Choi, S. Lee, and K. H. Koh, J. Vac. Sci. Technol. B **22**, 1308 (2004).
[84] M. A. Guillorn, T. E. McKnight, A. Melechko, V. I. Merkulov, P. F. Britt, D. W. Austin, D. H. Lowndes, and M. L. Simpson, J. Appl. Phys. **91**, 3824 (2002).
[85] B. A. Cruden, A. M. Cassell, Q. Ye, and M. Meyyappan, J. Appl. Phys. **94**, 4070 (2003).
[86] Y. Chen, L. P. Guo, D. J. Johnson, and R. H. Prince, J. Cryst. Growth **193**, 342 (1998).
[87] R. Haubner and B. Lux, Diamond Relat. Mater. **2**, 1277 (1993).
[88] D. Hash, D. Bose, T. R. Govindan, and M. Meyyappan, J. Appl. Phys. **93**, 6284 (2003).
[89] D. B. Hash and M. Meyyappan, J. Appl. Phys. **93**, 750 (2003).
[90] J. Han, W. S. Yang, J. B. Yoo, and C. Y. Park, J. Appl. Phys. **88**, 7363 (2000).
[91] Q. Yang, C. Xiao, W. Chen, A. K. Singh, T. Asai, and A. Hirose, Diamond Relat. Mater. **12**, 1482 (2003).
[92] K. M. Lee, H. J. Han, S. H. Choi, K. H. Park, S. Oh, S. Lee, and K. H. Koh, J. Vac. Sci. Technol. B **21**, 623 (2003).
[93] G. W. Ho, A. T. S. Wee, J. Lin, and W. C. Tjiu, Thin Solid Films **388**, 73 (2001).
[94] T. Hirata, N. Satake, G. H. Jeong, T. Kato, R. Hatakeyama, K. Motomiya, and K. Tohji, Appl. Phys. Lett. **83**, 1119 (2003).
[95] T. Ikuno *et al.*, Surf. Interface Anal. **35**, 15 (2003).
[96] S. S. Kim, H. Y. Chang, C. S. Chang, and N. S. Yoon, Appl. Phys. Lett. **77**, 492 (2000).
[97] P. E. Nolan, D. C. Lynch, and A. H. Cutler, J. Phys. Chem. B **102**, 4165 (1998).
[98] J. B. O. Caughman, L. R. Baylor, M. A. Guillorn, V. I. Merkulov, D. H. Lowndes, and L. F. Allard, Appl. Phys. Lett. **83**, 1207 (2003).
[99] O. M. Kuttel, O. Groening, C. Emmenegger, and L. Schlapbach, Appl. Phys. Lett. **73**, 2113 (1998).
[100] D. Ugarte, Nature (London) **359**, 707 (1992).
[101] L. C. Qin, D. Zhou, A. R. Krauss, and D. M. Gruen, Appl. Phys. Lett. **72**, 3437 (1998).
[102] C. Bower, W. Zhu, S. H. Jin, and O. Zhou, Appl. Phys. Lett. **77**, 830 (2000).
[103] M. Yoshimura, S. Jo, and K. Ueda, Jpn. J. Appl. Phys., Part 1 **42**, 4841 (2003).
[104] Y. S. Woo, D. Y. Jeon, I. T. Han, N. S. Lee, J. E. Jung, and J. M. Kim, Diamond Relat. Mater. **11**, 59 (2002).
[105] C. L. Tsai, C. F. Chen, and L. K. Wu, Appl. Phys. Lett. **81**, 721 (2002).
[106] H. Cui, O. Zhou, and B. R. Stoner, J. Appl. Phys. **88**, 6072 (2000).
[107] S. H. Tsai, C. W. Chao, C. L. Lee, and H. C. Shih, Appl. Phys. Lett. **74**, 3462 (1999).
[108] Q. Zhang, S. F. Yoon, J. Ahn, B. Gan, Rusli, and M. B. Yu, J. Phys. Chem. Solids **61**, 1179 (2000).
[109] Y. C. Choi, Y. M. Shin, S. C. Lim, D. J. Bae, Y. H. Lee, B. S. Lee, and D. C. Chung, J. Appl. Phys. **88**, 4898 (2000).
[110] Y. C. Choi, D. J. Bae, Y. H. Lee, B. S. Lee, I. T. Han, W. B. Choi, N. S. Lee, and J. M. Kim, Synth. Met. **108**, 159 (2000).
[111] H. Sato, H. Tagegawa, and Y. Saito, J. Vac. Sci. Technol. B **21**, 2564 (2003).
[112] M. Okai, T. Muneyoshi, T. Yaguchi, and S. Sasaki, Appl. Phys. Lett. **77**, 3468 (2000).
[113] C. H. Lin, H. L. Chang, C. M. Hsu, A. Y. Lo, and C. T. Kuo, Diamond Relat. Mater. **12**, 1851 (2003).
[114] D. J. Willins and R. L. F. Boyd, J. Phys. D **6**, 1447 (1973).
[115] A. Huczko, H. Lange, M. Sioda, Y. Q. Zhu, W. K. Hsu, and D. R. M. Walton, J. Phys. Chem. B **106**, 1534 (2002).
[116] Y. Y. Xia, Y. G. Mu, Y. C. Ma, S. Y. Li, H. D. Zhang, C. Y. Tan, and L. M. Mei, Nucl. Instrum. Methods Phys. Res. B **155**, 395 (1999).
[117] M. W. Li, Z. Hu, X. Z. Wang, Q. Wu, and Y. Chen, J. Mater. Sci. Lett. **22**, 1223 (2003).
[118] A. Marafee, C. J. Liu, G. H. Xu, R. Mallinson, and L. Lobban, Ind. Eng. Chem. Res. **36**, 632 (1997).
[119] V. I. Merkulov, A. V. Melechko, M. A. Guillorn, D. H. Lowndes, and M. L. Simpson, Appl. Phys. Lett. **80**, 476 (2002).
[120] J. Ma, C. Park, N. M. Rodriguez, and R. T. K. Baker, J. Phys. Chem. B **105**, 11 994 (2001).
[121] V. I. Merkulov, D. K. Hensley, A. V. Melechko, M. A. Guillorn, D. H. Lowndes, and M. L. Simpson, J. Phys. Chem. B **106**, 10 570 (2002).
[122] V. Merkulov, A. V. Melechko, M. A. Guillorn, D. H. Lowndes, and M. L. Simpson, Chem. Phys. Lett. **361**, 492 (2002).
[123] M. Laudon, N. N. Carlson, and M. P. Masqueller, Appl. Phys. Lett. **78**, 201 (2001).
[124] V. I. Merkulov, A. V. Melechko, M. A. Guillorn, M. L. Simpson, D. H. Lowndes, J. H. Whealton, and R. J. Raridon, Appl. Phys. Lett. **80**, 4816 (2002).
[125] A. V. Melechko, T. E. McKnight, D. K. Hensley, M. A. Guillorn, A. Y. Borisevich, V. I. Merkulov, D. H. Lowndes, and M. L. Simpson, Nanotechnology **14**, 1029 (2003).
[126] K. M. Ryu, M. Y. Kang, Y. D. Kim, and H. T. Jeon, Jpn. J. Appl. Phys., Part 1 **42**, 3578 (2003).
[127] M. Nihei, A. Kawabata, and Y. Awano, Jpn. J. Appl. Phys., Part 2 **42**, L721 (2003).
[128] P. M. Campbell, E. S. Snow, and J. P. Novak, Appl. Phys. Lett. **81**, 4586 (2002).
[129] C. J. Lee, S. C. Lyu, Y. R. Cho, J. H. Lee, and K. I. Cho, Chem. Phys. Lett. **341**, 245 (2001).
[130] L. Delzeit, B. Chen, A. Cassell, R. Stevens, C. Nguyen, and M. Meyyappan, Chem. Phys. Lett. **348**, 368 (2001).
[131] H. M. Christen, A. A. Puretzky, H. Cui, P. H. Belay, P. H. Fleming, D. B. Geohegan, and D. H. Lowndes, Nano Lett. **4**, 1939 (2004).
[132] S. Y. Zaginaichenko, D. V. Schur, and Z. A. Matysina, Carbon **41**, 1349 (2003).
[133] M. S. Kim, N. M. Rodriguez, and R. T. K. Baker, J. Catal. **131**, 60 (1991).
[134] P. D. Kichambare, D. Qian, E. C. Dickey, and C. A. Grimes, Carbon **40**, 1903 (2002).
[135] Y. Nishiyama and Y. Tamai, J. Catal. **33**, 98 (1974).
[136] K. Kamada *et al.*, Appl. Surf. Sci. **212**, 383 (2003).
[137] I. Alstrup, M. T. Tavares, C. A. Bernardo, O. Sorensen, and J. R. Rostrup-Nielsen, Mater. Corros. **49**, 367 (1998).
[138] A. Chambers, N. M. Rodriguez, and R. T. K. Baker, J. Mater. Res. **11**, 430 (1996).
[139] D. Pradhan, M. Sharon, M. Kumar, and Y. Ando, J. Nanosci. Nanotechnol. **3**, 215 (2003).
[140] W. Z. Li, J. G. Wen, and Z. F. Ren, Appl. Phys. Lett. **79**, 1879 (2001).
[141] C. A. Bernardo, I. Alstrup, and J. R. Rostrup-Nielsen, J. Catal. **96**, 517 (1985).
[142] L. B. Avdeeva, O. V. Goncharova, D. I. Kochubey, V. I. Zaikovskii, L. M. Plyasova, B. N. Novgorodov, and S. K. Shaikhutdinov, Appl. Catal., A **141**, 117 (1996).
[143] B. Gan *et al.*, Diamond Relat. Mater. **9**, 897 (2000).
[144] H. T. Ng, B. Chen, J. E. Koehne, A. M. Cassell, J. Li, J. Han, and M. Meyyappan, J. Phys. Chem. B **107**, 8484 (2003).

[145] A. M. Cassell, Q. Ye, B. A. Cruden, J. Li, P. C. Sarrazin, H. T. Ng, J. Han, and M. Meyyappan, Nanotechnology **15**, 9 (2004).
[146] D. H. Kim and H. R. Lee, J. Korean Phys. Soc. **44**, L208 (2004).
[147] A. G. Naumovets and Z. Y. Zhang, Surf. Sci. **500**, 414 (2002).
[148] H. Cui, X. Yang, M. L. Simpson, D. H. Lowndes, and M. Varela, Appl. Phys. Lett. **84**, 4077 (2004).
[149] T. Ichihashi, J. Fujita, M. Ishida, and Y. Ochiai, Phys. Rev. Lett. **92**, 215702 (2004).
[150] M. S. Dresselhaus, *Encyclopedia of Materials: Science and Technology* (Elsevier Science, New York, 2001).
[151] R. Bacon, J. Appl. Phys. **31**, 283 (1960).
[152] Y. Chen, D. T. Shaw, and L. P. Guo, Appl. Phys. Lett. **76**, 2469 (2000).
[153] M. Endo *et al.*, Carbon **41**, 1941 (2003).
[154] N. A. Kiselev *et al.*, Carbon **42**, 149 (2004).
[155] M. H. Kuang, Z. L. Wang, X. D. Bai, J. D. Guo, and E. G. Wang, Appl. Phys. Lett. **76**, 1255 (2000).
[156] L. Dong, J. Jiao, C. Pan, and D. W. Tuggle, Appl. Phys. A: Mater. Sci. Process. **78**, 9 (2004).
[157] S. B. Lee, K. B. K. Teo, M. Chhowalla, D. G. Hasko, G. A. J. Amaratunga, W. I. Milne, and H. Ahmed, Microelectron. Eng. **61–62**, 475 (2002).
[158] C. Schonenberger, A. Bachtold, C. Strunk, J. P. Salvetat, and L. Forro, Appl. Phys. A: Mater. Sci. Process. **A69**, 283 (1999).
[159] A. Thess *et al.*, Science **273**, 483 (1996).
[160] L. Zhang, D. Austin, V. I. Merkulov, A. V. Melechko, K. L. Klein, M. A. Guillorn, D. H. Lowndes, and M. L. Simpson, Appl. Phys. Lett. **84**, 3972 (2004).
[161] R. H. Fowler and L. Nordheim, Proc. R. Soc. London, Ser. A **119**, 173 (1928).
[162] T. Utsumi, IEEE Trans. Electron Devices **38**, 2276 (1991).
[163] F. S. Baker, J. Williams, and A. R. Osborn, Nature (London) **239**, 96 (1972).
[164] C. Lea, J. Phys. D **6**, 1105 (1973).
[165] K. A. Dean and B. R. Chalamala, Appl. Phys. Lett. **75**, 3017 (1999).
[166] L. R. Baylor (private communication).
[167] W. A. Deheer, A. Chatelain, and D. Ugarte, Science **270**, 1179 (1995).
[168] V. I. Merkulov, D. H. Lowndes, and L. R. Baylor, J. Appl. Phys. **89**, 1933 (2001).
[169] W. D. J. Callister, *Materials Science and Engineering an Introduction*, 6th ed. (Wiley, New York, 2003).
[170] B. McEnaney, *Encyclopedia of Materials: Science and Technology* (Amsterdam, New York, 2001), pp. 967–975.
[171] B. G. Demczyk, Y. M. Wang, J. Cumings, M. Hetman, W. Han, A. Zettl, and R. O. Ritchie, Mater. Sci. Eng., A **334**, 173 (2002).
[172] R. S. Ruoff, D. Qian, and W. K. Liu, C. R. Phys. **4**, 993 (2003).
[173] M. F. Yu, O. Lourie, M. J. Dyer, K. Moloni, T. F. Kelly, and R. S. Ruoff, Science **287**, 637 (2000).
[174] R. P. Gao, Z. L. Wang, Z. G. Bai, W. A. de Heer, L. M. Dai, and M. Gao, Phys. Rev. Lett. **85**, 622 (2000).
[175] E. T. Thostenson, Z. F. Ren, and T. W. Chou, Compos. Sci. Technol. **61**, 1899 (2001).
[176] M. C. Weisenberger, E. A. Grulke, D. Jacques, T. Rantell, and R. Andrews, J. Nanosci. Nanotechnol. **3**, 535 (2003).
[177] R. L. McCreery, in *Electroanalytical Chemistry*, edited by A. J. Bard (Marcel Dekker, New York, 1991).
[178] R. J. Chen, Y. G. Zhan, D. W. Wang, and H. J. Dai, J. Am. Chem. Soc. **123**, 3838 (2001).
[179] J. L. Bahr and J. M. Tour, J. Mater. Chem. **12**, 1952 (2002).
[180] E. T. Mickelson, C. B. Huffman, A. G. Rinzler, R. E. Smalley, R. H. Hauge, and J. L. Margrave, Chem. Phys. Lett. **296**, 188 (1998).
[181] G. T. Hermanson, *Boiconjugate Techniques* (Academic, San Diego, 1996).
[182] Y. H. Lin, F. Lu, Y. Tu, and Z. F. Ren, Nano Lett. **4**, 191 (2004).
[183] C. V. Nguyen, L. Delzeit, A. M. Cassell, J. Li, J. Han, and M. Meyyappan, Nano Lett. **2**, 1079 (2002).
[184] T. E. McKnight *et al.*, Nanotechnology **14**, 551 (2003).
[185] K. Kinoshita, *Carbon: Electrochemical and Physiological Properties* (Wiley, New York 1988).
[186] J. Li, A. Cassell, L. Delzeit, J. Han, and M. Meyyappan, J. Phys. Chem. B **106**, 9299 (2002).
[187] M. A. Murphy, G. D. Wilcox, R. H. Dahm, and F. Marken, Electrochem. Commun. **5**, 51 (2003).
[188] T. E. McKnight *et al.*, J. Phys. Chem. B **107**, 10722 (2003).
[189] Y. Tu, Y. H. Lin, and Z. F. Ren, Nano Lett. **3**, 107 (2003).
[190] J. Li, H. T. Ng, A. Cassell, W. Fan, H. Chen, Q. Ye, J. Koehne, J. Han, and M. Meyyappan, Nano Lett. **3**, 597 (2003).
[191] T. E. McKnight, A. V. Melechko, D. W. Austin, T. Sims, M. A. Guillorn, and M. L. Simpson, J. Phys. Chem. B **108**, 7115 (2004).
[192] J. H. Chen, Z. P. Huang, D. Z. Wang, S. X. Yang, W. Z. Li, J. G. Wen, and Z. F. Ren, Synth. Met. **125**, 289 (2001).
[193] J. Koehne, J. Li, A. M. Cassell, H. Chen, Q. Ye, H. T. Ng, J. Han, and M. Meyyappan, J. Mater. Chem. **14**, 676 (2004).
[194] L. Zhang, A. V. Melechko, V. I. Merkulov, M. A. Guillorn, M. L. Simpson, D. H. Lowndes, and M. J. Doktycz, Appl. Phys. Lett. **81**, 135 (2002).
[195] M. A. Guillorn, A. V. Melechko, V. I. Merkulov, E. D. Ellis, M. L. Simpson, L. R. Baylor, and G. J. Bordonaro, J. Vac. Sci. Technol. B **19**, 2598 (2001).
[196] T. Ikuno, M. Katayama, K. Y. Lee, T. Kuzuoka, J. G. Lee, S. Honda, H. Mori, and K. Oura, Jpn. J. Appl. Phys., Part 2 **43**, L987 (2004).
[197] S. M. Huang, L. M. Dai, and A. W. H. Mau, J. Phys. Chem. B **103**, 4223 (1999).
[198] T. Ito, L. Sun, and R. M. Crooks, Electrochem. Solid-State Lett. **6**, C4 (2003).
[199] B. J. Hinds, N. Chopra, T. Rantell, R. Andrews, V. Gavalas, and L. G. Bachas, Science **303**, 62 (2004).
[200] D. Temple, Mater. Sci. Eng., R. **24**, 185 (1999).
[201] X. P. Xu and G. R. Brandes, Appl. Phys. Lett. **74**, 2549 (1999).
[202] G. Pirio, P. Legagneux, D. Pribat, K. B. K. Teo, M. Chhowalla, G. A. J. Amaratunga, and W. I. Milne, Nanotechnology **13**, 1 (2002).
[203] X. Xu and G. R. Brandes, *Carbon nanotube-based vacuum microelectronic gated cathode*, in Materials Issues in Vacuum Microelectronics Symposium, 13–16 April 1998 (Materials Research Society, San Francisco, CA, 1998).
[204] K. B. K. Teo *et al.*, J. Vac. Sci. Technol. B **21**, 693 (2003).
[205] M. A. Guillorn *et al.*, J. Vac. Sci. Technol. B **22**, 35 (2004).
[206] L. R. Baylor *et al.*, J. Vac. Sci. Technol. B **22**, 3021 (2004).
[207] OxfordInstruments, Oxford instruments.
[208] H. Sugie, M. Tanemura, V. Filip, K. Iwata, K. Takahashi, and F. Okuyama, Appl. Phys. Lett. **78**, 2578 (2001).
[209] G. Z. Yue *et al.*, Appl. Phys. Lett. **81**, 355 (2002).
[210] T. Matsumoto and H. Mimura, Appl. Phys. Lett. **82**, 1637 (2003).
[211] R. A. Wallingford and A. G. Ewing, Anal. Chem. **59**, 1762 (1987).
[212] A. J. Bard, F. R. F. Fan, J. Kwak, and O. Lev, Anal. Chem. **61**, 132 (1989).
[213] R. M. Wightman *et al.*, Proc. Natl. Acad. Sci. U.S.A. **88**, 10754 (1991).
[214] G. L. Prasanna and T. Panda, Bioprocess Eng. **16**, 261 (1997).
[215] A. Radford, S. Pope, A. Sazci, M. J. Fraser, and J. H. Parish, Mol. Gen. Genet. **184**, 567 (1981).
[216] N. J. Taylor and C. M. Fauquet, DNA Cell Biol. **21**, 963 (2002).
[217] T. E. McKnight, A. V. Melechko, D. K. Hensley, D. G. J. Mann, G. D. Griffin, and M. L. Simpson, Nano Lett. **4**, 1213 (2004).
[218] G. Binnig, C. F. Quate, and C. Gerber, Phys. Rev. Lett. **56**, 930 (1986).
[219] L. Delzeit, C. Nguyen, R. Stevens, J. Han, and M. Meyyappan, Nanotechnology **13**, 280 (2002).
[220] C. V. Nguyen, K. J. Chao, R. M. D. Stevens, L. Delzeit, A. Cassell, J. Han, and M. Meyyappan, Nanotechnology **12**, 363 (2001).
[221] J. H. Hafner, C. L. Cheung, and C. M. Lieber, J. Am. Chem. Soc. **121**, 9750 (1999).
[222] P. Poncharal, Z. L. Wang, D. Ugarte, and W. A. de Heer, Science **283**, 1513 (1999).
[223] D. M. Eigler and E. K. Schweizer, Nature (London) **344**, 524 (1990).
[224] P. Kim and C. M. Lieber, Science **286**, 2148 (1999).
[225] S. Akita *et al.*, Appl. Phys. Lett. **79**, 1691 (2001).
[226] B. L. Fletcher *et al.*, Nano Lett. **4**, 1809 (2004).
[227] P. M. Ajayan and O. Z. Zhou, Top. Appl. Phys. **800**, 391 (2001).
[228] A. B. Dalton *et al.*, Nature (London) **423**, 703 (2003).
[229] A. Zuttel, P. Sudan, P. Mauron, T. Kiyobayashi, C. Emmenegger, and L. Schlapbach, Int. J. Hydrogen Energy **27**, 203 (2002).
[230] Y. S. Nechaev and O. K. Alexeeva, Int. J. Hydrogen Energy **28**, 1433 (2003).
[231] D. Lupu, A. R. Biris, I. Misan, A. Jianu, G. Holzhuter, and E. Burkel, Int. J. Hydrogen Energy **29**, 97 (2004).
[232] D. Lupu, A. R. Biris, I. Misan, N. Lupsa, A. S. Biris, D. A. Buzatu, and M. Kleeve, Part. Sci. Technol. **20**, 225 (2002).
[233] S. Orimo, A. Zuttel, L. Schlapbach, G. Majer, T. Fukunaga, and H. Fujii, J. Alloys Compd. **356**, 716 (2003).
[234] H. G. Schimmel, G. J. Kearley, M. G. Nijkamp, C. T. Visserl, K. P. de

Jong, and F. M. Mulder, Chem.-Eur. J. **9**, 4764 (2003).
[235] C. Cantalini, L. Valentini, I. Armentano, L. Lozzi, J. M. Kenny, and S. Santucci, Sens. Actuators B **95**, 195 (2003).
[236] P. Serp, M. Corrias, and P. Kalck, Appl. Catal., A **253**, 337 (2003).
[237] L. Pesant, G. Wine, J. Matta, R. Vieira, N. Keller, C. Pham-Huu, and G. Ledoux, Large Scale Synthesis of Carbon Nanofibers for Use as Catalyst Support in Liquid-Phase Reactions, in 12th Brazillian Congress on Catalysis, Augra dos Reis, Rio de Janeiro, 2003 (unpublished).
[238] M. Croci, I. Arfaoui, T. Stockli, A. Chatelain, and J.-M. Bonard, Microelectron. J. **35**, 329 (2004).
[239] G. H. Luo, Z. F. Li, F. Wei, L. Xiang, X. Y. Deng, and Y. Jin, Physica B **323**, 314 (2002).
[240] J. Li, C. Papadopoulos, and J. Xu, Nature (London) **402**, 253 (1999).
[241] W. Hofmeister, W. P. Kang, Y. M. Wong, and J. L. Davidson, J. Vac. Sci. Technol. B **22**, 1286 (2004).
[242] J. H. Hafner, M. J. Bronikowski, B. R. Azamian, P. Nikolaev, A. G. Rinzler, D. T. Colbert, K. A. Smith, and R. E. Smalley, Chem. Phys. Lett. **296**, 195 (1998).
[243] H. T. Ng, M. L. Foo, A. P. Fang, J. Li, G. Q. Xu, S. Jaenicke, L. Chan, and S. F. Y. Li, Langmuir **18**, 1 (2002).
[244] H. Terrones *et al.*, Chem. Phys. Lett. **343**, 241 (2001).
[245] M. L. Mabudafhasi, R. Bodkin, C. P. Nicolaides, X. Y. Liu, M. J. Witcomb, and N. J. Coville, Carbon **40**, 2737 (2002).
[246] A. W. Hull, Phys. Rev. **10**, 661 (1917).
[247] *Binary Alloy Phase Diagrams*, 2nd ed., edited by T. B. Massalski (ASM International, Metals Park, OH, 1990), Vol. 1 and 2.
[248] A. W. Hull and W. P. Davey, Phys. Rev. **14**, 54 (1919).
[249] *The Properties of Natural and Synthetic Diamond*, edited by J. E. Field (Academic, London, 1992).
[250] B. T. Kelly, *The Physics of Graphite* (Applied Science Publishers, London, 1981).
[251] D. P. Kim, Y. R. Suhng, and M. M. Labes, Carbon **30**, 729 (1992).
[252] E. W. Wong, P. E. Sheehan, and C. M. Lieber, Science **277**, 1971 (1997).
[253] M. S. Dresselhaus, G. Dresselhaus, and P. C. Eklund, *Science of Fullerenes and Carbon Nanotubes* (Academic, San Diego, 1996).
[254] A. Krishnan, E. Dujardin, T. W. Ebbesen, P. N. Yianilos, and M. M. J. Treacy, Phys. Rev. B **58**, 14013 (1998).
[255] M. M. J. Treacy, T. W. Ebbesen, and J. M. Gibson, Nature (London) **381**, 678 (1996).
[256] R. Bacon, J. Appl. Phys. **31**, 323 (1960).
[257] J. D. H. Hughes, J. Phys. D **20**, 276 (1987).
[258] T. Hashishin, H. Kohara, H. Iwanaga, and S. Takeuchi, J. Ceram. Soc. Jpn. **110**, 772 (2002).
[259] R. L. Jacobsen, T. M. Tritt, J. R. Guth, A. C. Ehrlich, and D. J. Gillespie, Carbon **33**, 1217 (1995).